REVIEWS OF TOPICAL PROBLEMS

Impurities in multiband superconductors

Physics – Uspekhi **59** (12) 1211 – 1240 (2016)

REVIEWS OF TOPICAL PROBLEMS

PACS numbers: 74.20.Rp, **74.25.–q**, 74.62.Dh

100th ANNIVERSARY OF THE BIRTH OF V L GINZBURG

Impurities in multiband superconductors

M M Korshunov, Yu N Togushova, O V Dolgov

DOI: https://doi.org/10.3367/UFNe.2016.07.037863

Contents

1. Introduction **1211**
1.1 Comparison of iron pnictides and chalcogenides with cuprates; 1.2 Role of disorder in cuprates; 1.3 Specific features of iron-based superconductors
2. Strong coupling formalism and the $\mathcal{T}$-matrix approximation **1217**
3. Born approximation for one- and two-band superconductors **1219**
3.1 Qualitative analysis; 3.2 Clean and Born limits
4. Nonmagnetic impurities in two-band superconductors **1221**
4.1 Solution of Eliashberg equations in the $\mathcal{T}$-matrix approximation; 4.2 Critical temperature of the superconducting transition; 4.3 Results of the numerical solution
5. Magnetic disorder in multiband superconductors **1225**
5.1 Eliashberg equations in the $\mathcal{T}$-matrix approximation; 5.2 Results of calculations
6. Experimental situation with disorder-induced superconductivity suppression in iron-based materials **1229**
7. Dynamical properties of dirty superconductors **1231**
7.1 Density of states and penetration depth; 7.2 ARPES; 7.3 Optical conductivity; 7.4 NMR spin-lattice relaxation rate
8. Conclusions **1237**
References **1239**

Abstract. Disorder — impurities and defects violating the ideal long-range order — is always present in solids. It can result in interesting and sometimes unexpected effects in multiband superconductors, especially if the superconductivity is unconventional, thus having symmetry other than the usual s-wave. This paper uses the examples of iron-based pnictides and chalcogenides to examine how both nonmagnetic and magnetic impurities affect superconducting states with $s_{\pm}$ and s_{++} order parameters. We show that disorder causes the transition between $s_{\pm}$ and s_{++} states and examine what observable effects this transition can produce.

M M Korshunov Kirensky Institute of Physics, Federal Research Center Krasnoyarsk Science Center SB RAS,
ul. Akademgorodok 50, str. 38, 660036 Krasnoyarsk, Russian Federation;
Siberian Federal University,
Svobodnyi prosp. 79, 660041 Krasnoyarsk, Russian Federation
E-mail: mkor@iph.krasn.ru
Yu N Togushova Siberian Federal University,
Svobodnyi prosp. 79, 660041 Krasnoyarsk, Russian Federation
E-mail: togushova@bk.ru
O V Dolgov Max-Planck-Institut für Festkörperforschung,
D-70569, Stuttgart, Germany;
Lebedev Physical Institute, Russian Academy of Sciences,
Leninskii prosp. 53, 119991 Moscow, Russian Federation
E-mail: o.dolgov@fkf.mpg.de

Received 18 May 2016, revised 8 July 2016
Uspekhi Fizicheskikh Nauk **186** (12) 1315 – 1347 (2016)
DOI: https://doi.org/10.3367/UFNr.2016.07.037863
Translated by M M Korshunov; edited by A Radzig

Keywords: unconventional superconductors, iron pnictides, iron chalcogenides, impurity scattering

For two dangers never cease threatening the world: order and disorder.
Paul Valery, "Crisis of the Mind" (1919)

1. Introduction

The phenomenon of superconductivity has always attracted much attention of the scientific community. It was observed for the first time in Kamerlingh Onnes's Leiden cryogenic laboratory in 1911. Almost half a century passed before the microscopic theory was developed — only in 1957 did Bardeen, Cooper, and Schrieffer published an article [1] where the superconductivity phenomenon was explained by the formation of the condensate of Cooper pairs of electrons having opposite momenta and spins due to the electron–phonon interaction being attractive at small frequencies. The theory of superconductivity developed later by Gor'kov, Abrikosov, and Dzyaloshinskii in the frames of the Green's functions method [2] allowed formalizing the approach to the phenomenon and describing many of its interesting features. From the second-order phase transitions point of view, superconductivity is a transition to the state with broken gauge invariance. The phenomenological Ginzburg–Landau theory of superconductivity based on free energy functional expansion depends on the complex superconducting order parameter Δ. According to a theoretical-group classification, the order parameter of an ordinary superconductor in crystals obeying the tetragonal symmetry belongs to the simplest

representation, A_{1g}, and is isotropic in momentum space, i.e., exhibits an s-wave symmetry [3, 4]. In the simplest case, the gap opening in the spectrum of Fermi quasiparticles is determined by the absolute value of the order parameter, $|\Delta|$. Superconductivity as the fundamental ground state occurs in almost all metals and doped semiconductors, which are not magnetic at low temperatures.

An interesting development in the superconductivity theory occurred during investigations of superconducting states in ^{3}He, heavy-fermion materials, and magnetic superconductors (see, for example, Refs [5–7]). An important feature was the 'unconventional', non-s-wave, symmetry of the order parameter. For example, the order parameter in ^{3}He has a p-wave symmetry.

The next important milestone was the discovery of so-called high-temperature superconductivity (HTSC) in copper oxides, or simply, cuprates, in 1986 [8]. One of their features is that the critical temperature of the transition to the superconducting state, T_c, exceeded the critical temperatures of superconductors known at that time by four to five times. In addition, the cuprates have an unconventional symmetry of the superconducting gap — that is, most materials bear a d-wave order parameter belonging to the B_{2g} representation of the tetragonal symmetry group [5, 9].

In the 1990s and 2000s, superconductivity in fullerides [10] and magnesium diboride (MgB_2) [11] was discovered, which was explained in the framework of the electron–phonon interaction contrary to the cuprates. A characteristic feature of these materials was their significantly multiband nature, i.e., several bands originating from the mixture of different orbitals cross the Fermi level and form a multiply connected Fermi surface consisting of several sheets. Thus, to describe such systems, it is necessary to apply a multiband approach. On the contrary, a single-band approach works well in the cuprates despite their multiband nature.

The discovery of a new class of superconductors in 2008 — iron-based materials — started a new phase of unconventional superconductivity studies [12]. While Fe-based systems have not yet led to a technological breakthrough (these days, T_c in bulk materials is only 15 K higher than that in MgB_2; besides, just like the cuprates, they are expensive to make and difficult to work with), the conceptual importance of their discovery is hard to overestimate. Indeed, like the cuprates, fullerides and magnesium diboride reveal many unusual features; however, Cooper pairing in them arises due to the electron–phonon interaction, while in the cuprates the mechanism of superconductivity probably has a nonphononic origin. Not surprisingly, there has been a growing feeling among physicists that phonon superconductivity will probably never grow past 50–60 K, while true high-temperature superconductivity is probably due to strong correlations and limited to the unique family of layered cuprates. What the discovery of iron-based systems brought to the table was the understanding that however unique cuprates may be, these features are not prerequisites for nonphonon, high-temperature superconductivity. And, if that is true, there are likely many other crystallochemical families to be discovered, some of which may have higher critical temperatures or be better suited for applications than cuprates and iron-based superconductors. For example, the discovery of superconductivity in sulfur hydrates under pressure with the record $T_c \approx 200$ K was claimed recently [13, 14].

Superconducting Fe-based materials can be divided into two subclasses, pnictides and chalcogenides. The square lattice of Fe is the basic element of all the construction. Iron is surrounded by As or P pnictogens situated in the tetrahedral positions within the first subclass, and by Se, Te, or S chalcogens within the second subclass. Fe d-orbitals are significantly overlapped and, apart from that, out-of-plane pnictogen or chalcogen are well hybridized with the t_{2g}-subset of the iron d-orbitals, and all of them contribute to the Fermi surface. The minimal model is then a significantly multiband model. In this regard, iron-based materials are more similar to ruthenates and magnesium diboride than to cuprates. The multiband electronic structure of the cuprates can be described basically within an effective low-energy single-band model due to the dominating contribution from the in-plane $d_{x^2-y^2}$ copper orbital.

Various mechanisms of Cooper pair formation currently being discussed result in the distinct superconducting gap symmetry and structure in iron-based materials [15]. In particular, the random-phase approximation spin fluctuation (RPA-SF) approach in the clean limit gives the extended s-wave gap that changes sign between hole and electron Fermi surface sheets (the so-called $s_\pm$ state) as the main instability for the wide range of doping concentrations [16–20]. On the other hand, orbital fluctuations enhanced by the electron–phonon interaction lead to the state with the sign-preserving order parameter, the so-called s_{++} state [21]. Electron–phonon interaction by itself (without Coulomb repulsion) also leads to the s_{++} gap [22, 23]. Thus, probing the gap structure is a fundamental issue that might help in elucidating the underlying mechanism of superconductivity.

Varying amounts of disorder are present in all actually existing materials. Moreover, cuprates and iron-based materials in most cases become superconducting when doped, i.e., some atoms are replaced by others and, consequently, the potential is changed at sites where the replacement was made. In this regard, disorder is the inherent part of the observed picture of superconductivity and one has to bear a clear-eyed understanding of its role and impact on the features of studied systems.

1.1 Comparison of iron pnictides and chalcogenides with cuprates

High-T_c cuprates are known for their high critical temperature, unconventional superconducting state, and unusual normal state properties. Fe-based superconductors, with T_c up to 58 K in bulk materials [24], and probably up to 110 K in FeSe monolayer at the $SrTiO_3$ substrate [25–29], stand in second place after cuprates. When superconductivity in iron-based materials was discovered, the question immediately arose — how similar are they to cuprates? Let us compare some of their properties.

At first glance, the phase diagrams of cuprates and many Fe-based superconductors are similar. In both cases, the undoped materials exhibit antiferromagnetism, which vanishes with doping; superconductivity occurs at some nonzero doping and then disappears, such that T_c forms a 'dome'. While in cuprates the long-range ordered Néel phase vanishes before superconductivity appears, in iron-based materials the competition between these orders can take several forms. In LaFeAsO, for example, there appears to be a transition between the magnetic and superconducting states at a critical doping value, whereas in the 122 systems ($BaFe_2As_2$ and similar ones) the superconducting phase coexists with magnetism over a finite range and then persists to higher doping. It is tempting to conclude that the two

classes of superconducting materials show generally very similar behavior, but there are profound differences as well. The first striking difference lies in the fact that undoped cuprates are Mott insulators, whereas iron-based materials are metals. This suggests that the Mott–Hubbard physics of a half-filled Hubbard model is not a good starting point for pnictides, although some authors have pursued strong-coupling approaches. It does not, of course, rule out effects of correlations in iron-based materials, but they may be moderate or small. In any case, density functional theory-based approaches describe the observed Fermi surface and band structure reasonably well in the whole phase diagram, contrary to the situation in cuprates, especially in undoped and underdoped regimes.

The second important difference pertains to normal state properties. Underdoped cuprates reveal pseudogap behavior in both one-particle and two-particle charge and/or spin excitations, while a similar robust behavior is absent in iron-based materials. Generally speaking, the term 'pseudogap' implies a dip in the density of states near the Fermi level. There are, however, a wide variety of unusual features of the pseudogap state in cuprates. For example, a strange metal phase near optimal doping level in hole-doped cuprates is characterized by linear-T resistivity over a wide range of temperatures. In iron-based materials, different temperature power laws for the resistivity, including linear T-dependence of the resistivity for some materials, have been observed near optimal doping and interpreted as being due to multiband physics and interband scattering [30]. There are, however, indications of a pseudogap formation in densities of states of some pnictide bands; see, e.g., Refs [31, 32].

The mechanism of doping deserves additional discussion. Doping in cuprates is accomplished by replacing one of the spacer ions with another ion having a different valence, as in $La_{2-x}Sr_xCuO_2$ and $Nd_{2-x}Ce_xCuO_2$, or adding extra out-of-plane oxygen, as in $YBa_2Cu_3O_{6+\delta}$. The additional electron or hole is then assumed to dope the plane in an itinerant state. In iron-based materials, the nature of doping is not completely understood — similar phase diagrams are obtained by replacing the spacer ion or by in-plane substitution of Fe with Co or Ni. For example, $LaFeAsO_{1-x}F_x$, $Ba_{1-x}K_xFe_2As_2$, and $Sr_{1-x}K_xFe_2As_2$ belong to the first case, while $Ba(Fe_{1-x}Co_x)_2As_2$ and $Ba(Fe_{1-x}Ni_x)_2As_2$ belong to the second one. Whether these heterovalent substitutions dope the FeAs or FeP plane as in the cuprates was not initially clear [33], but now it is well established that they affect the Fermi surface, consistent with formal electron count doping [34, 35]. Another mechanism to vary electronic and magnetic properties takes advantage of the possibility of isovalent doping with phosphorous in $BaFe_2(As_{1-x}P_x)_2$ or ruthenium in $BaFe_2(As_{1-x}Ru_x)_2$. 'Dopants' can act as potential scatterers and change the electronic structure because of the difference in ionic sizes or simply by diluting the magnetic ions with nonmagnetic ones. In iron-based materials, therefore, some of the doping mechanisms are connected with the changes in the transition metal layer. But the phase diagrams of all Fe-based materials in the first approximation are quite similar, challenging workers in the field to seek a systematic structural observable which correlates with the variation of T_c. Among several proposals, the height of the pnictogen or chalcogen above the Fe plane has frequently been noted as playing some role in the overall doping dependence [36–38].

It is well established that the superconducting state in cuprates is universally d-wave. By contrast, the gap symmetry and structure of the iron-based materials can be quite different from material to material. Nevertheless, it seems quite possible that the ultimate source of the pairing interaction in both systems is fundamentally similar, although essential details, such as pairing symmetry and the gap structure in iron-based materials, depend on the Fermi surface geometry, orbital character of bands, and degree of correlations [15, 39].

1.2 Role of disorder in cuprates

Conventional superconductors behave differently depending on the type of introduced impurities. So, nonmagnetic impurities do not suppress superconducting critical temperature T_c according to Anderson's theorem [40], while, on the contrary, magnetic impurities cause T_c suppression with the rate following the Abrikosov–Gor'kov theory [41].

Cuprate superconductors reveal a more complicated picture. Phase diagram asymmetry for hole- and electron-doped cuprates is closely related to the impact of nonmagnetic and magnetic impurities replacing copper sites on superconducting properties. In electron-doped systems (n-type), the situation is analogous to the conventional superconductors — nonmagnetic impurities weakly suppress T_c, while magnetic ones cause a collapse of superconductivity for an impurity concentration of about one percent, which is in close agreement with the Abrikosov–Gor'kov theory. These results follow from studies of both polycrystalline samples [42, 43] and $Pr_{2-x}Ce_xCu_{1-y}M_yO_{4+z}$ single crystals with $M = Ni, Co$ [44].

Contrary to the n-type cuprates, hole-doped counterparts show a different behavior. Early studies on $YBa_2Cu_3O_7$ (Y-123) [45] revealed the suppression of superconductivity via replacement of copper not only by magnetic (Fe, Co, Ni), but also by nonmagnetic (Zn, Al, Ga) ions. Notice, however, that to compare effects of different types of impurities on T_c, it is more convenient to study the lanthanum-based system $La_{2-x}Sr_xCu_{1-y}M_yO_4$ (with y being the amount of $M = Fe, Co, Ni, Zn, Al, Ga$), where all impurities are located in the CuO_2 layer, as opposed to the Y-123 system. In the latter system, copper in-plane sites are replaced by divalent ions, while trivalent ions generally occupy Cu–O chains, which reduces their effect on T_c and thus complicates interpretation of the results.

The problem described is absent in the $La_{1.85}Sr_{0.15}Cu_{1-y}M_yO_4$ compound, for which the following results were obtained in Ref. [46]: both magnetic impurity, Co, and nonmagnetic impurities, Zn, Al, Ga, result in almost the same $T_c(y)$ dependence. At the same time, Fe causes the most rapid suppression of T_c, while Ni gives a slowest decrease in it, though both should be magnetic due to their atomic structure. To clarify the relation between superconductivity and the magnetic nature of impurities, static susceptibility measurements were made [46, 47]. They revealed the presence of an effective magnetic moment at the impurity site in all systems studied. Moreover, it become clear that the rate of T_c suppression has a weak correlation with the impurity valence. Furthermore, the magnitude of the moment strongly correlates with the critical impurity concentration at which T_c vanishes. This argues in favor of the magnetic mechanism of pairbreaking and against pairbreaking originating from the change in the hole doping level.

The authors of Ref. [46] suggested a qualitative explanation for the concentration dependence of $T_c(y)$ and for the magnetic properties of impurities. It is based on indications

that all impurities with zero spin (nonmagnetic Zn, Al, Ga, as well as Co^{3+} in the low-spin state) induce an effective magnetic moment in close proximity to the Cu^{2+} moment. That is, one has to consider the copper ion spin removed by the impurity. For an impurity with an open d-shell (Fe, Co, Ni), it is necessary to consider not only the removed copper spin but also its own impurity moment. The experimental value of the Fe^{3+} ion effective moment suggests that it resides in a high-spin state with $S = 5/2$ in the lanthanum system, and it generates an effective moment significantly larger than the Cu^{2+} moment. On the other hand, the anomalously small experimental value of the Ni^{2+} effective moment suggests that the spin should be no more than 0.32, instead of the expected $S = 1$. The authors of Ref. [46] explain this by the significant delocalization of the Ni spin state, in contrast to the strong localization of the Fe state.

Besides a qualitative explanation of the anomalous result of Cu with Ni replacement, proper treatment of the multi-electron effects in the correlated band structure leads to a quantitative description of the $T_c(y)$ dependence [48]. With the diamagnetic replacement of copper with zinc, the fraction of ions in configuration d^{10} (Zn^{2+}) is equal to y. The model for such systems is the antiferromagnetic lattice of $S = 1/2$ spins with one empty site that behaves as one paramagnetic center due to the uncompensation of sublattices. As for the copper replacement with nickel, the nickel ion Ni^{2+}, which formally should be in the d^8 state with the spin $S = 1$, due to strong intraatomic Coulomb repulsion acquires an intermediate valence. The probability of it being in the nonmagnetic d^{10} state with the spin $S = 0$ is equal to u_0^2, and the probability of the d^9 state with $S = 1/2$ is $v_0^2 = 1 - u_0^2$. As follows from the summary of optical, photoemission, and magnetic data on La_2CuO_4, the weights of these states, u_0^2 and v_0^2, are expressed via such parameters of the multiband p–d model of copper oxides [49] as energies of p and d holes in the crystal field and matrix elements of Coulomb interaction. This way, the nickel ion should have the effective spin $S = v_0^2\,(1/2)$ instead of a nominal Ni^{2+} state with $S = 1$. Calculated values of $v_0^2 = 0.72$ and $S = 0.36$ [48] are in good agreement with the experimental data.

Therefore, with the substitution of nickel for copper, the amount of impurity ions in the d^{10} state (the same state as for zinc) is equal to $u_0^2 y$. The probability of ions being in the d^9 state is $v_0^2 y$, and since their magnetic and charge characteristics are almost the same as those of copper, such ions should not suppress superconductivity. The resulting ratio of $T_c(y)$ slopes for nickel and zinc impurities is $u_0^2 = 0.28$, which is close to the experimental value of 0.38 for $La_{1.85}Sr_{0.15}Cu_{1-y}M_yO_4$ [46].

The change in the impurity effect with doping can be summarized as follows. Suppression of T_c by impurities in overdoped systems does not depend on the doping level p, while in underdoped samples it is strongly doping-dependent [50]. Given that the pseudogap state occurs exactly at low doping, the observed p-dependence emphasizes the importance of the ground state in the response of the system to the disorder.

It should be noted that an alternative to the chemical introduction of impurities is the creation of defects via fast neutron irradiation. Such a method benefits from avoiding some of the difficulties related to the replacement of some atoms with others. Suppression of T_c in this case, as well as other physical characteristics of cuprates being irradiated by neutrons, are extensively described in Refs [51–53].

Summarizing, strong electronic correlations causing the formation of local moments due to the presence of formally nonmagnetic impurities complicates significantly the interpretation of disorder effects on T_c suppression. Among other factors preventing the formulation of a consistent theory for the role of defects in superconductivity of cuprates are the absence of the theory for the correlated ground state, difficulties with controling the disorder parameters, and the presence of anisotropy in impurity scattering. Since a detailed discussion of cuprate physics with the important role of strong correlations is not the goal of the present review, here we mentioned only a few important points of impurity scattering. We direct the curious reader to other reviews, like Refs [54–60].

Nor are we going further into the details of d-wave superconductivity and related problems in cuprates. This topic is extensively reviewed in many papers concerning both the theories of impurity scattering in a d-wave superconductor [61–70] and the effect of impurities on observable properties of cuprates [71–79]. Let us just mention that the single-band d-wave superconductor can be approximately treated as a two-band superconductor with opposite signs of the gaps in different bands — the analogy of the $s_\pm$ state [80]. In other words, parts of the Fermi surface with different signs of the order parameter are considered to originate from different bands. Though this is a rough approximation, it can give some qualitative results.

1.3 Specific features of iron-based superconductors

Under normal conditions, iron is ferromagnetic. Under pressure, however, once the Fe atoms form an hcp lattice, iron becomes nonmagnetic and even superconducting at $T < 2$ K [81], most probably due to electron–phonon interaction [82]. On the other hand, iron-based superconductors are quasi-two-dimensional materials with the conducting square lattice of Fe ions. The Fermi level is occupied by the $3d^6$ states of Fe^{2+}. This was established in early DFT (density functional theory) calculations [16, 83, 84] which are in quite good agreement with the results of quantum oscillations and ARPES (angle-resolved photoemission spectroscopy). All five orbitals, $d_{x^2-y^2}$, $d_{3z^2-r^2}$, d_{xy}, d_{xz}, and d_{yz}, are at or near the Fermi level. This results in a significantly 'multiorbital' and multiband low-energy electronic structure, which could not be described within the single-band model. For example, within the five-orbital model [17] correctly reproducing the DFT band structure [85], the Fermi surface comprises four sheets: two hole pockets around the point $(0, 0)$, and two electron pockets around the points $(\pi, 0)$ and $(0, \pi)$. Such **k**-space geometry results in the possibility of spin-density wave (SDW) instability due to the nesting between hole and electron Fermi surface sheets at the wave vector $\mathbf{Q} = (\pi, 0)$ or $(0, \pi)$. Upon doping x, the long-range SDW order is destroyed. If electrons are doped, then for the large x hole pockets disappear, leaving only electron Fermi surface sheets, as observed in $K_xFe_{2-y}Se_2$ and in FeSe monolayers [26]. Upon increasing hole doping, first, a new hole pocket appears around the point (π, π) and then electron sheets vanish. KFe_2As_2 just corresponds to the latter case. ARPES confirms that the maximal contribution to the bands at the Fermi level comes from the $d_{xz, yz}$ and d_{xy} orbitals [86, 87]. At the same time, as will be pointed out later, the presence of a few pockets and the multiorbital band character significantly affect superconducting pairing.

Soon after high-quality samples of cuprates were prepared, the $d_{x^2-y^2}$ symmetry of the gap, with the $\cos k_x - \cos k_y$ structure, was empirically established by penetration depth, ARPES, NMR, and phase sensitive Josephson tunneling experiments. No similar consensus on any universal gap structure has been reached even after several years of intensive research on high-quality single crystals of iron-based superconductors. There is strong evidence that small differences in electronic structure can lead to a strong diversity in superconducting gap structures, including nodal states and states with a full gap on the Fermi surface. The actual symmetry class of most of the materials may be generalized A_{1g} (extended s-wave symmetry), probably involving a sign change of the order parameter between Fermi surface sheets or its parts [15]. Understanding the symmetry character of the superconducting ground states, as well as a detailed structure of the order parameter should provide clues to the microscopic pairing mechanism in iron-based materials and thereby lead to a deeper insight into the phenomenon of high-temperature superconductivity.

The group-theoretical classification of gap structures in unconventional superconductors is rather complicated and has been reviewed in, e.g., Ref. [9]. In the absence of spin–orbit coupling, the total spin of the Cooper pair is well defined and can be either $S = 1$ or $S = 0$. The easiest and most accurate way to probe whether the pair is spin-triplet is via the Knight shift measurements. These experiments have been performed on several iron-based materials, including $Ba(Fe_{1-x}Co_x)_2As_2$ [88], $LaFeAsO_{1-x}F_x$ [89], $PrFeAsO_{0.89}F_{0.11}$ [90], $Ba_{1-x}K_xFe_2As_2$ [91, 92], LiFeAs [93, 94], and $BaFe_2(As_{0.67}P_{0.33})_2$ [95]. It was found that the Knight shift decreases in all crystallographic directions. This effectively ruled out triplet symmetries, such as p-wave or f-wave.

Having ruled out the spin-triplet states, we focus first on simple tetragonal point group symmetry. In a three-dimensional tetragonal system, group theory allows only five one-dimensional irreducible representations according to how the order parameter transforms under rotations by 90° and other operations of the tetragonal group: A_{1g} ('s-wave'), B_{1g} ('d-wave', $x^2 - y^2$), B_{2g} ('d-wave', xy), A_{2g} ('g-wave', $xy(x^2 - y^2)$), and E_g ('d-wave', xz, yz). Notice that the s_{++} and $s_{\pm}$ states all have the same symmetry, i.e., neither changes sign if the crystal axes are rotated through 90°. By contrast, the d-wave state changes sign under such a rotation. Notice further that the mere existence of the hole and electron pockets leads to new ambiguities in the sign structure of the various states. In addition to a global change of sign, which is equivalent to a gauge transformation, we can have individual rotations on single pockets and still preserve symmetry. For example, if for the d-wave case we rotate the gap in the hole pocket, 90°, but keep the electron pocket signs fixed, it still represents a B_{1g} state. B_{2g} states are also possible by symmetry and would have nodes on the electron pockets. Further, more complicated, gap functions with differing relative phases become possible when more pockets are present and when three-dimensional effects are included.

It is important to note that, while the d-wave does not necessarily imply the existence of gap nodes, in combination with a quasi-two-dimensional Fermi surface at the center of the Brillouin zone such nodes are unavoidable: either vertical for the B_{1g}, B_{2g}, and A_{2g} symmetries, or horizontal for the E_g symmetry. Since such a Fermi surface exists in pnictides, the experimentally proven absence of nodes on it would evidence against the d-wave symmetry. As for experiments, surface probes such as ARPES show full gaps on the central Fermi surface sheet. Moreover, the full gap on the whole Fermi surface is observed in tunneling and bulk probes in hole-doped systems, as well as in materials with a small electron doping.

There are also direct experiments that provide evidence against the d-wave. The Josephson current in the c-direction, when the studied superconductor is coupled to a known s-wave superconductor, would confirm the s-type of the former. Exactly such current was observed in 122 single crystals [96].

Another piece of evidence comes from the absence of the so-called anomalous Meissner effect (or Wohlleben effect) [97]. This effect manifests itself in polycrystalline samples with random orientation of grains. It was predicted at the beginning of the cuprates era [98] and since then it has been routinely observed only in d-wave superconductors. The Wohlleben effect appears due to the fact that the response to a weak external magnetic field is paramagnetic, i.e., opposite to the standard diamagnetic response of an s-wave superconductor. This happens because half of the weak links have a zero phase shift, and the other half have a π phase shift.

The described separate pieces of evidence strongly suggest that the pairing symmetry is s-wave, not d-wave. However, we want to stress that direct testing similar to that performed in cuprates, namely a single-crystal experiment with a 90° Josephson junction forming a closed loop, is still lacking, and it is highly desirable to make an ultimate conclusion.

It should also be borne in mind that nothing forbids different iron-based materials from having different order parameter symmetries, although our previous experience with other superconductors tends to argue against this. Indeed, there are several theories claiming that, while most iron-based systems have the s-wave gap symmetry, those with unusual Fermi surfaces with either electron or hole pockets can have the d-wave symmetry of the order parameter [20, 99–103].

Notice that the term *symmetry* should be distinguished from the term *structure* of the *gap*. The latter is used to designate the **k**-dependent variation of an order parameter within a given symmetry class. Gaps with the same symmetry may have very different structures. Let us illustrate this for the s-wave symmetry (Fig. 1). Fully gapped s-states without nodes on the Fermi surface differ only by a relative gap sign between the hole and electron pockets, which is positive in the s_{++} state and negative in the $s_{\pm}$ state. On the other hand, the gap vanishes in nodal s-states at certain points on the electron pockets. These states are called 'nodal $s_{\pm}$' ('nodal s_{++}') and are characterized by the opposite (same) averaged signs of the order parameter on the hole and electron pockets. Nodes of this type are sometimes described as 'accidental', since their existence is not dictated by symmetry, in contrast to the symmetry nodes of the d-wave gap. Therefore, they can be removed continuously, resulting in either an $s_{\pm}$ or an s_{++} state [104, 105].

Superconducting states with different symmetries and structures of order parameters differently respond when subject to the disorder. As we have mentioned earlier, nonmagnetic impurities in the single-band s-wave superconductors do not suppress T_c, while magnetic impurities do it in accordance with the Abrikosov–Gor'kov theory [41]. In unconventional superconductors, suppression of the critical temperature as a function of parameter Γ characterizing impurity scattering may follow a complicated, yet very

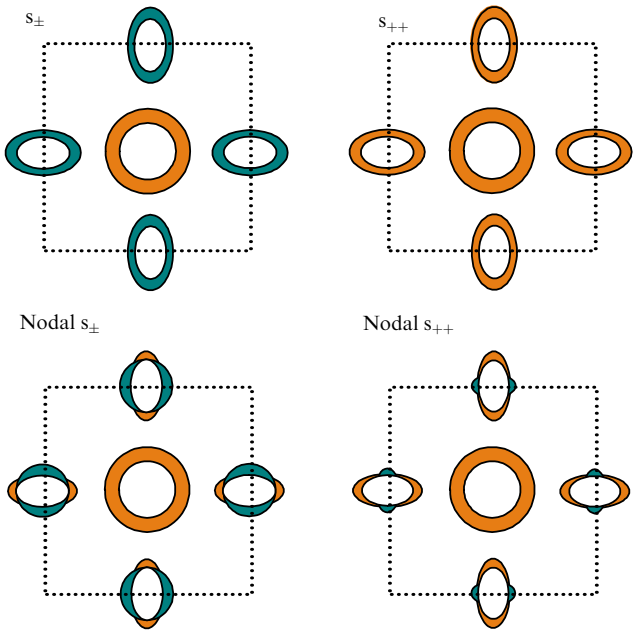

Figure 1. (Color online.) Schematic diagrams of four types of order parameter *structures* having the s-wave symmetry in the two-dimensional Brillouin zone (dotted square) corresponding to one iron atom per unit cell. Different colors stands for different signs of the order parameter.

explicit, law. That is why many authors desire to attribute the observed $T_c(\Gamma)$ dependence as pointing towards a particular gap structure is not surprising.

Several experiments on iron-based systems show that T_c suppression is much weaker than expected in the framework of the Abrikosov–Gor'kov theory for both nonmagnetic [106–112] and magnetic disorder [107, 113–116]. It is worth advising the reader to interpret T_c suppression results with caution for several reasons. First, in some cases not all the nominal concentration of impurity substitutes in the crystal. Second, 'slow' and 'fast' T_c suppression cannot be determined by plotting T_c vs impurity concentration, but only vs a scattering rate directly comparable to the theoretical scattering rate, which is generally difficult to determine from experiments. The alternative is to plot T_c vs residual resistivity change $\Delta\rho$, but this is only possible, first, if the $\rho(T)$ curve shifts rigidly with disorder and, second, if comparisons with theory include a proper treatment of the transport rather than the quasiparticle lifetime. Finally, the effect of a chemical substitution in an iron-based superconductor is quite clearly not describable solely in terms of a potential scatterer, but the impurity may dope the system or cause other electronic structure changes which influence the pairing interaction. The most promising alternatives are irradiation experiments, since the disorder is introduced without altering the chemical composition of the studied material. Experiments of this kind include irradiation by protons [109, 117, 118], neutrons [106], electrons [105, 112, 119, 120], and heavy ions [121–123]. There are some specific complications though. For example, consider the work on neutron irradiation by Karkin et al. [106]. As seen from other work by the same group [124], the structure of the studied material changed after neutron irradiation. The doping is also accompanied by changes to the structural parameters that correlate with the T_c changes [36–38, 125]. And it might seem that the problem of separating the role of defects and changes to structural parameters with neutron irradiation is not a simple one. Given the many uncertainties present in the basic modeling of a single impurity, as well as the multiband nature of iron-based materials, it is reasonable to assume that systematic disorder experiments may not play a decisive role in determining the order parameter symmetry and structure. Nevertheless, one can extract useful information from the qualitative effects appearing on the level of simple multiband models of disorder [126, 127].

In this review, we demonstrate the basics of impurity effects on multiband superconductivity using the simple model for iron-based materials as an example. In particular, within the $\mathcal{T}$-matrix approximation, we discuss the role of scattering on nonmagnetic and magnetic impurities for the $s_{\pm}$ and s_{++} states in a two-band model. We show that for the finite nonmagnetic impurity scattering rate, the transition from $s_{\pm}$ to s_{++} occurs, i.e., one of two gaps changes sign when going through zero. The transition happens for the positive sign of the superconducting coupling constant averaged over the bands. At the same time, T_c stays finite and almost independent of the impurity scattering rate, which is proportional to the impurity concentration and magnitude of the scattering potential. There are two cases for scattering on magnetic impurities when the transition temperature T_c is not fully suppressed, in contrast to the Abrikosov–Gor'kov theory, but the saturation of it appears in the regime of a large scattering rate. The first case is characterized by purely interband impurity scattering. At the same time, the $s_{\pm}$ gap is preserved, while the s_{++} state transforms into the $s_{\pm}$ state with increasing magnetic disorder. The second case corresponds to the unitary limit of scattering with the gap structure remaining intact. The reason for the $s_{\pm} \leftrightarrow s_{++}$ transitions is the following: if one of the two competing superconducting interactions leads to a state robust against impurity scattering, then, although it was not dominant in the clean limit, it should become dominant while the other state is destroyed by impurity scattering. Since the transitions between the $s_{\pm}$ and s_{++} states go through the gapless regime, they should reveal themselves in thermodynamic and transport properties of the system and thus be observable in optical and tunneling experiments, as well as in photoemission spectroscopy. Because one of the gaps vanishes near the transition, ARPES should reveal the gapless spectra and, in the optical conductivity, the transition should result in the 'restoring' of the Drude frequency dependence of $\mathrm{Re}\,\sigma(\omega)$. We ignored the complicated question of nonmagnetic and magnetic scattering channels coexisting due to its poor development in the multiband case at the time of writing.

The layout of the review is as follows. In Section 2 we present the Eliashberg formalism for a multiband superconductor and the $\mathcal{T}$-matrix approximation for the impurity self-energy. The approximation is then applied to the simple two-band model, in which either the $s_{\pm}$ or s_{++} state occurs, depending on the parameters. Section 3 contains a discussion of qualitative impurity scattering effects in the Born limit. In Sections 4 and 5, the roles of nonmagnetic and magnetic impurities are described, respectively. Section 6 is devoted to a short review of the experimental findings on the impact of impurities on the superconducting state of pnictides and chalcogenides. In Section 7, we discuss the effect of disorder on such experimentally observable dynamical characteristics as the density of states, the spectral function, optical conductivity, and the magnetic field penetration depth. Conclusions are contained in the final Section 8.

2. Strong coupling formalism and the $\mathcal{T}$-matrix approximation

For the sake of simplicity, we begin by considering a two-band model with the interaction leading to superconductivity with a spin-singlet order parameter that is isotropic in each band. Results can be easily generalized for a larger number of bands, as will follow from the equations below. The isotropy of the order parameter allows us to obtain some results analytically, though it is a heavy restriction of the theory. On the other hand, with it, one can pursue the approximate treatment of superconductors with sign-changing gap, like the d-wave cuprates, where parts of the Fermi surface with different signs of the gap can be roughly considered to be contributions from different bands [80].

For the considered task of impurity scattering, the Hamiltonian can be written out in the following form

$$H = \sum_{\mathbf{k},\,\alpha,\,\sigma} \xi_{\mathbf{k}\alpha} c^{\dagger}_{\mathbf{k}\alpha\sigma} c_{\mathbf{k}\alpha\sigma} + H_{\mathrm{sc}} + H_{\mathrm{imp}}\,, \tag{1}$$

where $c_{\mathbf{k}\alpha\sigma}$ is the annihilation operator of the electron with momentum $\mathbf{k}$, spin σ, and band index α that equals a (first band) or b (second one), and $\xi_{\mathbf{k}\alpha}$ is the electron dispersion that, for simplicity, we treat as linearized near the Fermi level, $\xi_{\mathbf{k}\alpha} = \mathbf{v}_{\mathrm{F}\alpha}(\mathbf{k} - \mathbf{k}_{\mathrm{F}\alpha})$, with $\mathbf{v}_{\mathrm{F}\alpha}$ and $\mathbf{k}_{\mathrm{F}\alpha}$ being the Fermi velocity and the Fermi momentum of the band α, respectively.

Superconductivity occurs in our system due to the interaction H_{sc}. It has a different form for different mechanisms of pairing. That is, when the superconductivity is mediated by spin and/or orbital fluctuations, it is the on-site Coulomb (Hubbard) electron–electron interaction [17, 18, 128, 129]:

$$H^{\mathrm{sf}}_{\mathrm{sc}} = U \sum_{f,l} n_{fl\uparrow} n_{fl\downarrow} + U' \sum_{f,l<l'} n_{fl} n_{fl'} + J \sum_{f,l<l'} \sum_{\sigma,\sigma'} c^{\dagger}_{fl\sigma} c^{\dagger}_{fl'\sigma'} c_{fl\sigma'} c_{fl'\sigma} + J' \sum_{f,l\neq l'} c^{\dagger}_{fl\uparrow} c^{\dagger}_{fl\downarrow} c_{fl'\downarrow} c_{fl'\uparrow}\,, \tag{2}$$

where $n_{fl} = n_{fl\uparrow} + n_{fl\downarrow}$ is the number of particles operator, f is the site index, l and l' are orbital indices, U and U' are intra- and interorbital Hubbard repulsions, J is Hund's exchange, and J' is pair-hopping. Usually, parameters obey the spin-rotational invariance, which leads to relations $U' = U - 2J$ and $J' = J$, thus reducing the number of free parameters in the theory.

In the case of electron–phonon interaction inducing superconductivity, one of the examples of the Hamiltonian is given by

$$H^{\mathrm{e-ph}}_{\mathrm{sc}} = \sum_{\mathbf{q},\,\lambda} \omega_{\mathbf{q}\lambda} \left(b^{\dagger}_{\mathbf{q}\lambda} b_{\mathbf{q}\lambda} + \frac{1}{2} \right) + \frac{1}{\sqrt{N}} \sum_{\mathbf{k},\,\mathbf{q},\,\lambda,\,\alpha,\,\sigma} g_{\lambda}(\mathbf{k},\,\mathbf{q}) (b_{\mathbf{q}\lambda} + b^{\dagger}_{-\mathbf{q}\lambda})\, c^{\dagger}_{\mathbf{k}+\mathbf{q}\alpha\sigma} c_{\mathbf{k}\alpha\sigma}\,. \tag{3}$$

Here, $b_{\mathbf{q}\lambda}$ is the annihilation operator of the phonon with momentum $\mathbf{q}$, polarization λ, and frequency $\omega_{\mathbf{q}\lambda}$, and $g_{\lambda}(\mathbf{k},\mathbf{q})$ is the electron–phonon interaction matrix element.

We assume hereinafter that the problem of finding the effective dynamical superconducting interaction has already been solved, and both coupling constants and the bosonic spectral function have been obtained. The latter describes the effective electron–electron interaction via an intermediate boson. In the case of Hubbard interaction (2), intermediate excitations are spin or charge fluctuations, while in the case of electron–phonon interaction (3) they are phonons. Moreover, if the retarded nature of the interaction in the case of phonons is obvious from the beginning, for the Hubbard Hamiltonian it is revealed only after the summation of a particular diagram series [130]. The nature of the effective dynamical interaction is not important for the following analysis of the role played by disorder in a superconducting state. Rather, what is important is the fact that the corresponding bosonic spectral function is maximal at small frequencies and drops with a further increase in frequency. For example, inelastic neutron scattering experiments confirm such a behavior for spin fluctuations.

Notice that though the dynamical interaction has a complicated structure and is hard to write in a unified form, everything becomes simplified in the mean-field approximation and can be cast in the Hamiltonian

$$H^{\mathrm{MF}}_{\mathrm{sc}} = \sum_{\mathbf{k},\,\alpha} \left(\Delta_{\alpha} c^{\dagger}_{\mathbf{k}\alpha\uparrow} c^{\dagger}_{-\mathbf{k}\alpha\downarrow} + \mathrm{h.c.} \right), \tag{4}$$

where Δ_{α} is a mean-field spin-singlet order parameter. For example, $\operatorname{sgn}\Delta_a = \operatorname{sgn}\Delta_b$ for the two-band superconductor in the s_{++} state, while for the $s_{\pm}$ state it is $\operatorname{sgn}\Delta_a = -\operatorname{sgn}\Delta_b$.

Impurity scattering is described by the H_{imp} term containing nonmagnetic ($\mathcal{U}$) and magnetic ($\mathcal{V}$) impurity scattering potentials:

$$H_{\mathrm{imp}} = \sum_{\mathbf{R}_i,\,\sigma,\,\sigma',\,\alpha,\,\beta} \left(\mathcal{U}^{\alpha\beta}_{\mathbf{R}_i} \delta_{\sigma\sigma'} + \mathcal{V}^{\alpha\beta}_{\mathbf{R}_i} \hat{S}_{\mathbf{R}_i} \hat{\sigma}_{\sigma\sigma'} \right) c^{\dagger}_{\mathbf{R}_i\alpha\sigma} c_{\mathbf{R}_i\beta\sigma'}\,, \tag{5}$$

where $\hat{S}_{\mathbf{R}_i}$ is the operator of an impurity spin at site $\mathbf{R}_i$ with the spin quantum number $S_{\mathbf{R}_i}$, and $\hat{\boldsymbol{\sigma}}$ are the Pauli spin matrices

$$\hat{\sigma}_0 = \begin{pmatrix} 1 & 0 \\ 0 & 1 \end{pmatrix}, \quad \hat{\sigma}_1 = \begin{pmatrix} 0 & 1 \\ 1 & 0 \end{pmatrix},$$
$$\hat{\sigma}_2 = \begin{pmatrix} 0 & -\mathrm{i} \\ \mathrm{i} & 0 \end{pmatrix}, \quad \hat{\sigma}_3 = \begin{pmatrix} 1 & 0 \\ 0 & -1 \end{pmatrix}.$$

In what follows, we will use the Eliashberg approach generalized for multiband superconductors [131]. To describe the thermodynamics of the superconducting state, we are interested in Green's function $\hat{\mathbf{G}}(\mathbf{k},\omega_n)$ of the quasiparticle with momentum $\mathbf{k}$ and Matsubara frequency $\omega_n = (2n+1)\,\pi T$. Green's function is a matrix in the band space and combined Nambu and spin spaces (we indicate quantities in the band space in bold face, and quantities in the combined Nambu and spin spaces by the circumflex accent). For definiteness, we assume that the index $\alpha = a, b$ denotes the band space, and Pauli matrices $\hat{\tau}_i$ and $\hat{\sigma}_i$ denote the Nambu ($\hat{\tau}_i$) and spin ($\hat{\sigma}_i$) spaces. As a result of the direct product (operation $\otimes$) of all matrices, for the two-band model we have Green's function matrix with the dimension 8×8.

Dyson equation

$$\hat{\mathbf{G}}(\mathbf{k},\omega_n) = \left(\hat{\mathbf{G}}_0^{-1}(\mathbf{k},\omega_n) - \hat{\boldsymbol{\Sigma}}(\mathbf{k},\omega_n) \right)^{-1} \tag{6}$$

establishes a connection among the full Green's function, the 'bare' Green's function (without interelectron interactions and impurities)

$$\hat{G}^{\alpha\beta}_0(\mathbf{k},\omega_n) = \left(\mathrm{i}\omega_n \hat{\tau}_0 \otimes \hat{\sigma}_0 - \xi_{\mathbf{k}\alpha} \hat{\tau}_3 \otimes \hat{\sigma}_0 \right)^{-1} \delta_{\alpha\beta}\,, \tag{7}$$

and the self-energy matrix $\hat{\boldsymbol{\Sigma}}(\mathbf{k}, \omega_n)$. Further, we assume that the latter does not depend on the wave vector $\mathbf{k}$, but keep the frequency and band index dependences:

$$\hat{\boldsymbol{\Sigma}}(\omega_n) = \sum_{i=0}^{3} \Sigma_{(i)\,\alpha\beta}(\omega_n)\,\hat{\tau}_i\,. \tag{8}$$

In this case, the problem can be simplified by averaging over $\mathbf{k}$. Thus, all equations will be written down in terms of quasiclassical ξ-integrated Green's functions:

$$\hat{\mathbf{g}}(\omega_n) = \int \mathrm{d}\xi \hat{\mathbf{G}}(\mathbf{k}, \omega_n) = \begin{pmatrix} \hat{g}_{an} & 0 \\ 0 & \hat{g}_{bn} \end{pmatrix}, \tag{9}$$

where

$$\hat{g}_{\alpha n} = g_{0\alpha n}\hat{\tau}_0 \otimes \hat{\sigma}_0 + g_{2\alpha n}\hat{\tau}_2 \otimes \hat{\sigma}_2\,. \tag{10}$$

Here, $g_{0\alpha n}$ and $g_{2\alpha n}$ are the normal and anomalous (Gor'kov) ξ-integrated Green's functions in the Nambu representation:

$$g_{0\alpha n} = -\frac{\mathrm{i}\pi N_\alpha \tilde{\omega}_{\alpha n}}{\sqrt{\tilde{\omega}_{\alpha n}^2 + \tilde{\phi}_{\alpha n}^2}}\,, \quad g_{2\alpha n} = -\frac{\pi N_\alpha \tilde{\phi}_{\alpha n}}{\sqrt{\tilde{\omega}_{\alpha n}^2 + \tilde{\phi}_{\alpha n}^2}}\,. \tag{11}$$

They depend on the density of states per spin at the Fermi level in the corresponding band ($N_{a,b}$), and on the order parameter $\tilde{\phi}_{\alpha n}$ and frequency $\tilde{\omega}_{\alpha n}$ renormalized by the self-energy:

$$\mathrm{i}\tilde{\omega}_{\alpha n} = \mathrm{i}\omega_n - \Sigma_{0\alpha}(\omega_n) - \Sigma_{0\alpha}^{\mathrm{imp}}(\omega_n)\,, \tag{12}$$

$$\tilde{\phi}_{\alpha n} = \Sigma_{2\alpha}(\omega_n) + \Sigma_{2\alpha}^{\mathrm{imp}}(\omega_n)\,. \tag{13}$$

Often, it is convenient to introduce the renormalization factor $Z_{\alpha n} = \tilde{\omega}_{\alpha n}/\omega_n$ that enters into the gap function $\Delta_{\alpha n} = \tilde{\phi}_{\alpha n}/Z_{\alpha n}$. It is the gap function that generates peculiarities in the density of states.

A part of the self-energy due to spin fluctuations or any other retarded interaction (electron–phonon, retarded Coulomb interaction) can be written out in the following way:

$$\Sigma_{0\alpha}(\omega_n) = T\sum_{\omega_{n'},\beta} \lambda_{\alpha\beta}^{Z}(n-n')\,\frac{g_{0\beta n'}}{N_\beta}\,, \tag{14}$$

$$\Sigma_{2\alpha}(\omega_n) = -T\sum_{\omega_{n'},\beta} \lambda_{\alpha\beta}^{\phi}(n-n')\,\frac{g_{2\beta n'}}{N_\beta}\,. \tag{15}$$

Coupling functions

$$\lambda_{\alpha\beta}^{\phi,Z}(n-n') = 2\lambda_{\alpha\beta}^{\phi,Z}\int_0^\infty \mathrm{d}\Omega\,\frac{\Omega B(\Omega)}{(\omega_n - \omega_{n'})^2 + \Omega^2}$$

are represented by coupling constants $\lambda_{\alpha\beta}^{\phi,Z}$, which include density of states N_β, and by the normalized bosonic spectral function $B(\Omega)$, shown in Fig. 2. The matrix elements $\lambda_{\alpha\beta}^{\phi}$ can be positive (attractive), as well as negative (repulsive) due to the interplay between spin fluctuations and electron–phonon coupling [130, 132], while the matrix elements $\lambda_{\alpha\beta}^{Z}$ are always positive. For simplicity's sake, we set $\lambda_{\alpha\beta}^{Z} = |\lambda_{\alpha\beta}^{\phi}| \equiv |\lambda_{\alpha\beta}|$ and neglect possible anisotropy in each order parameter $\tilde{\phi}_{\alpha n}$. Effects due to anisotropy in the $s_\pm$ state have been examined, for example in Ref. [104].

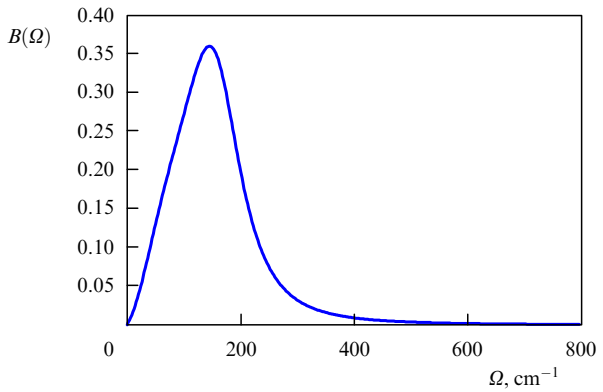

Figure 2. Spectral function $B(\Omega)$ reproducing the frequency dependence of spin fluctuations [132–134].

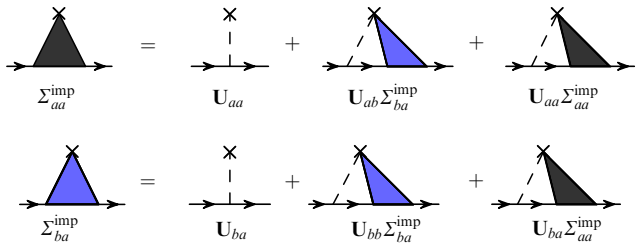

Figure 3. System of equations for the intra- and interband parts of the impurity self-energy $\hat{\boldsymbol{\Sigma}}^{\mathrm{imp}}$ in the self-consistent $\mathcal{T}$-matrix approximation [135]. Here, $\mathbf{U}_{aa(bb)}$ and $\mathbf{U}_{ab(ba)}$ are the intraband and interband components of the impurity potential, respectively.

We use a noncrossing approximation (graphically sketched in Fig. 3) to calculate the impurity self-energy $\hat{\boldsymbol{\Sigma}}^{\mathrm{imp}}$:

$$\hat{\boldsymbol{\Sigma}}^{\mathrm{imp}}(\omega_n) = n_{\mathrm{imp}}\hat{\mathbf{U}} + \hat{\mathbf{U}}\hat{\mathbf{g}}(\omega_n)\,\hat{\boldsymbol{\Sigma}}^{\mathrm{imp}}(\omega_n)\,, \tag{16}$$

where $\hat{\mathbf{U}}$ is the matrix of the impurity potential, and n_{imp} is the concentration of impurities. Equation (16) represents the $\mathcal{T}$-matrix approximation.

The impurity scattering matrix $\hat{\mathbf{U}}$ is derived from Hamiltonian (5). The procedure of further calculations is the following: (i) solve equation (16); (ii) calculate renormalizations of frequency (12) and order parameter (13) self-consistently, and (iii) use them to obtain Green's functions (9) and (11).

The solution of equation (16) depends on the explicit form of the impurity potential. Further, we consider two cases separately: nonmagnetic ($\mathcal{U}_{\mathbf{R}_i}^{\alpha\beta} \neq 0$, $\mathcal{V}_{\mathbf{R}_i}^{\alpha\beta} = 0$) and magnetic ($\mathcal{U}_{\mathbf{R}_i}^{\alpha\beta} = 0$, $\mathcal{V}_{\mathbf{R}_i}^{\alpha\beta} \neq 0$) impurities, respectively.

At the end of the present section, we write down expressions for some of the observables which are affected by the detailed structure of impurity scattering. In the first place, this is the density of states that can be measured in tunneling experiments and by ARPES:

$$N(\omega) = \sum_\alpha N_\alpha(\omega) = \sum_{\mathbf{k},\alpha} A_\alpha(\mathbf{k}, \omega) = -\frac{1}{\pi}\sum_\alpha \mathrm{Im}\, g_{0\alpha}(\omega)\,, \tag{17}$$

where $g_{0\alpha}(\mathrm{i}\omega_n \to \omega + \mathrm{i}\delta)$ is the retarded Green's function that is Matsubara Green's function (11) analytically continued to the real frequency axis, $N_\alpha(\omega)$ is the partial density of states for band α, $A_\alpha(\mathbf{k}, \omega)$ is the quasiparticle spectral function, ω is the real frequency, and $\delta \to 0+$.

Another important characteristic of a superconductor is the temperature dependence of the London magnetic field penetration depth $\lambda_{\rm L}$. In the local limit, it is related to the imaginary part of the optical conductivity:

$$\frac{1}{\lambda^2_{{\rm L},xx'}} = \lim_{\omega\to 0}\frac{4\pi\omega}{c^2}\,{\rm Im}\,\sigma^{xx'}(\omega,\mathbf{q}=0)\,, \tag{18}$$

where x and x' are axis directions of the Cartesian coordinates, c is the speed of light, and $\sigma^{xx'}(\omega,\mathbf{q}=0)$ is the optical conductivity at zero momentum $\mathbf{q}$ (in the local, i.e., London, limit). If we ignore the effects of strong coupling and, in general, Fermi-liquid effects, then for a clean uniform superconductor at zero temperature we have $1/\lambda_{{\rm L},xx'} = \omega_{{\rm p}\alpha}^{xx'}/c$, where $\omega_{{\rm p}\alpha}^{xx'} = [8\pi e^2 N_\alpha(0)\langle v_{{\rm F}\alpha}^x v_{{\rm F}\alpha}^{x'}\rangle]^{1/2}$ is the electron plasma frequency. For impurity scattering, vertex corrections from noncrossing diagrams vanish due to the $\mathbf{q}=0$ condition. Thus, the penetration depth for the multiband system can be calculated via the following expression:

$$\frac{1}{\lambda^2_{{\rm L},xx'}} = \sum_\alpha\left(\frac{\omega_{{\rm p}\alpha}^{xx'}}{c}\right)^2 T\sum_n \frac{g^2_{2\alpha n}}{\pi N_\alpha^2\sqrt{\tilde\omega^2_{\alpha n}+\tilde\phi^2_{\alpha n}}}\,. \tag{19}$$

A so-called 'superfluid plasma frequency' $\omega_{\rm SF}^{xx'} = c/\lambda_{{\rm L},xx'}$ can be introduced. It is often mentioned in literature that this function corresponds to the charge density of the superfluid condensate. Notice that this is true only in a noninteracting clean system at zero temperature.

We consider hereinafter a square lattice with x and x' in the *ab* plane. In this case, we denote the penetration depth and corresponding plasma frequency by $\lambda_{\rm L}$ and $\omega_{{\rm p}\alpha}$, respectively.

Optical conductivity is the third important observable characteristic. In the local (London) limit with $\mathbf{q}=0$ in the *ab* plane, it is equal to

$$\sigma(\omega) = \sum_\alpha \sigma_\alpha(\omega) = {\rm i}\sum_\alpha \frac{\Pi_\alpha^{xx}({\rm i}\omega_m\to\omega+{\rm i}\delta)}{\omega}\,, \tag{20}$$

where the polarization operator is given by

$$\Pi_\alpha^{xx'}(\omega_m) = \frac{T}{N_{\mathbf{k}}}\sum_{\mathbf{k},\omega_n}{\rm Tr}\, e v_\alpha^x\hat\tau_0\otimes\hat\sigma_0\hat G^{\alpha\alpha}(\mathbf{k},\omega_n+\omega_m) \times\hat G^{\alpha\alpha}(\mathbf{k},\omega_n)\,\hat\gamma_\alpha^{x'}\,. \tag{21}$$

Here, $N_{\mathbf{k}}$ is the normalization coefficient of the sum over momenta, $\hat\gamma_\alpha^{x'}$ is a vertex function, and the trace is taken over the Nambu and spin spaces. As was mentioned before, vertex corrections from noncrossing diagrams for the impurity scattering at $\mathbf{q}=0$ vanish due to the vector nature of the optical conductivity vertex, and the scalar character of the impurity scattering. Thus, the zeroth order is a good approximation for the vertex [136], in which the vertex is equal to $ev_\alpha^{x'}\hat\tau_0\otimes\hat\sigma_0$. It is also convenient to go over from the summation over momenta to the integration over energy and averaging over the Fermi surface, which results in $2e^2N_\alpha(0)\langle v_{{\rm F}\alpha}^x v_{{\rm F}\alpha}^{x'}\rangle \approx (\omega_{{\rm p}\alpha}^{xx'})^2/(4\pi)$. After the transformation, the polarization operator becomes equal to [136]

$$\Pi_\alpha^{xx'}(\omega_m) = \frac{(\omega_{{\rm p}\alpha}^{xx'})^2}{4\pi}\,\pi T\sum_{\omega_n} S_\alpha^{nm}\,, \tag{22}$$

where $S_\alpha^{nm} = \tilde\phi^2_{\alpha n}/Q^3_{\alpha n}$ at $m=0$, $S_\alpha^{nm} = 1/Q_{\alpha n}$ at $m=-2n-1$, and

$$S_\alpha^{nm} = \frac{\tilde\omega_{\alpha n}(\tilde\omega_{\alpha n}+\tilde\omega_{\alpha n+m})+\tilde\phi_{\alpha n}(\tilde\phi_{\alpha n}-\tilde\phi_{\alpha n+m})}{Q_{\alpha n}P_{\alpha nm}} - \frac{\tilde\omega_{\alpha n+m}(\tilde\omega_{\alpha n+m}+\tilde\omega_{\alpha n})+\tilde\phi_{\alpha n+m}(\tilde\phi_{\alpha n+m}-\tilde\phi_{\alpha n})}{Q_{\alpha n+m}P_{\alpha nm}}$$

in all other cases. Here, $Q_{\alpha n} = (\tilde\omega^2_{\alpha n}+\tilde\phi^2_{\alpha n})^{1/2}$ and $P_{\alpha nm} = \tilde\omega^2_{\alpha n}-\tilde\omega^2_{\alpha n+m}+\tilde\phi^2_{\alpha n}-\tilde\phi^2_{\alpha n+m}$.

To obtain the optical conductivity, one has to perform an analytical continuation of the polarization operator given above to real frequencies (${\rm i}\omega_m\to\omega+{\rm i}\delta$). Another approach is to make the analytical continuation together with the integration [137–142]. This leads to the polarization operator in the following form:

$$\begin{aligned}\Pi_\alpha^{xx}(\omega) = \frac{(\omega_{{\rm p}\alpha}^{xx})^2}{4\pi}\int{\rm d}\omega'\Bigg[&\frac{\tanh\left[\omega_-/(2T)\right]}{Q_+^{\rm R}+Q_-^{\rm R}}\\ &\times\left(1-\frac{\tilde\omega_-^{\rm R}\tilde\omega_+^{\rm R}+\tilde\phi_-^{\rm R}\tilde\phi_+^{\rm R}}{Q_-^{\rm R}Q_+^{\rm R}}\right)-\frac{\tanh\left[\omega_+/(2T)\right]}{Q_+^{\rm A}+Q_-^{\rm A}}\\ &\times\left(1-\frac{\tilde\omega_-^{\rm A}\tilde\omega_+^{\rm A}+\tilde\phi_-^{\rm A}\tilde\phi_+^{\rm A}}{Q_-^{\rm A}Q_+^{\rm A}}\right)\\ &-\frac{\tanh\left[\omega_+/(2T)\right]-\tanh\left[\omega_-/(2T)\right]}{Q_+^{\rm R}-Q_-^{\rm A}}\\ &\times\left(1-\frac{\tilde\omega_-^{A}\tilde\omega_+^{\rm R}+\tilde\phi_-^{\rm A}\tilde\phi_+^{\rm R}}{Q_-^{\rm A}Q_+^{\rm R}}\right)\Bigg]\,,\end{aligned} \tag{23}$$

where $Q_\pm^{\rm R,A} = \sqrt{(\tilde\omega_\pm^{\rm R,A})^2-(\tilde\phi_\pm^{\rm R,A})^2}$, indices $\pm$ set the frequency $\omega_\pm = \omega'\pm\omega/2$ which enters the corresponding function, the band index α is omitted in the integrand, and indices R and A refer to retarded and advanced branches of a complex function F, i.e., $F^{\rm R(A)} = {\rm Re}\,F \pm {\rm i}\,{\rm Im}\,F$.

Notice that the optical conductivity in the normal state is expressed as

$$\sigma^{\rm N}(\omega) = \sum_\alpha\frac{(\omega_{{\rm p}\alpha}^{xx})^2}{8{\rm i}\pi\omega} \times\int_{-\infty}^{+\infty}{\rm d}z\,\frac{\tanh\left[(z+\omega)/(2T)\right]-\tanh\left[z/(2T)\right]}{\tilde\omega_\alpha(z+\omega)-\tilde\omega_\alpha(z)}\,. \tag{24}$$

In the following, we will utilize expressions from this section to describe properties of different systems and their observable characteristics.

3. Born approximation for one- and two-band superconductors

3.1 Qualitative analysis

Nonmagnetic impurities in a conventional two-band superconductor with two isotropic gaps lead to scattering of quasiparticles between bands or within each band. Interband processes shown in Fig. 4 result in averaging the gaps and, therefore, to the initial suppression of $T_{\rm c}$, after which $T_{\rm c}$ saturates and stays constant until localization effects become important [143, 144]. Interband scattering in a two-band

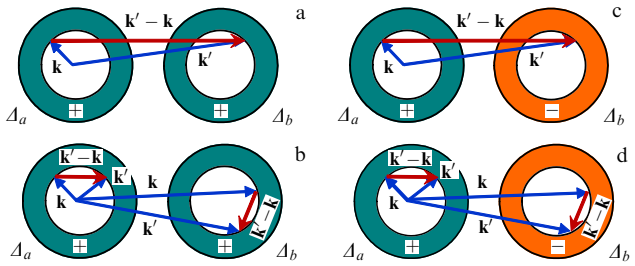

Figure 4. Diagram of two Fermi surfaces with the superconducting gaps Δ_a and Δ_b having the same signs (a, b), and opposite signs (c, d). Interband impurity scattering (panels a and c) mixes states with Δ_a and Δ_b, while the intraband scattering (panels b and d) involves states within the boundaries of each Fermi surface.

system with the sign-changing order parameter leads to a much more complicated behavior [68, 80, 135, 145]. In this case, nonmagnetic impurities with the interband component of the scattering potential destroy the superconductivity even for equal magnitudes of gaps and densities of states (the so-called symmetric model). The reason is quite simple — interband scattering results in averaging the gaps in two different bands and, since Δ_a and Δ_b have opposite signs in the $s_\pm$ state, their average goes to zero. Critical temperature T_c would then vanish for the finite critical impurity concentration, similar to the theory of magnetic impurity scattering in a single-band s-wave superconductor [41]. Such a characteristic feature of iron-based superconductors was quickly noticed by different groups of researchers [16, 132, 146–148].

As for the effect of nonmagnetic and magnetic disorder on a multiband anisotropic superconductor, the simple (and naive!) qualitative rule of thumb is as follows: when a nonmagnetic impurity scatters a pair from one point on the Fermi surface to another point, such that the order parameter does not change sign, scattering is not pair breaking; if the order parameter flips its sign, it is pair breaking. For a magnetic impurity, the opposite is true: scattering with an order parameter sign change is not pairbreaking, otherwise it is. As follows from calculations for some particular cases, however, such a naive qualitative rule collapses and quite unexpected results appear, which we discuss in Sections 4–7. But before going further, we apply the simplest Born limit in Section 3.2 to demonstrate the general results in single- and two-band models.

3.2 Clean and Born limits

Here, we consider a *weak coupling* example, i.e., the case of $\lambda_{\alpha\beta} \ll 1$, and describe the effect of disorder on a macroscopic characteristic — the critical temperature of the superconducting transition T_c. Scattering on static impurities would results only in a decrease of T_c from its clean limit value T_{c0}.

Order parameter $\Delta_{\alpha n}$ in a multiband superconductor in the clean limit is a solution of the equation that follows from expressions (13) and (15). Neglecting the frequency dependence of the coupling functions (which is the essence of weak coupling), we have

$$\Delta_\alpha = -T\sum_{\omega_n,\,\beta} \lambda_{\alpha\beta}\,\frac{g_{2\beta n}}{N_\beta}\,. \tag{25}$$

Summation over the Matsubara frequencies ω_n goes until a cut-off frequency ω_c. In the limit $T \to T_{c0}$, we have $\Delta_\alpha \to 0$ and $g_{2\alpha n} \to -\pi N_\alpha \Delta_\alpha/|\omega_n|$. Then, expression (25) becomes the equation for the critical temperature in the clean limit, i.e., for T_{c0}:

$$1 = \pi T_{c0}\sum_\beta \lambda_{\alpha\beta}\sum_{\omega_n}\frac{1}{\Delta_\alpha}\,\frac{\Delta_\beta}{|\omega_n|} = 2\pi T_{c0}\sum_\beta \lambda_{\alpha\beta}\sum_{\omega_n\geqslant 0}\frac{1}{\Delta_\alpha}\,\frac{\Delta_\beta}{\omega_n}\,. \tag{26}$$

The single-band case is realized at $\lambda_{\alpha\beta} = \lambda\delta_{\alpha\beta}$:

$$\begin{aligned} 1 &= 2\pi T_{c0}\lambda\sum_{\omega_n\geqslant 0}^{\omega_c}\frac{1}{\omega_n} = \lambda\sum_{n\geqslant 0}^{N_c}\frac{1}{n+1/2}\\ &= \lambda\left[\Psi\left(N_c+\frac{3}{2}\right)-\Psi\left(\frac{1}{2}\right)\right]\\ &= \lambda\left[\Psi\left(\frac{\omega_c}{2\pi T_{c0}}+1\right)+C\right] \to \lambda\left[\ln\frac{\omega_c}{2\pi T_{c0}}+C\right], \end{aligned}$$

where we have taken into account that $\omega_n = (2n+1)\,\pi T_{c0}$, $(2N_c+1)\,\pi T_{c0} = \omega_c$, $\Psi(1/2) = -\gamma - 2\ln 2 \equiv -C$, and $\Psi(z+1) \to \ln z$ as $z \to \infty$. Here, Ψ is the digamma function, and γ is the Euler constant. Since $\exp C/(2\pi) \approx 1.13$, the solution of the above equation gives the well-known expression for the superconducting critical temperature $T_{c0} = 1.13\omega_c \exp(-1/\lambda)$. Notice again that the coupling constant includes the density of states, $\lambda \propto N_a$.

Expression (26) in a two-band case is a system of two equations in Δ_a and Δ_b gaps. From the consistency condition of the system (determinant of the corresponding matrix should be equal to zero), one can derive the expression for T_{c0}:

$$\ln\frac{1.13\omega_c}{T_{c0}} = \max\left[\frac{\lambda_{aa}+\lambda_{bb}\pm\sqrt{(\lambda_{aa}-\lambda_{bb})^2+4\lambda_{ab}\lambda_{ba}}}{2(\lambda_{aa}\lambda_{bb}-\lambda_{ab}\lambda_{ba})}\right]. \tag{27}$$

Let us consider the simplest case of treating the impurity scattering by replacing the 'bare' Green's function $g_{2\beta n}$ in equation (25) with the full one (11) containing the renormalized order parameter $\tilde\phi_{\alpha n}$ and frequency $\tilde\omega_{\alpha n}$:

$$\Delta_\alpha = \pi T\sum_{\omega_n,\,\beta}\lambda_{\alpha\beta}\,\frac{\tilde\phi_{\beta n}}{Q_{\beta n}}\,, \tag{28}$$

where $Q_{\beta n} = (\tilde\omega_{\beta n}^2 + \tilde\phi_{\beta n}^2)^{1/2}$. As $T \to T_c$, we have $g_{0\alpha n} \to -i\pi N_\alpha\tilde\omega_{\alpha n}/|\tilde\omega_{\alpha n}| = -i\pi N_\alpha \operatorname{sgn}\omega_n$ and $g_{2\alpha n} \to -\pi N_\alpha\tilde\phi_{\alpha n}/|\omega_{\alpha n}|$. The equation for the critical temperature becomes

$$1 = 2\pi T_c\sum_\beta\lambda_{\alpha\beta}\sum_{\omega_n\geqslant 0}\left(\frac{1}{\Delta_\alpha}\,\frac{\tilde\phi_{\beta n}}{\tilde\omega_{\beta n}}\right)\Bigg|_{T\to T_c}. \tag{29}$$

As follows from a comparison with equation (26), T_c does not depend on impurity scattering if the following condition is satisfied:

$$\frac{\tilde\phi_{\beta n}}{\tilde\omega_{\beta n}} = \frac{\Delta_\beta}{\omega_n}\,. \tag{30}$$

In the Born approximation, only the contribution from double scattering at the same impurity is allowed, $\hat\Sigma^{\rm imp}(\omega_n) \approx n_{\rm imp}\hat U + n_{\rm imp}\hat U\hat g(\omega_n)\,\hat U$. We can now derive

expressions for the frequency and order parameters:

$$\tilde{\omega}_{an} = \omega_n + \gamma_{aa}\frac{\tilde{\omega}_{an}}{Q_{an}} + \gamma_{ab}\frac{\tilde{\omega}_{bn}}{Q_{bn}}\,, \tag{31}$$

$$\tilde{\phi}_{an} = \Delta_a \pm \gamma_{aa}\frac{\tilde{\phi}_{an}}{Q_{an}} \pm \gamma_{ab}\frac{\tilde{\phi}_{bn}}{Q_{bn}}\,, \tag{32}$$

where $\gamma_{\alpha\beta} \propto n_{\rm imp}(\mathbf{U})^2_{\alpha\beta}$ is the scattering rate parameter; the sign + (−) corresponds to nonmagnetic (magnetic) impurities. The different signs for magnetic disorder occur due to the spin operators accompanying the impurity potential $\mathcal{V}^{\alpha\beta}_{\mathbf{R}_i}$ in $H_{\rm imp}$.

Let us first consider the single-band case. Then, $\gamma_{ab} = 0$ and $\tilde{\omega}_{an} = \omega_n + \gamma_{aa}\tilde{\omega}_{an}/Q_{an}$, $\tilde{\phi}_{an} = \Delta_a \pm \gamma_{aa}\tilde{\phi}_{an}/Q_{an}$, $\gamma_{aa} = 2\pi N_a n_{\rm imp}\mathcal{U}^2$. Equations for nonmagnetic impurities are as follows: $\tilde{\omega}_{an}(1 - \gamma_{aa}/Q_{an}) = \omega_n$ and $\tilde{\phi}_{an}(1 - \gamma_{aa}/Q_{an}) = \Delta_a$, which immediately lead to relation (30). Therefore, $T_{\rm c}$ is independent of impurity concentration. This is the essence of Anderson's theorem.

For magnetic impurities, the appropriate equations are $\tilde{\omega}_{an}(1 - \gamma_{aa}/Q_{an}) = \omega_n$ and $\tilde{\phi}_{an}(1 + \gamma_{aa}/Q_{an}) = \Delta_a$. Thus, condition (30) is violated. Instead of it, we have

$$\left(\frac{\tilde{\phi}_{an}}{\Delta_a}\frac{1}{\tilde{\omega}_{an}}\right)\Bigg|_{T\to T_{\rm c}} = \left(\frac{1}{1+\gamma_{aa}/Q_{an}}\frac{1}{\tilde{\omega}_{an}}\right)\Bigg|_{T\to T_{\rm c}}$$
$$= \frac{1}{\tilde{\omega}_{an}|_{T\to T_{\rm c}} + \gamma_{aa}} = \frac{1}{\omega_n + \gamma_{aa}\,\tilde{\omega}_{an}/|\tilde{\omega}_{an}| + \gamma_{aa}}$$
$$= \frac{1}{\omega_n + 2\gamma_{aa}}\,,$$

since for the $T_{\rm c}$ equation we are interested in the case of $\omega_n \geqslant 0$. In the equation for the critical temperature, an additional factor $2\gamma_{aa}$ appears in the denominator:

$$1 = 2\pi T_{\rm c}\lambda \sum_{\omega_n \geqslant 0}^{\omega_{\rm c}} \frac{1}{\omega_n + 2\gamma_{aa}}$$
$$= \lambda\left[\Psi\left(\frac{\omega_{\rm c}}{2\pi T_{\rm c}} + \frac{\gamma_{aa}}{\pi T_{\rm c}} + 1\right) - \Psi\left(\frac{\gamma_{aa}}{\pi T_{\rm c}} + \frac{1}{2}\right)\right].$$

In the $\omega_{\rm c} \to \infty$ limit, the last equation takes the form

$$1 = \lambda\left[\ln\frac{\omega_{\rm c}}{2\pi T_{\rm c}} - \Psi\left(\frac{\gamma_{aa}}{\pi T_{\rm c}} + \frac{1}{2}\right)\right].$$

Combining this equation with the corresponding expression in the clean limit, $1 = \lambda\,[\ln\,\omega_{\rm c}/(2\pi T_{\rm c0}) - \Psi(1/2)]$, we finally have

$$\ln\frac{T_{\rm c0}}{T_{\rm c}} = \Psi\left(\frac{\gamma_{aa}}{\pi T_{\rm c}} + \frac{1}{2}\right) - \Psi\left(\frac{1}{2}\right), \tag{33}$$

which represents the formula for $T_{\rm c}$ suppression according to the Abrikosov–Gor'kov theory [41].

Let us now consider the two-band case. For impurity scattering within only one band ('intraband impurities'), $\gamma_{ab} = 0$, equations (31) and (32) for different bands are not coupled. Therefore, all conclusions made for the single-band case above are also true here for each band in the presence of both nonmagnetic and magnetic impurities.

When both intra- and interband nonmagnetic impurity scattering channels are present, from equations (31) and (32) we have

$$\tilde{\omega}_{an}\left(1 - \frac{\gamma_{aa}}{Q_{an}} - \frac{\gamma_{ab}^2}{Q_{an}}\frac{1}{Q_{bn}-\gamma_{bb}}\right) = \omega_n\left(1 + \frac{\gamma_{ab}}{Q_{bn}-\gamma_{bb}}\right),$$

$$\tilde{\phi}_{an}\left(1 - \frac{\gamma_{aa}}{Q_{an}} - \frac{\gamma_{ab}^2}{Q_{an}}\frac{1}{Q_{bn}-\gamma_{bb}}\right) = \Delta_a + \Delta_b\frac{\gamma_{ab}}{Q_{bn}-\gamma_{bb}}\,.$$

Evidently, if $\Delta_a = \Delta_b$, then condition (30) holds and, thus, $T_{\rm c}$ is independent of the disorder. Therefore, there is no impurity effect on the multiband isotropic s-wave superconducting state. If, however, $\Delta_a \neq \Delta_b$, then condition (30) is violated and $T_{\rm c}$ will be suppressed by scattering on impurities.

For a magnetic impurity, equations (31) and (32) lead to

$$\tilde{\omega}_{an}\left(1 - \frac{\gamma_{aa}}{Q_{an}} - \frac{\gamma_{ab}^2}{Q_{an}}\frac{1}{Q_{bn}-\gamma_{bb}}\right) = \omega_n\left(1 + \frac{\gamma_{ab}}{Q_{bn}-\gamma_{bb}}\right),$$

$$\tilde{\phi}_{an}\left(1 + \frac{\gamma_{aa}}{Q_{an}} - \frac{\gamma_{ab}^2}{Q_{an}}\frac{1}{Q_{bn}+\gamma_{bb}}\right) = \Delta_a - \Delta_b\frac{\gamma_{ab}}{Q_{bn}+\gamma_{bb}}\,.$$

Obviously, condition (30) holds true only for $\Delta_b = -\Delta_a$ and $\gamma_{aa} = \gamma_{bb} = 0$. That is, the $s_\pm$ state with the equal absolute values of gaps is not susceptible to the scattering by magnetic impurities having an interband scattering channel only ('interband impurities'). In all other cases, $T_{\rm c}$ would decrease with increasing concentration and potential of magnetic impurities.

4. Nonmagnetic impurities in two-band superconductors

Since we found out what happens in the simplest cases, we move on to solving Eliashberg equations in the $\mathcal{T}$-matrix approximation (16). Here, nonmagnetic impurities are considered first.

As was mentioned in Section 3, in the $s_\pm$ state, any nonmagnetic impurity scattering *only* between the bands with different signs of the gaps leads to suppression of the critical temperature $T_{\rm c}$, similar to magnetic impurity scattering in a single-band BCS superconductor [145, 149]. Then, $T_{\rm c}$ is determined from the Abrikosov–Gor'kov formula (33). Critical impurity scattering rate Γ determined by the equation $T_{\rm c}(\Gamma^{\rm crit}) = 0$ satisfies the relation $\Gamma^{\rm crit}/T_{\rm c0} \approx 1.12$ in the Abrikosov–Gor'kov theory. On the other hand, several experiments on iron-based superconductors, for example, the introduction of zinc or proton irradiation [107–110], reveal that $T_{\rm c}$ suppression is much weaker than expected in the framework of the Abrikosov–Gor'kov theory. Therefore, it was even suggested that the $s_\pm$ state is not realized in these systems and the order parameter should be of an s_{++} type [21, 148].

The problem of disorder in iron-based superconductors is much more intricate than the simple arguments may suggest. Even assuming isotropic gaps on two different Fermi surface sheets and nonmagnetic scattering, we find the suppression of superconductivity for a system with mainly intraband scattering to be slower than expected. Anderson's theorem is applicable in the limit of pure intraband scattering, the system is 'insensitive' to the signs of the gaps, and $T_{\rm c}$ is not suppressed.

Therefore, the $T_{\rm c}$ suppression rate depends on the ratio between intra- and interband scattering rates, and making conclusions about the superconducting state on the basis of systematic disorder studies is harder than in the single-band

case. One approach to the problem is to try to determine intra- and interband impurity potentials from first principles methods for different materials and types of impurities [16, 34, 150]; however, the quantitative applicability of band structure calculations here is questionable.

4.1 Solution of Eliashberg equations in the $\mathcal{T}$-matrix approximation

In the case of a nonmagnetic disorder, we can simplify the problem by reducing the dimension of matrices due to spin degeneracy. Thus, instead of expressions (9) and (10), we have 4×4 quasiclassical matrix Green's function in Nambu and band spaces:

$$\hat{\mathbf{g}}(\omega_n)=\begin{pmatrix} g_{0an} & 0\\ 0 & g_{0bn}\end{pmatrix}\otimes\hat{\tau}_0+\begin{pmatrix} g_{2an} & 0\\ 0 & g_{2bn}\end{pmatrix}\otimes\hat{\tau}_2\,, \quad (34)$$

where $\hat{\tau}_i$ are Pauli matrices corresponding to the Nambu space.

The impurity potential matrix entering the $\mathcal{T}$-matrix equation (16) is $\hat{\mathbf{U}}=\mathbf{U}\otimes\hat{\tau}_3$, where $(\mathbf{U})_{\alpha\beta}=\mathcal{U}^{\alpha\beta}_{\mathbf{R}_i}$. Without loss of generality, we set $\mathbf{R}_i=0$ for the single-impurity problem studied here. For simplicity, intraband and interband parts of the impurity potential are set equal to v and u, respectively, such that $(\mathbf{U})_{\alpha\beta}=(v-u)\,\delta_{\alpha\beta}+u$.

From equations (16) and (34), we then have

$$\hat{\Sigma}^{\rm imp}_{aa}=n_{\rm imp}v\hat{\tau}_3+v\hat{\tau}_3(g_{0an}\hat{\tau}_0+g_{2an}\hat{\tau}_2)\,\hat{\Sigma}^{\rm imp}_{aa} + u\hat{\tau}_3(g_{0bn}\hat{\tau}_0+g_{2bn}\hat{\tau}_2)\hat{\Sigma}^{\rm imp}_{ba}\,, \quad (35)$$

$$\hat{\Sigma}^{\rm imp}_{ba}=n_{\rm imp}u\hat{\tau}_3+u\hat{\tau}_3(g_{0an}\hat{\tau}_0+g_{2an}\hat{\tau}_2)\hat{\Sigma}^{\rm imp}_{aa} + v\hat{\tau}_3(g_{0bn}\hat{\tau}_0+g_{2bn}\hat{\tau}_2)\,\hat{\Sigma}^{\rm imp}_{ba}\,. \quad (36)$$

Renormalizations of frequencies and gaps come from $\Sigma^{\rm imp}_{0a}=(1/2)\,{\rm Tr}\,(\hat{\Sigma}^{\rm imp}_{aa}\,\hat{\tau}_0)$ and $\Sigma^{\rm imp}_{2a}=(1/2)\,{\rm Tr}\,(\hat{\Sigma}^{\rm imp}_{aa}\,\hat{\tau}_2)$, respectively. Equations for $\Sigma^{\rm imp}_{0b}$ and $\Sigma^{\rm imp}_{2b}$ are derived through the replacement $a\leftrightarrow b$ in the equations above. Considering the relation $g^2_{0\alpha n}-g^2_{2\alpha n}=-\pi^2N^2_\alpha$, we derive the following solution for $\Sigma^{\rm imp}_{0a}$ and $\Sigma^{\rm imp}_{2a}$:

$$\Sigma^{\rm imp}_{0a}=\frac{n_{\rm imp}}{D}\,\left[g_{0bn}u^2+g_{0an}v^2+g_{0an}(u^2-v^2)^2\pi^2N_b^2\right], \quad (37)$$

$$\Sigma^{\rm imp}_{2a}=-\frac{n_{\rm imp}}{D}\left[g_{2bn}u^2+g_{2an}v^2+g_{2an}(u^2-v^2)^2\pi^2N_b^2\right], \quad (38)$$

where

$$D=1+\pi^2N_a^2v^2+\pi^4N_a^2N_b^2(u^2-v^2)^2 + \pi^2N_b^2v^2-2u^2(g_{0an}g_{0bn}-g_{2an}g_{2bn})\,.$$

In what follows, apart from the general case, we will also consider two important limits: the Born, weak scattering, limit with $\pi uN_{a,b}\ll 1$, and the opposite limit of very strong scattering with $\pi uN_{a,b}\gg 1$, called the unitary limit.

It is convenient to introduce the generalized cross-section parameter

$$\sigma=\frac{\pi^2N_aN_bu^2}{1+\pi^2N_aN_bu^2}\to\begin{cases}0, & \text{Born limit,}\\ 1, & \text{unitary limit,}\end{cases} \quad (39)$$

and the impurity scattering rate

$$\Gamma_{a(b)}=2n_{\rm imp}\pi N_{b(a)}u^2(1-\sigma)=\frac{2n_{\rm imp}\sigma}{\pi N_{a,b}}\to \to\begin{cases}2n_{\rm imp}\pi N_{b,a}u^2\,, & \text{Born limit}\,,\\ \dfrac{2n_{\rm imp}}{\pi N_{a,b}}\,, & \text{unitary limit}\,.\end{cases} \quad (40)$$

Parameter η controls the ratio between intra- and interband scattering potentials:

$$v=\eta u\,. \quad (41)$$

With the introduced notations, we rewrite equations for frequency (12) and order parameter (13) taking the impurity self-energy (37), (38) into account:

$$\tilde{\omega}_{an}=\omega_n+{\rm i}\Sigma_{0a}(\omega_n)+\frac{\Gamma_a}{2D}\left[\sigma\,\frac{\tilde{\omega}_{an}}{Q_{an}}(1-\eta^2)^2 + (1-\sigma)\left(\frac{N_a\tilde{\omega}_{an}}{N_bQ_{an}}\,\eta^2+\frac{\tilde{\omega}_{bn}}{Q_{bn}}\right)\right], \quad (42)$$

$$\tilde{\phi}_{an}=\Sigma_{2a}(\omega_n)+\frac{\Gamma_a}{2D}\left[\sigma\,\frac{\tilde{\phi}_{an}}{Q_{an}}\,(1-\eta^2)^2 + (1-\sigma)\left(\frac{N_a\tilde{\phi}_{an}}{N_bQ_{an}}\,\eta^2+\frac{\tilde{\phi}_{bn}}{Q_{bn}}\right)\right], \quad (43)$$

where

$$D=(1-\sigma)^2+\sigma(1-\sigma) \times\left(2\,\frac{\tilde{\omega}_{an}\tilde{\omega}_{bn}+\tilde{\phi}_{an}\tilde{\phi}_{bn}}{Q_{an}Q_{bn}}+\frac{N_a^2+N_b^2}{N_aN_b}\,\eta^2\right)+\sigma^2(1-\eta^2)^2\,.$$

Let us examine important limiting cases. In the Born limit, we have $\sigma\to 0$ (weak scattering, $\pi uN_{a,b}\ll 1$); thus, $D=1$, $\Gamma_a=2n_{\rm imp}\pi N_bu^2$, and

$$\tilde{\omega}_{an}=\omega_n+{\rm i}\Sigma_{0a}(\omega_n)+\frac{\gamma_{aa}}{2}\,\frac{\tilde{\omega}_{an}}{Q_{an}}+\frac{\gamma_{ab}}{2}\,\frac{\tilde{\omega}_{bn}}{Q_{bn}}\,, \quad (44)$$

$$\tilde{\phi}_{an}=\Sigma_{2a}(\omega_n)+\frac{\gamma_{aa}}{2}\,\frac{\tilde{\phi}_{an}}{Q_{an}}+\frac{\gamma_{ab}}{2}\,\frac{\tilde{\phi}_{bn}}{Q_{bn}}\,, \quad (45)$$

where $\gamma_{aa}=2\pi n_{\rm imp}N_au^2\eta^2$ and $\gamma_{ab}=2\pi n_{\rm imp}N_bu^2$. Evidently, for the finite interband scattering γ_{ab}, i.e., finite η, different bands are mixed in equations. This leads to the suppression of $T_{\rm c}$, similar to the one following from the Abrikosov–Gor'kov expression (33).

In the unitary limit, with $\sigma\to 1$ (strong scattering, $\pi uN_{a,b}\gg 1$), we have $\Gamma_a=2n_{\rm imp}/(\pi N_a)$, and one must distinguish two cases:

(1) Uniform impurity potential with $\eta=1$. We the have

$$\tilde{\omega}_{an}=\omega_n+{\rm i}\Sigma_{0a}(\omega_n)+\frac{n_{\rm imp}}{\pi N_aN_bD_{\rm uni}}\left[N_a\,\frac{\tilde{\omega}_{an}}{Q_{an}}+N_b\,\frac{\tilde{\omega}_{bn}}{Q_{bn}}\right], \quad (46)$$

$$\tilde{\phi}_{an}=\Sigma_{2a}(\omega_n)+\frac{n_{\rm imp}}{\pi N_aN_bD_{\rm uni}}\left[N_a\,\frac{\tilde{\phi}_{an}}{Q_{an}}+N_b\,\frac{\tilde{\phi}_{bn}}{Q_{bn}}\right], \quad (47)$$

where

$$D_{\rm uni}=2\,\frac{\tilde{\omega}_{an}\tilde{\omega}_{bn}+\tilde{\phi}_{an}\tilde{\phi}_{bn}}{Q_{an}Q_{bn}}+\frac{N_a^2+N_b^2}{N_aN_b}\,.$$

Obviously, different bands are mixed in equations for the renormalized frequency and order parameter, so this leads to a suppression of T_c.

(2) All other cases with $\eta \neq 1$. We then have

$$\tilde{\omega}_{an} = \omega_n + i\Sigma_{0a}(\omega_n) + \frac{n_{imp}}{\pi N_a}\frac{\tilde{\omega}_{an}}{Q_{an}}, \quad (48)$$

$$\tilde{\phi}_{an} = \Sigma_{2a}(\omega_n) + \frac{n_{imp}}{\pi N_a}\frac{\tilde{\phi}_{an}}{Q_{an}}. \quad (49)$$

We get the same result as for the intraband impurities, since the other band (b) does not contribute to the equations. Surprisingly, Anderson's theorem works here independently of the gap signs in different bands. Thus, T_c should be finite for any impurity concentration.

In this way, there is a special case of T_c suppression in the unitary limit for the uniform impurity potential $\eta = 1$. Such a situation arises due to the structure of the denominator D in equations (42), (43). It vanishes at $\eta = \sigma = 1$ and we have to accurately pass first to the limit $\eta \to 1$, and only then put $\sigma \to 1$. This is a $\eta = 1$ case, which was considered in Ref. [148]. For all other values of η (even for a slight difference between intra- and interband potentials), impurities are not going to affect the critical temperature. Of course, from the physical point of view, the former situation is improbable, since it is hard to imagine an impurity in a multiorbital system where intra- and interband scatterings have equal intensities.

4.2 Critical temperature of the superconducting transition

As $T \to T_c$, the equations become significantly simplified, because the order parameter vanishes and $Q_{\alpha n} = (\tilde{\omega}_{\alpha n}^2 + \tilde{\phi}_{\alpha n}^2)^{1/2} \to |\tilde{\omega}_{\alpha n}|$. Thus, the linearized Eliashberg equations (12), (13) for the renormalization factors $Z_{\alpha n} = \tilde{\omega}_{\alpha n}/\omega_n$ and gap functions $\Delta_{\alpha n} = \tilde{\phi}_{an}/Z_{\alpha n}$ [131] can be rewritten, in view of expressions (42), (43), as follows:

$$Z_{\alpha n} = 1 + \sum_\beta \frac{\tilde{\Gamma}_{\alpha\beta}}{|\omega_n|} + \pi T_c \sum_{\omega_{n'},\beta} \left|\lambda_{\alpha\beta}(n-n')\right| \frac{\operatorname{sgn}\omega_{n'}}{\omega_n}, \quad (50)$$

$$Z_{\alpha n}\Delta_{\alpha n} = \sum_\beta \frac{\tilde{\Gamma}_{\alpha\beta}\Delta_{\beta n}}{|\omega_n|} + \pi T_c \sum_{\omega_{n'},\beta} \lambda_{\alpha\beta}(n-n')\frac{\Delta_{\beta n'}}{|\omega_{n'}|}, \quad (51)$$

where we have introduced renormalized impurity scattering rates $\tilde{\Gamma}_{\alpha\beta}$ [126]:

$$\tilde{\Gamma}_{ab(ba)} = \Gamma_{a(b)}\frac{1-\sigma}{\sigma(1-\sigma)\eta^2(N_a+N_b)^2/(N_aN_b) + (\sigma\eta^2-1)^2}, \quad (52)$$

$$\tilde{\Gamma}_{aa} = \Gamma_a\frac{\sigma(1-\eta^2)^2 + (1-\tilde{\sigma})\eta^2 N_a/N_b}{\sigma(1-\sigma)\eta^2(N_a+N_b)^2/(N_aN_b) + (\sigma\eta^2-1)^2}. \quad (53)$$

After substituting $Z_{\alpha n}$ from Eqn (50) to (51), we obtain the equation for the critical temperature T_c:

$$\Delta_{\alpha n} + \pi T_c \sum_{n',\beta}\left[\left|\lambda_{\alpha\beta}(n-n')\right|\operatorname{sgn}\omega_{n'}\frac{\Delta_{\alpha n}}{\omega_n} - \lambda_{\alpha\beta}(n-n')\frac{\Delta_{\beta n'}}{|\omega_{n'}|}\right] + \sum_\beta \tilde{\Gamma}_{\alpha\beta}\frac{\Delta_{\alpha n}-\Delta_{\beta n}}{|\omega_n|} = 0. \quad (54)$$

The last term is finite only for $\alpha \neq \beta$. Therefore, intraband terms $\propto \tilde{\Gamma}_{aa}$ and $\tilde{\Gamma}_{bb}$ are cancelled and do not contribute to T_c, in agreement with Anderson's theorem. From the expression for scattering rates (52), we recover explicitly the well-known but counterintuitive result that in the unitary limit $\tilde{\Gamma}_{ab} = 0$ — that is, nonmagnetic impurities do not affect T_c in the $s_\pm$ state [68, 135].

Since T_c depends only on parameter $\tilde{\Gamma}_{ab}$, we call it the effective impurity scattering rate.

4.3 Results of the numerical solution

To determine T_c, we must solve numerically either equation (54) or Eliashberg equations (50), (51) and vary T to find the highest temperature at which nontrivial solution exists [126]. For definiteness, we choose $N_b/N_a = 2$. The resulting T_c and gap $\Delta_{\alpha,n=1}$ as functions of Γ_a in the s_{++} state are depicted in Fig. 5. Generally, the superconductivity is not suppressed completely, though there is an initial drop of T_c due to the scattering between bands with initially unequal gaps. Notice that the system in the unitary limit seems not to care about disorder — neither critical temperature nor gaps depend on Γ_a. As seen from equations (46), (47), there is, however, an isolated point, $\eta = 1$, corresponding to the vanishing of determinant D. That is, superconductivity is suppressed for the uniform impurity potential, $v = u$ (see Fig 5).

Figure 6 demonstrates T_c as a function of Γ_a for the $s_\pm$ state. As follows from calculations, T_c behavior is qualitatively different for different signs of the coupling constant averaged over the Fermi surface [126]:

$$\langle\lambda\rangle \equiv (\lambda_{aa}+\lambda_{ab})\frac{N_a}{N} + (\lambda_{ba}+\lambda_{bb})\frac{N_b}{N}, \quad (55)$$

where $N = N_a + N_b$ is the total density of states in the normal phase. We choose the following coupling constants for illustrative purpose: $(\lambda_{aa}, \lambda_{ab}, \lambda_{ba}, \lambda_{bb}) = (3, -0.2, -0.1, 0.5)$ for $\langle\lambda\rangle > 0$ [133, 134], $(1, -2, -1, 1)$ for $\langle\lambda\rangle < 0$, and $(2, -2, -1, 1)$ at $\langle\lambda\rangle = 0$. For the first set in the clean limit, a critical temperature is $T_{c0} = 30\ \text{cm}^{-1}$, for the second set it is $T_{c0} = 27.96\ \text{cm}^{-1}$, and for the third set it is $T_{c0} = 31.47\ \text{cm}^{-1}$, which correspond to 43.1 K, 40.2 K, and 45.2 K. It should be noted that the strongest T_c suppression occurs in the Born limit for the pure interband potential, i.e., $\eta = 0$. In the opposite limit of pure intraband scattering with $u = 0$ ($\eta \to \infty$), pairbreaking is absent because $\tilde{\Gamma}_{ab} \to 0$. Such a situation appears in the unitary limit. As for the dependence of T_c on $\tilde{\Gamma}_{ab}$ (52), shown in Fig. 7, all cases with different sets of σ and η fall onto one of the universal T_c curves, depending on the sign of the coupling constant averaged over the Fermi surface, $\langle\lambda\rangle$. It is clearly seen from Fig. 7 that, depending on the sign of $\langle\lambda\rangle$, one gets two types of T_c behavior for the $s_\pm$ state: (1) the critical temperature vanishes at a finite impurity scattering rate $\tilde{\Gamma}_{ab}^{\text{crit}}$ for $\langle\lambda\rangle < 0$, and (2) for $\langle\lambda\rangle > 0$, the critical temperature remains finite as $\tilde{\Gamma}_{ab} \to \infty$. In the marginal case of $\langle\lambda\rangle = 0$, we find that $\tilde{\Gamma}_{ab}^{\text{crit}} \to \infty$ but with exponentially small T_c. Therefore, we have found the universal behavior of T_c controlled by a single parameter $\langle\lambda\rangle$.

While the behavior of type (1) systems is in agreement with the qualitative statement that $s_\pm$ superconductivity is destroyed by nonmagnetic interband impurities due to the 'mixing' of gaps with different signs [145, 149], the behavior of type (2) systems with $\langle\lambda\rangle > 0$ is surprising. To understand what happens in this case, we calculated the gap $\Delta_{\alpha n}$ for the first Matsubara frequency $n = 1$ at $T = 0.016T_{c0}$. Results are shown in Figs 8 and 9 for zero and finite intraband potential v, respectively. Coupling constants $\lambda_{\alpha\beta}$ are chosen to have $T_{c0} \approx 40$ K. It is seen that gaps on both bands, $\Delta_{a(b)n}$,

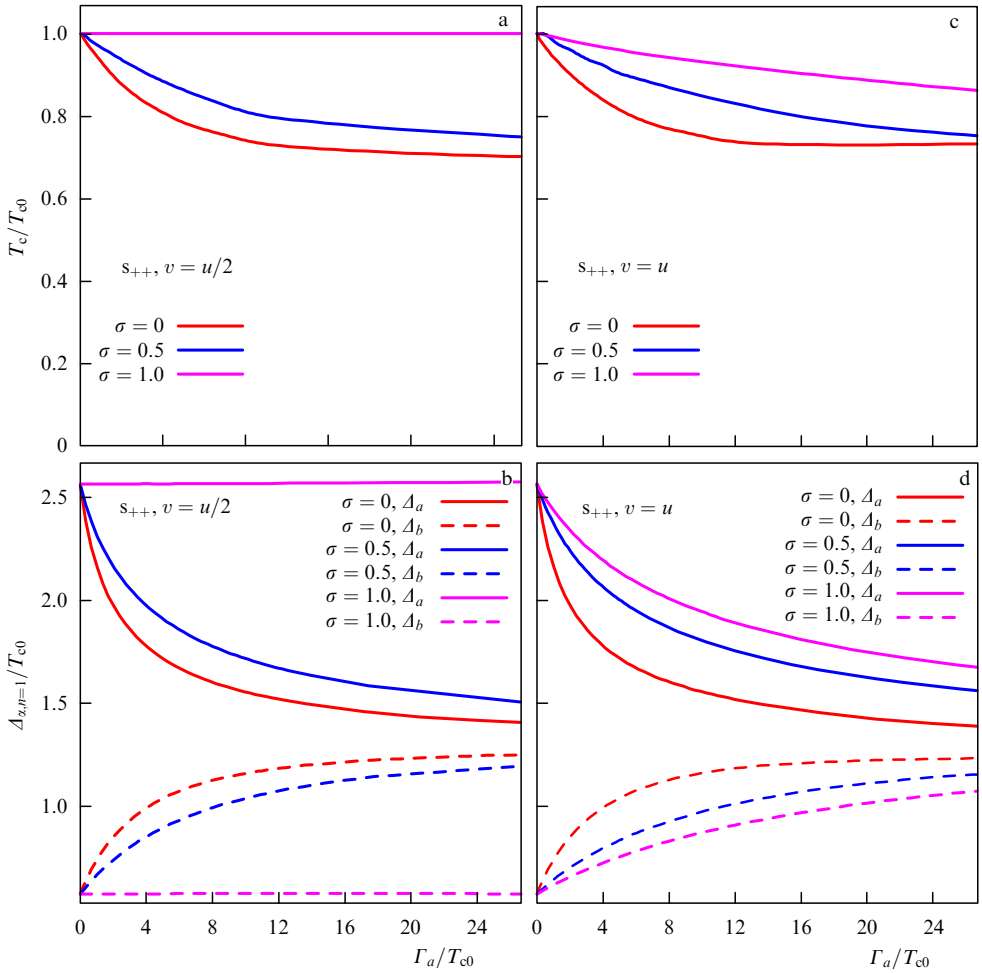

Figure 5. (Color online.) Dependences of T_c (a, c) and the order parameter $\Delta_{\alpha,n=1}$ at $T = 0.016T_{c0}$ (b, d) on the impurity scattering rate Γ_a for the s_{++} state with $v = u/2$ (a, b) and $v = u$ (c, d). At $v = u$, the suppression of superconductivity occurs even in the unitary limit. Here, the coupling constants are $(\lambda_{aa}, \lambda_{ab}, \lambda_{ba}, \lambda_{bb}) = (3, 0.2, 0.1, 0.5)$, which gives $T_{c0} = 43.1$ K.

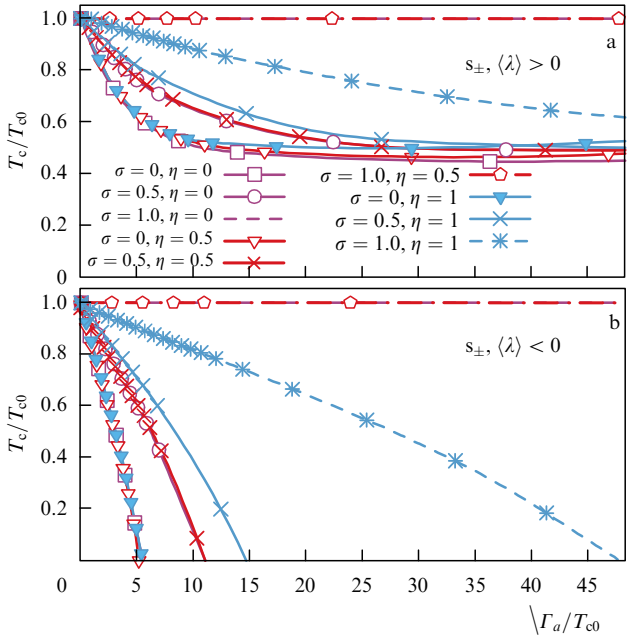

Figure 6. Critical temperature for various σ and η as a function of the impurity scattering rate Γ_a for different signs of an average coupling constant $\langle\lambda\rangle$.

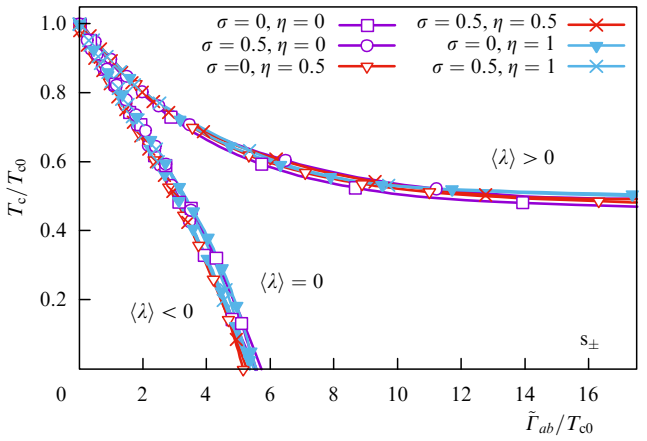

Figure 7. (Color online.) Critical temperature T_c for various σ and η as a function of the effective interband scattering rate $\tilde{\Gamma}_{ab}$. Notice that curves for different sets of σ and η overlap and fall onto one of the three universal curves, depending on the sign of $\langle\lambda\rangle$. Visible deviations originate from the numerical calculating errors. Curve for the case of $\langle\lambda\rangle = 0$ is situated slightly above the curve for $\langle\lambda\rangle < 0$, and they almost overlap.

converge to the same value $\Delta_{\Gamma_{a(b)}\to\infty}$, while T_c quickly saturates. The initially negative order parameter Δ_{bn} (corresponding to the smaller gap) increases and at some point in time passes through zero and becomes positive. After that,

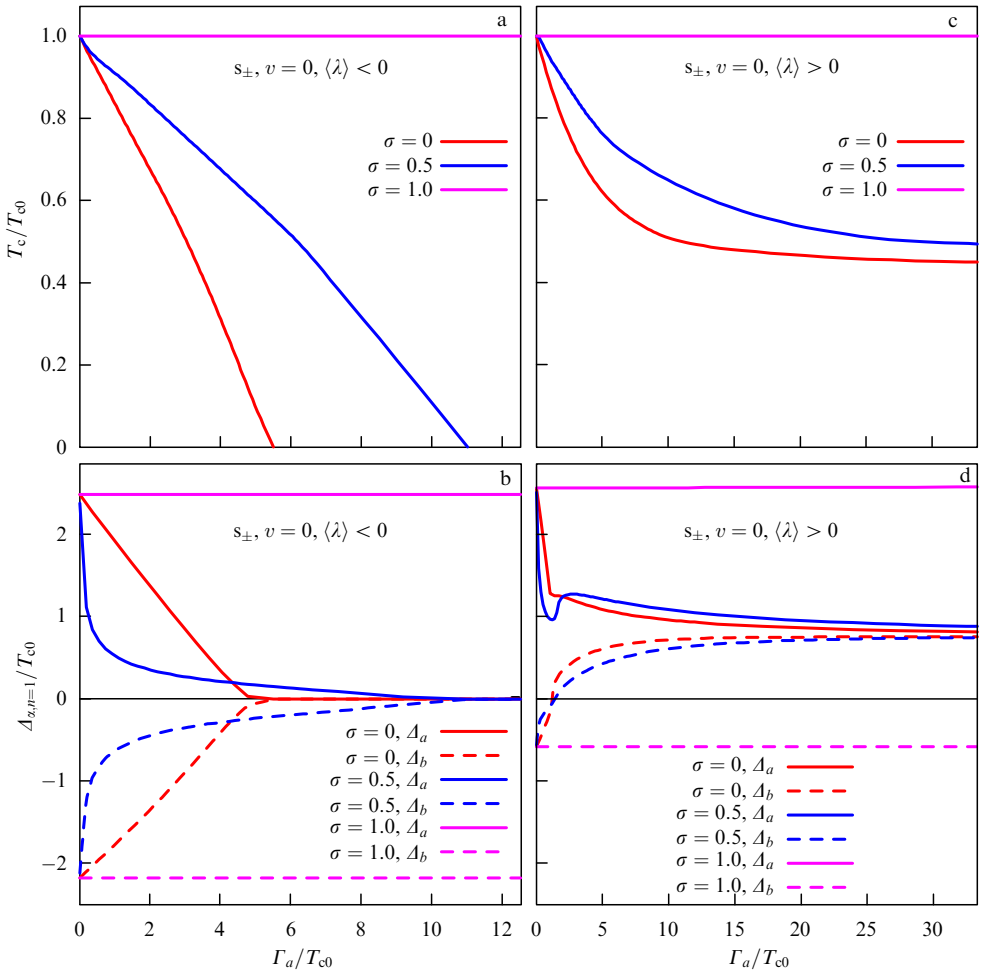

Figure 8. (Color online.) Dependences of T_c (a, c) and Matsubara gaps $\Delta_{\alpha,n=1}$ (b, d) on the impurity scattering rate Γ_a for the $s_\pm$ state with $v = 0$ for $\langle\lambda\rangle < 0$ (panels a and b), and for $\langle\lambda\rangle > 0$ (panels c and d). For $\langle\lambda\rangle < 0$, gaps in both bands vanish, making T_c drop to zero. For $\langle\lambda\rangle > 0$, smaller gap Δ_b passes through zero and its sign become the same as the sign of the larger gap Δ_a, i.e., the system experiences transition to the s_{++} state. The unitary limit is always an exceptional case with constant T_c and gaps. Gaps are shown for the Matsubara frequency $\omega_n = \pi T(2n+1)$ with $n = 1$ at $T = 0.016T_{c0}$.

since the gap signs for both bands are equal, we have the s_{++} state. Due to Anderson's theorem, this state is robust against impurity scattering, thus having a finite T_c up to $\Gamma_a \to \infty$. Therefore, T_c stays finite in type (2) systems due to the $s_\pm \to s_{++}$ transition.

The transition is also seen in gap functions $\mathrm{Re}\,\Delta_\alpha(\omega)$ analytically continued to real frequencies, which are shown in Fig. 10.

Similar to the s_{++} state, there is no disorder effect on the critical temperature or gaps in the unitary limit except for the case of $\eta = 1$, where the $s_\pm \to s_{++}$ transition occurs (see Fig. 9), which again makes the case of uniform scattering somehow unique [68].

There is a simple physical reason for the transition: with increasing interband scattering, order parameters on different Fermi surfaces 'mix' due to the scattering processes and converge to the same value. At the same time, the larger gap 'attracts' the smaller one that passes through zero and changes its sign. Similar effects were discussed in Refs [145, 149, 152, 153] for the two-band s_{++} superconductor, and in Ref. [104], where node lifting in the extended $s_\pm$ state on the electron pocket was investigated. The discovered $s_\pm \to s_{++}$ transition allows us to explain the much slower suppression of critical temperature than that following from the well-known Abrikosov–Gor'kov equation. Qualitatively, this result was confirmed by agreement with the numerical solution of the Bogoliubov–de Gennes equations [154, 155].

5. Magnetic disorder in multiband superconductors

Here, we focus on magnetic impurities and their effect on the properties of the $s_\pm$ and s_{++} models. We show that there are few cases when the critical temperature T_c saturates and stays finite in contrast to T_c following from the prediction of the Abrikosov–Gor'kov theory for single-band superconductors [127].

5.1 Eliashberg equations in the $\mathcal{T}$-matrix approximation

In the case of magnetic impurities, we have to consider a Green's function matrix entering into equation (9) with the dimension 8×8. This considerably complicates the problem in comparison with the study of nonmagnetic disorder. The impurity potential for the noncorrelated impurities can be written out as $\hat{\mathbf{U}} = \mathbf{V} \otimes \hat{S}$, where

$$\hat{S} = \begin{pmatrix} \hat{\boldsymbol{\sigma}}\,\mathbf{S} & 0 \\ 0 & -(\hat{\boldsymbol{\sigma}}\,\mathbf{S})^{\mathrm{T}} \end{pmatrix} \tag{56}$$

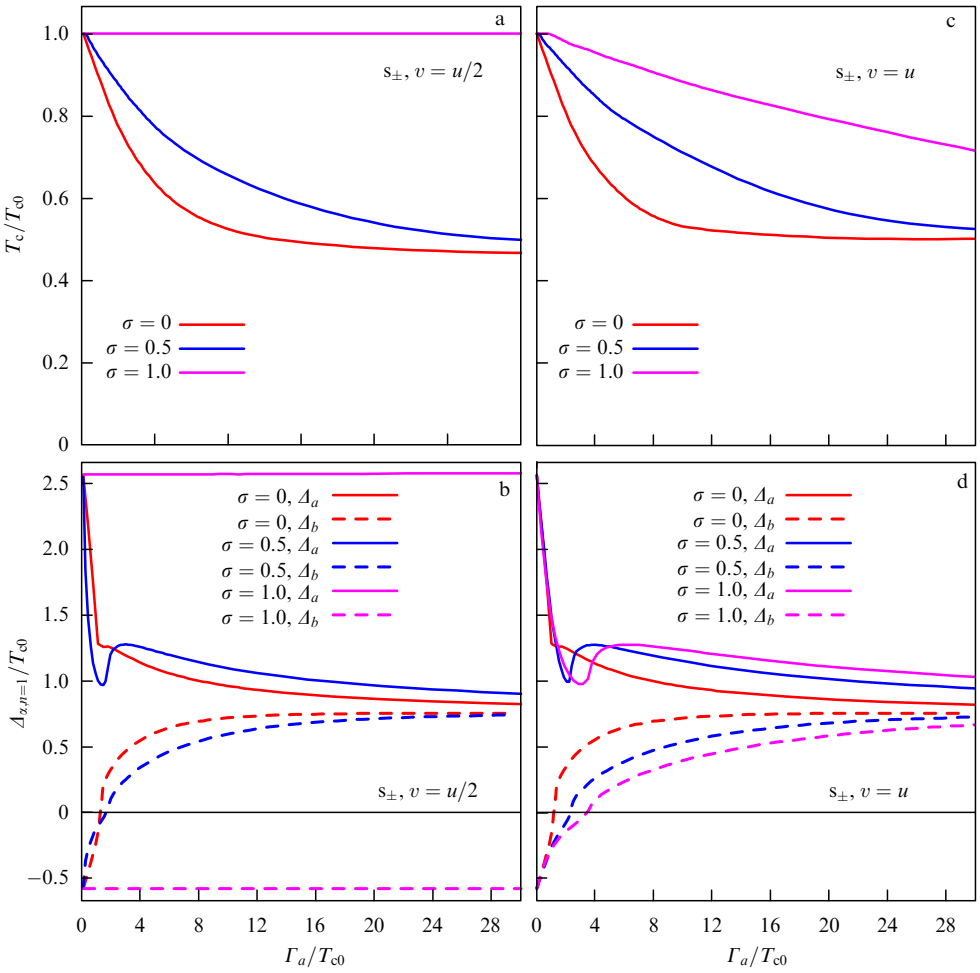

Figure 9. (Color online.) Dependences of T_c (a, c) and Matsubara gaps $\Delta_{\alpha,n=1}$ (b, d) on the impurity scattering rate Γ_a for the $s_\pm$ state with $\langle\lambda\rangle > 0$ at $v = u/2$ (panels a and b) and at $v = u$ (panels c and d). In both cases, the $s_\pm \to s_{++}$ transition occurs. At $v = u$, the superconductivity is suppressed even in the unitary limit.

is the 4×4 matrix, with $(...)^T$ being the matrix transpose, and $\mathbf{S} = (S_x, S_y, S_z)$ being the classic spin vector [156]. The vector $\hat{\boldsymbol{\sigma}}$ is composed of Pauli τ-matrices, $\hat{\boldsymbol{\sigma}} = (\hat{\tau}_1, \hat{\tau}_2, \hat{\tau}_3)$. The potential strength is determined by $(\mathbf{V})_{\alpha\beta} = \mathcal{V}^{\alpha\beta}_{\mathbf{R}_i=0}$. For simplicity, the intraband and interband parts of the potential are set equal to $\mathcal{I}$ and $\mathcal{J}$, respectively, such that $(\mathbf{V})_{\alpha\beta} = (\mathcal{I} - \mathcal{J})\,\delta_{\alpha\beta} + \mathcal{J}$. Then, $\mathbf{V}$ is given by

$$\mathbf{V} = \begin{pmatrix} \mathcal{I} & \mathcal{J} \\ \mathcal{J} & \mathcal{I} \end{pmatrix}. \tag{57}$$

Components of the impurity potential matrix $\hat{\mathbf{U}}$ are then $\hat{U}_{aa,\,bb} = \mathcal{I}\hat{S}$ and $\hat{U}_{ab,\,ba} = \mathcal{J}\hat{S}$, and the matrix itself takes the form

$$\hat{\mathbf{U}} = \begin{pmatrix} \mathcal{I}\hat{S} & \mathcal{J}\hat{S} \\ \mathcal{J}\hat{S} & \mathcal{I}\hat{S} \end{pmatrix}. \tag{58}$$

Coupled $\mathcal{T}$-matrix equations (16) for the aa and ba components of the self-energy in the introduced notations become

$$\hat{\Sigma}^{\text{imp}}_{aa} = n_{\text{imp}}\hat{U}_{aa} + \hat{U}_{aa}\hat{g}_a\hat{\Sigma}^{\text{imp}}_{aa} + \hat{U}_{ab}\hat{g}_b\hat{\Sigma}^{\text{imp}}_{ba}\,, \tag{59}$$

$$\hat{\Sigma}^{\text{imp}}_{ba} = n_{\text{imp}}\hat{U}_{ba} + \hat{U}_{ba}\hat{g}_a\hat{\Sigma}^{\text{imp}}_{aa} + \hat{U}_{bb}\hat{g}_b\hat{\Sigma}^{\text{imp}}_{ba}\,. \tag{60}$$

The solution of the system of equations in the matrix form is given by

$$\hat{\Sigma}^{\text{imp}}_{aa} = n_{\text{imp}}\big(\hat{1} - \hat{U}_{aa}\hat{g}_a - \hat{U}_{ab}\hat{g}_b\hat{\zeta}\hat{U}_{ba}\hat{g}_a\big)^{-1} \times \big(\hat{U}_{aa} + \hat{U}_{ab}\hat{g}_b\hat{\zeta}\hat{U}_{ba}\big)\,, \tag{61}$$

$$\hat{\Sigma}^{\text{imp}}_{ba} = \hat{\zeta}\hat{U}_{ba}\big(n_{\text{imp}} + \hat{g}_a\hat{\Sigma}^{\text{imp}}_{aa}\big)\,, \tag{62}$$

where $\hat{\zeta} = (\hat{1} - \hat{U}_{bb}\hat{g}_b)^{-1}$. Renormalizations of frequencies and gaps come from

$$\Sigma^{\text{imp}}_{0a} = \frac{1}{4}\,\text{Tr}\left[\hat{\Sigma}^{\text{imp}}_{aa}\,(\hat{\tau}_0 \otimes \hat{\sigma}_0)\right], \tag{63}$$

$$\Sigma^{\text{imp}}_{2a} = \frac{1}{4}\,\text{Tr}\left[\hat{\Sigma}^{\text{imp}}_{aa}\,(\hat{\tau}_2 \otimes \hat{\sigma}_2)\right]. \tag{64}$$

Equations for Σ^{imp}_{0b} and Σ^{imp}_{2b} are derived from above equations via replacement $a \leftrightarrow b$.

We assume that spins are not polarized and $s^2 = \langle S^2\rangle = S(S+1)$. Since s enters everywhere together with the components $\mathcal{I}$ and $\mathcal{J}$ of the impurity potential (see expression (58) for $\hat{\mathbf{U}}$), without loss of generality we later set $s = 1$, assuming that $\mathcal{I}$ and $\mathcal{J}$ are renormalized to include s in themselves.

As follows from the calculations, similar to the results presented in Section 4, expressions for $\Sigma^{\text{imp}}_{0\alpha}$ and $\Sigma^{\text{imp}}_{2\alpha}$ are

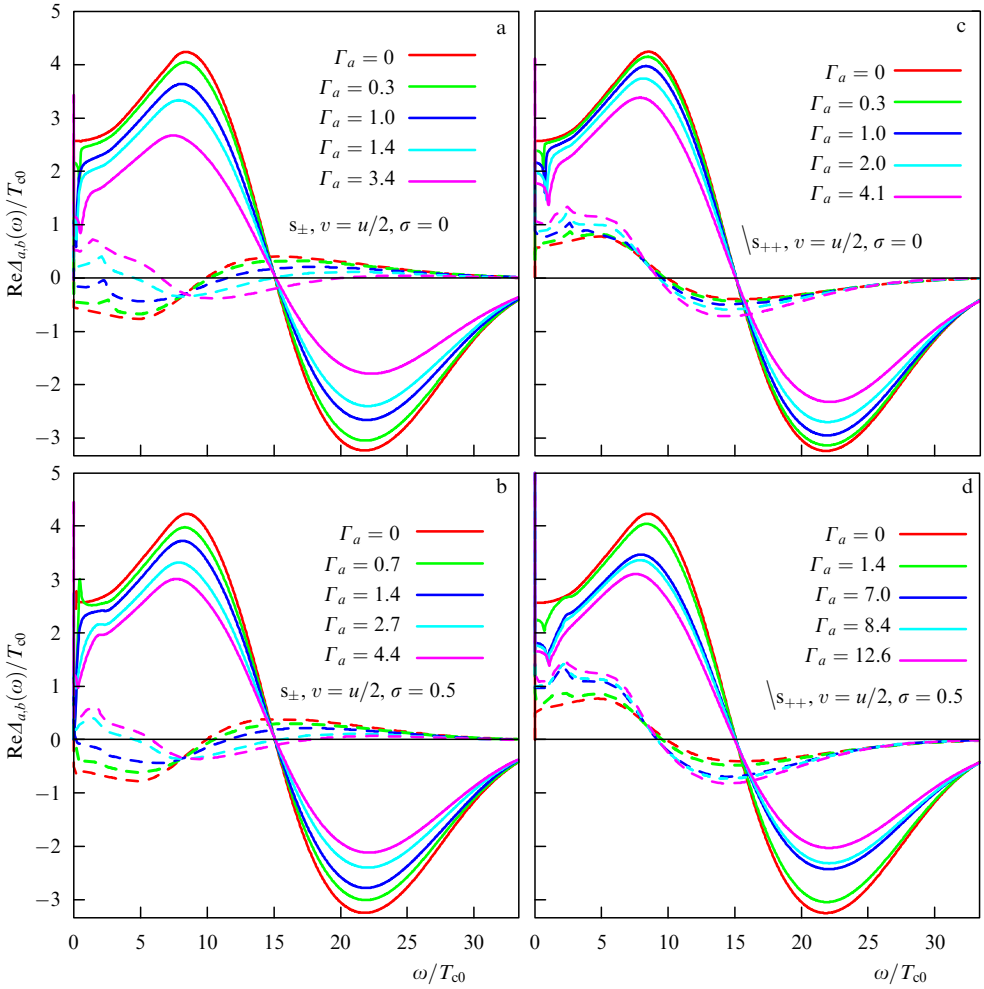

Figure 10. (Color online.) Frequency dependences of a real part of the gap function $\mathrm{Re}\,\Delta_\alpha(\omega)$ for $s_\pm$ (a, b) and s_{++} (c, d) superconductors with $v = u/2$ and for various Γ_a. Γ_a is given in units of T_{c0}. The gap in the band $\alpha = a$ ($\alpha = b$) is shown by the straight (dashed) curve. The Born limit, $\sigma = 0$, is shown in panels a and c, while the intermediate impurity scattering limit with $\sigma = 0.5$ is shown in panels b and d.

proportional to the impurity scattering rate $\Gamma_{a,b}$ and contain the generalized cross-section parameter σ that helps to control the approximation for the 'strength' of impurity scattering. This ranges from the Born limit (weak scattering, $\pi\mathcal{J}N_{a,b} \ll 1$) to the unitary limit (strong scattering, $\pi\mathcal{J}N_{a,b} \gg 1$):

$$\Gamma_{a,b} = 2\pi n_{\mathrm{imp}}\mathcal{J}^2(1-\sigma)\,N_{b,a} = \frac{2n_{\mathrm{imp}}\sigma}{\pi N_{a,b}} \to \begin{cases} 2\pi\mathcal{J}^2 n_{\mathrm{imp}} N_{b,a}\,, & \text{Born limit,} \\ \dfrac{2n_{\mathrm{imp}}}{\pi N_{a,b}}\,, & \text{unitary limit,} \end{cases} \tag{65}$$

$$\sigma = \frac{\pi^2\mathcal{J}^2 N_a N_b}{1+\pi^2\mathcal{J}^2 N_a N_b} \to \begin{cases} 0\,, & \text{Born limit,} \\ 1\,, & \text{unitary limit.} \end{cases} \tag{66}$$

We also introduce the parameter η to control the ratio between intra- and interband scattering potentials, $\mathcal{I} = \eta\mathcal{J}$.

Expressions for $\Sigma^{\mathrm{imp}}_{0(2)a}$ at arbitrary temperature and η are too complicated and noninformative to write them down here. It is much more convenient to consider limiting cases. We also consider the three special forms of the impurity potential: the uniform potential with $\eta = 1$ ($\mathcal{I} = \mathcal{J}$), the interband-only potential with $\eta = 0$ ($\mathcal{I} = 0$, $\mathcal{J} \neq 0$), and the intraband-only potential with $\mathcal{J} = 0$, $\mathcal{I} \neq 0$ (formally, $\eta = \infty$).

The Born limit corresponds to $\sigma = 0$. Eliashberg equations (12), (13) are then written out as follows:

$$\tilde{\omega}_{an} = \omega_n + \mathrm{i}\Sigma_{0a}(\omega_n) + \pi\mathcal{J}^2 n_{\mathrm{imp}}\left(\eta^2 N_a\frac{\tilde{\omega}_{an}}{Q_{an}} + N_b\frac{\tilde{\omega}_{bn}}{Q_{bn}}\right), \tag{67}$$

$$\tilde{\phi}_{an} = \Sigma_{2a}(\omega_n) - \pi\mathcal{J}^2 n_{\mathrm{imp}}\left(\eta^2 N_a\frac{\tilde{\phi}_{an}}{Q_{an}} + N_b\frac{\tilde{\phi}_{bn}}{Q_{bn}}\right). \tag{68}$$

One of the significant differences between this expression and the analogous one for nonmagnetic impurities [see formula (44) and (45)] is the minus sign before the term originating from impurity scattering in equation (68). In the presence of interband-only scattering ($\eta = 0$), we derive here the remarkable result

$$\tilde{\omega}_{an} = \omega_n + \mathrm{i}\Sigma_{0a}(\omega_n) + \pi\mathcal{J}^2 n_{\mathrm{imp}} N_b\frac{\tilde{\omega}_{bn}}{Q_{bn}}\,, \tag{69}$$

$$\tilde{\phi}_{an} = \Sigma_{2a}(\omega_n) - \pi\mathcal{J}^2 n_{\mathrm{imp}} N_b\frac{\tilde{\phi}_{bn}}{Q_{bn}}\,. \tag{70}$$

Indeed, for the s_{++} state we have $\mathrm{sgn}\,\tilde{\phi}_{bn} = \mathrm{sgn}\,\tilde{\phi}_{an}$ and equations written above correspond to the generalization of the Abrikosov–Gor'kov theory to the two-band case; there-

fore, impurities should suppress superconductivity. This, however, as we will see later, is not always true due to the complicated structure of equations, and their self-consistent solution may lead to unexpected results. On the other hand, for the $s_\pm$ state we have $\operatorname{sgn}\tilde{\phi}_{bn} = -\operatorname{sgn}\tilde{\phi}_{an}$ and the sign of the last term in formula (70), originating from impurity scattering, changes and the equations become similar to expressions for a two-band superconductor with *nonmagnetic impurities*. That is, T_c is not suppressed by disorder, except when $\eta = 1$.

For the uniform impurity potential, we have $\eta = 1$, then $\tilde{\omega}_{an} = \omega_n + i\Sigma_{0a}(\omega_n) + \pi\mathcal{J}^2 n_{\text{imp}}(N_a\,\tilde{\omega}_{an}/Q_{an} + N_b\,\tilde{\omega}_{bn}/Q_{bn})$ and $\tilde{\phi}_{an} = \Sigma_{2a}(\omega_n) - \pi\mathcal{J}^2 n_{\text{imp}}(N_a\,\tilde{\phi}_{an}/Q_{an} + N_b\,\tilde{\phi}_{bn}/Q_{bn})$. Here, contributions from both the a and b bands are mixed, so we expect a suppression of T_c by the disorder [151].

When the interband component is absent ($\eta = \infty$), equations for different bands are decoupled:

$$\tilde{\omega}_{an} = \omega_n + i\Sigma_{0a}(\omega_n) + \pi\mathcal{I}^2 n_{\text{imp}} N_a \frac{\tilde{\omega}_{an}}{Q_{an}}\,,$$

$$\tilde{\phi}_{an} = \Sigma_{2a}(\omega_n) - \pi\mathcal{I}^2 n_{\text{imp}} N_a \frac{\tilde{\phi}_{an}}{Q_{an}}\,,$$

and we have the suppression of superconductivity in each band, following the Abrikosov-Gor'kov theory.

It is remarkable that equations in the unitary limit are exactly the same as in the unitary limit for *nonmagnetic impurities* (46)–(49). Therefore, all conclusions about suppression of superconductivity for $\eta \neq 1$ and $\eta = 1$ are the same.

Now, we write down the Eliashberg equations for special shapes of the impurity potential. For the intraband-only impurity potential ($\mathcal{I} = 0$), terms in equations corresponding to bands a and b are separated, namely

$$\tilde{\omega}_{an} = \omega_n + i\Sigma_{0a}(\omega_n) + \frac{\Gamma_a}{2D}\left[\sigma\,\frac{\tilde{\omega}_{an}}{Q_a} + (1-\sigma)\,\frac{\tilde{\omega}_{bn}}{Q_b}\right], \quad (71)$$

$$\tilde{\phi}_{an} = \Sigma_{2a}(\omega_n) + \frac{\Gamma_a}{2D}\left[\sigma\,\frac{\tilde{\phi}_{an}}{Q_a} - (1-\sigma)\,\frac{\tilde{\phi}_{bn}}{Q_b}\right], \quad (72)$$

where

$$D = 1 - 2(1-\sigma)\,\sigma\left(1 - \frac{\tilde{\omega}_{an}\tilde{\omega}_{bn} - \tilde{\phi}_{an}\tilde{\phi}_{bn}}{Q_a Q_b}\right).$$

For the impurity potential scattering solely between different bands ($\mathcal{J} = 0$), equations for different bands decouple:

$$\tilde{\omega}_{an} = \omega_n + i\Sigma_{0a}(\omega_n) + \Gamma_a\,\frac{N_a}{2D}\,\frac{\tilde{\omega}_{an}}{Q_a}\left[\sigma N_a + (1-\sigma)\,N_b\right], \quad (73)$$

$$\tilde{\phi}_{an} = \Sigma_{2a}(\omega_n) + \Gamma_a\,\frac{N_a}{2D}\,\frac{\tilde{\phi}_{an}}{Q_a}\left[\sigma N_a - (1-\sigma)\,N_b\right], \quad (74)$$

where

$$D = \sigma^2 N_a^2 + (1-\sigma)^2 N_b^2 + 2\sigma(1-\sigma)\,N_a N_b\,\frac{\tilde{\omega}_{an}^2 - \tilde{\phi}_{an}^2}{Q_a^2}\,.$$

5.2 Results of calculations

The results that follow were obtained by solving self-consistently frequency and gap equations (12) and (13) with the impurity self-energy from the solution of equations (59), (60) for both arbitrary finite temperatures below T_c and at T_c [127]. Hereinafter, we consider for illustrative purposes the case of $N_b/N_a = 2$ and choose coupling constants as $(\lambda_{aa}, \lambda_{ab}, \lambda_{ba}, \lambda_{bb}) = (3, -0.2, -0.1, 0.5)$ for the $s_\pm$ state with $\langle\lambda\rangle > 0$ [133, 134], and as $(3, 0.2, 0.1, 0.5)$ for the s_{++} state. Critical temperature in the clean limit for both sets is $T_{c0} = 30\ \text{cm}^{-1}$, which corresponds to 43.1 K.

In Figs 11–13, we plot T_c and Matsubara gaps $\Delta_{\alpha n}$ for the first Matsubara frequency $\omega_{n=1} = 3\pi T$ as functions of Γ_a for both $s_\pm$ and s_{++} superconductors and for various values of σ. The real part of the analytical continuation of $\Delta_{\alpha n}$ to real frequencies, the gap function $\operatorname{Re}\Delta_\alpha(\omega)$, is shown in Fig. 14.

First, we discuss the $s_\pm$ state. Critical temperature T_c becomes insensitive to impurities for the pure interband scattering, $\mathcal{I} = 0$. This partially confirms qualitative arguments that the $s_\pm$ state with magnetic impurities behaves like the s_{++} state with nonmagnetic disorder [145, 149], and agrees with theoretical calculations in the Born limit [157]. For the initially unequal gaps, $|\Delta_a| \neq |\Delta_b|$, there is an initial decrease in T_c for small Γ_a until the renormalized gaps become equal and then T_c saturates, since the analog of Anderson's theorem is achieved. For the finite $\mathcal{I}$, intraband scattering on the magnetic disorder averages gaps up to zero and, thus, suppresses T_c. On the other hand, in the unitary limit ($\sigma = 1$) a $T \to T_c$ we obtains

$$\tilde{\omega}_{an} = \omega_n + i\Sigma_{0a}(\omega_n) + \frac{\Gamma_a}{2}\operatorname{sgn}\omega_n\,,$$

$$\tilde{\phi}_{an} = \Sigma_{2a}(\omega_n) + \frac{\Gamma_a}{2}\,\frac{\tilde{\phi}_{an}}{|\tilde{\omega}_{an}|}$$

for arbitrary values of η, including the case of intraband-only impurities, $1/\eta = 0$. This form of equation is the same as for nonmagnetic impurities and, thus, there is no impurity contribution to the T_c equation, in analogy to Anderson's theorem. The only exception here is the special case of uniform impurities, $\eta = 1$, when

$$\tilde{\omega}_{an} = \omega_n + i\Sigma_{0a}(\omega_n) + \frac{n_{\text{imp}}}{\pi(N_a + N_b)}\operatorname{sgn}\omega_n\,,$$

$$\tilde{\phi}_{an} = \Sigma_{2a}(\omega_n) + \frac{n_{\text{imp}}}{\pi(N_a + N_b)^2}\left(N_a\,\frac{\tilde{\phi}_{an}}{|\tilde{\omega}_{an}|} + N_b\,\frac{\tilde{\phi}_{bn}}{|\tilde{\omega}_{bn}|}\right).$$

Both gaps are mixed in the equation for $\tilde{\phi}_{an}$; thus, they tend to zero with an increasing amount of disorder. That is also true away from the unitary limit (see Fig. 13) and is the source for the claim that the uniform potential with $\mathcal{I} = \mathcal{J}$ is a special case with the strongest T_c suppression.

In general, the multiband s_{++} state should always be fragile against paramagnetic disorder, since magnetic scattering between bands having gaps of the same sign is equivalent to pairbreaking scattering within the single (quasi)isotropic band. Surprisingly, we found a regime with the saturation of T_c for the finite amount of disorder right after the initial downfall (similar to the one following from the Abrikosov–Gor'kov theory) (Fig. 12b). The saturation of T_c is observed for interband-only impurities, while the presence of the intraband magnetic disorder ultimately suppresses T_c to zero. However, depending on the 'strength' of scattering σ, a decrease in T_c may proceed quite slow compared to the one predicted by the Abrikosov–Gor'kov theory.

To understand the origin of the T_c saturation, we analyzed the gap function dependence on the scattering rate Γ_a (see Fig. 12). For the s_{++} state after a certain value of the

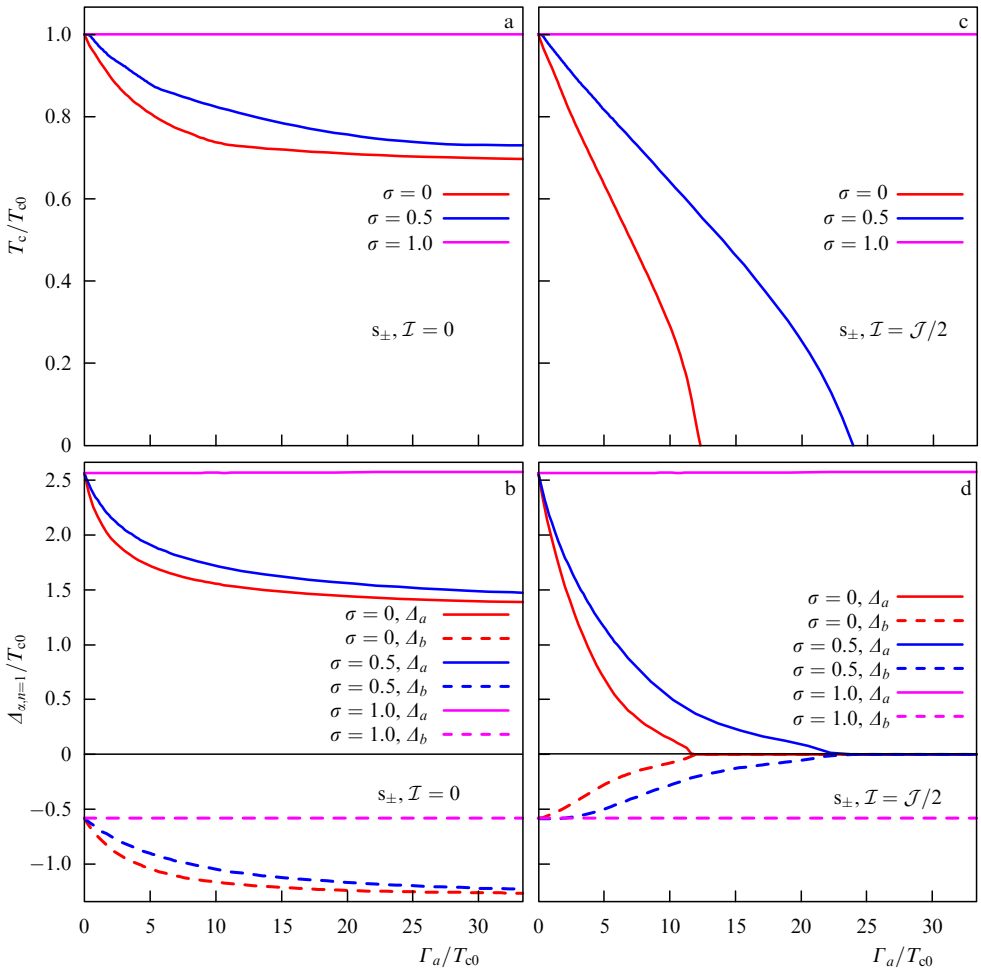

Figure 11. (Color online.) Dependences of T_c (a, c) and Matsubara gaps $\Delta_{\alpha,n=1}$ (b, d) on the impurity scattering rate Γ_a for the $s_\pm$ superconductor with only interband scattering, $\mathcal{I} = 0$, in panels a and b, and with $\mathcal{I} = \mathcal{J}/2$ in panels c and d.

scattering rate, the smaller gap, Δ_b, becomes negative. What we see is the $s_{++} \to s_\pm$ transition. As soon as the system becomes effectively $s_\pm$, scattering on magnetic impurities cancels out in the T_c equation, similar to Anderson's theorem, and T_c saturates. Before the saturation, the initial downfall akin to the one following from the Abrikosov–Gor'kov theory occurs. The transition is also seen in the frequency dependence of the gap function on a real frequency axis (see Fig. 14).

Similar to the $s_\pm \to s_{++}$ transition for nonmagnetic disorder, there is a simple physical argument behind the $s_{++} \to s_\pm$ transition here. Namely, with increasing interband magnetic disorder, the gap functions on different Fermi surfaces tend to the same value and, if one of the gaps is smaller than another, it crosses zero and changes sign. A similar effect has been mentioned in Refs [145, 149, 152] for a two-band systems with s_{++} symmetry in the Born limit.

Notice that here we do not consider a time-reversal symmetry broken $s_\pm + is_{++}$ state. It may appear for $T \lesssim T_c$ in cases when translational symmetry is violated [158].

6. Experimental situation with disorder-induced superconductivity suppression in iron-based materials

Presently, there are not so many experimental studies of impurity effects on the superconducting state of iron pnictides and chalcogenides. Moreover, it is hard to determine exactly whether the impurity is nonmagnetic or magnetic, because of the possible magnetic moment induced by nonmagnetic ions or irradiated particles, e.g., neutrons [106]. Other concomitant difficulties in the interpretation of results include changes in the crystal structure with the replacement of one ion with another, and possible effective doping also affecting the superconducting critical temperature. That is why further we describe the effects of various kinds of disorder on the critical temperature T_c without going into the details of the nature of the disorder.

Let us systemize the data in the following way: first, we discuss the subset of studies on introducing impurities via replacing one ion with another, and, second, we do a short review of irradiation studies.

The chemical substitution of iron with copper or nickel in the 122 system, $Ba_{0.6}K_{0.4}(Fe_{1-x}M_x)_2As_2$ with $M = Cu$ or Ni, resulted in the full suppression of T_c for $x \sim 0.1$ with the rates of -3.5 K per 1% of Cu, and -2.9 K per 1% of Ni [159]. With the chemical substitution in $Ba_{0.5}K_{0.5}(Fe_{1-x}M_x)_2As_2$ of iron with zinc ($M = Zn$), the effect on T_c is practically absent, while with a change for manganese ($M = Mn$), T_c is completely suppressed for $x \sim 0.08$ [107].

Another study of the $Ba_{0.5}K_{0.5}Fe_{2-2x}M_{2x}As_2$ system with $M = Fe$, Mn, Ru, Co, Ni, Cu, Zn revealed that all types of chemical substitution result in full T_c suppression except for $M = Ru$, when T_c changes quite weakly [116]. Rates of

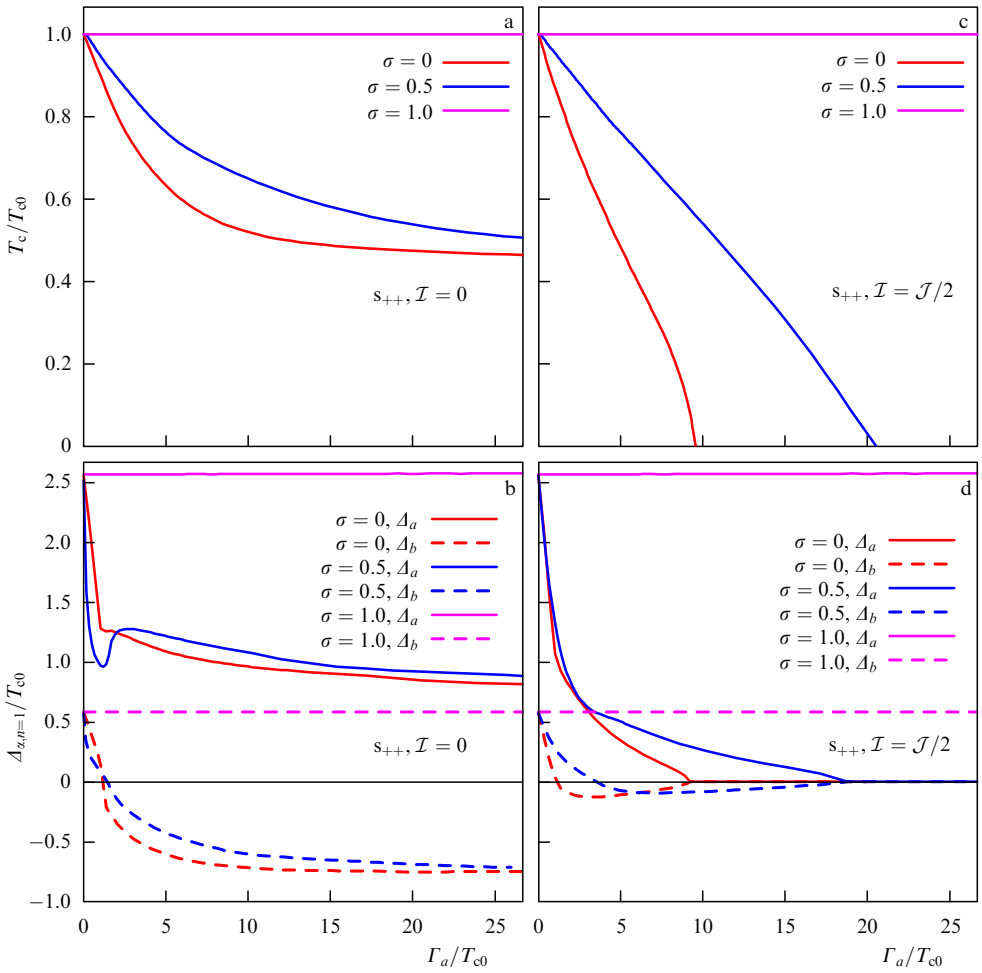

Figure 12. (Color online.) Dependences of T_c (a, c) and Matsubara gaps $\Delta_{\alpha,n=1}$ (b, d) on the impurity scattering rate Γ_a for the s_{++} superconductor with only interband scattering, $\mathcal{I} = 0$, in panels a and b, and with $\mathcal{I} = \mathcal{J}/2$ in panels c and d.

suppression for Mn, Co, Ni, Cu, and Zn are equal to 6.98, 1.73, 2.21, 2.68, and 2.22 K per 1% of Fe replacement with these atoms, respectively. Differences in T_c suppression by zinc in Refs [107, 116] are attributed to the technological difficulties in zinc doping at atmospheric pressure and, possibly, that in Ref. [107] zinc concentration did not exceed 2% in polycrystalline samples. The consistent study of zinc's effect on the superconductivity in $LaFe_{1-y}Zn_yAsO_{1-x}F_x$ revealed the dependence of this effect on x: T_c slightly increases in underdoped samples ($x = 0.05$), stays practically unchanged at optimal doping ($x = 0.1$), and becomes rapidly suppressed in overdoped samples ($x = 0.15$) [108]. In $BaFe_{1.89-2x}Zn_{2x}Co_{0.11}As_2$, zinc suppress T_c at the rate of 3.63 K per 1% of Zn [160], which is considerably weaker than expected from the Abrikosov–Gor'kov theory. Chemical substitution in $LaFe_{1-x}M_xPO_{0.95}F_{0.05}$ results in the T_c suppression rate of -2.2 K per 1% for $M = Co$, and -9.3 K per 1% for $M = Mn$ [161]. According to magnetoresistance measurements, the authors of Ref. [161] claim that cobalt (manganese) is a nonmagnetic (magnetic) impurity. For $K_{0.8}Fe_{2-y-x}M_xSe_2$ with $M = Cr$, Co, and Zn, a rapid suppression of T_c is observed that is absent for $M = Mn$ [114]. At the same time, based on electronic paramagnetic resonance (EPR) measurements, the authors of Ref. [114] report that the introduction of Cr, Co, and Zn cause the formation of large local magnetic moments, in contrast to the Mn case. Replacement of iron in $Fe_{1-y}M_yTe_{0.65}Se_{0.35}$ ($M = Co$, Ni, Cu) results in the following T_c-suppression rates: 5.8, 2.6, and 1.3 K per 1% for Cu, Ni, and Co, respectively [162]. Strong T_c suppression was observed in $LaFe_{1-x}Zn_xAsO_{0.85}$ with the rate of 9 K per 1% of Zn [163]. Isovalent replacement of potassium with sodium in $K_{1-x}Na_xFe_2As_2$ causes a drop in T_c from 3.5 K at $x = 0$ to 2.8 K at $x = 0.07$ [111]. With isovalent ruthenium doping in $NdFe_{1-y}Ru_yAsO_{0.89}F_{0.11}$ [164] and $LaFe_{1-y}Ru_yAsO_{0.89}F_{0.11}$ [163], T_c decreases much more weakly than when iron is replaced with cobalt in $NdFe_{1-y}Co_yAsO_{0.89}F_{0.11}$ and than expected from the Abrikosov–Gor'kov theory. In $SmFe_{1-x}Ru_xAsO_{0.85}F_{0.15}$, the isovalent substitution of iron with ruthenium results in rapid (slow) T_c suppression for $x < 0.5$ ($x > 0.5$) [110]. The authors of Ref. [110] connected such a change in the behavior to the change in the role played by ruthenium — initially it serves as nonmagnetic impurity and then, for $x > 0.5$, the metallic behavior is restored due to the large ruthenium concentration and its larger contribution to the band structure.

In the $K(Fe_{1-x}Co_x)_2As_2$ system, cobalt doping causes the same rapid T_c suppression, as in the cuprates $YBa_2(Cu_{1-x}Zn_x)_3O_{6.93}$ and $La_{1.85}Sr_{0.15}Cu_{1-x}Ni_xO_4$, and at $x \approx 0.4$ superconductivity vanishes [166]. Perhaps an analogy with the cuprates arises here due to the presence of line nodes in both cuprates and KFe_2As_2 [167].

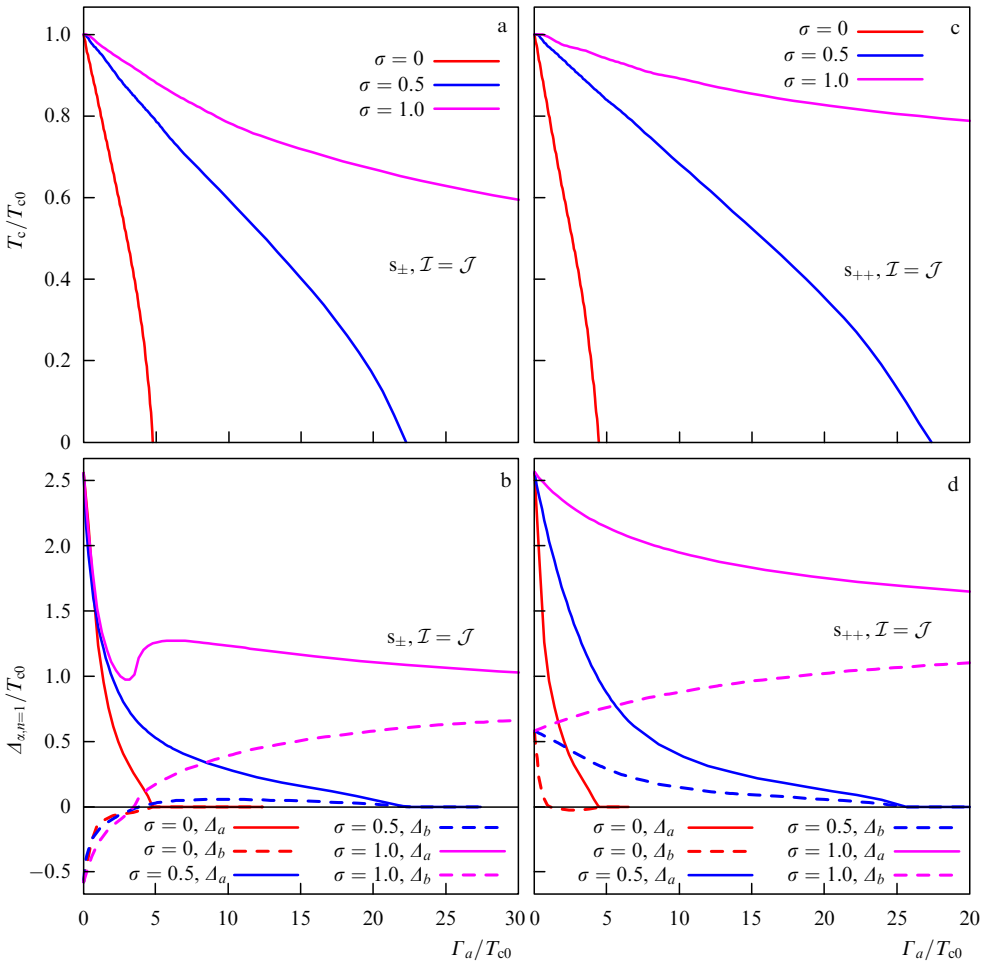

Figure 13. (Color online.) The same as in Figs 11 and 12, but for the special case of $\mathcal{I} = \mathcal{J}$.

There are also unusual situations, for example, $LaO_{0.9}F_{0.1}FeAs_{1-\delta}$, where the arsenic disorder with $\delta \approx 0.06$ causes not a decrease, but a slight increase in T_c [115].

Let us now switch to particle irradiation studies. Here, the situation, in general, is less diversified than with the chemical substitution of ions. In particular, the suppression of T_c is observed, though it is much weaker than expected from the Abrikosov–Gor'kov formula. This is true for irradiation by neutrons of $LaFeAsO_{0.9}F_{0.1}$ [106], by protons of $Ba(Fe_{1-x}Co_x)_2As_2$ ($x = 0.045, 0.075, 0.113$) [109] and $Ba(Fe_{0.9}Co_{0.1})_2As_2$ [117], by electrons of $Ba_{1-x}K_xFe_2As_2$ ($x = 0.19,\ 0.26,\ 0.32,\ 0.34$) [120] and $Ba(Fe_{1-x}Ru_x)_2As_2$ ($x = 0.24$) [112], by alpha-particles of $NdFeAsO_{0.7}F_{0.3}$ [113], and by heavy ions of $Ba(Fe_{1-x}M_x)_2As_2$ (M = Co, Ni) [121] and $Ba(Fe_{1-x}Co_x)_2As_2$ [122]. In the latter case, optimally doped $Ba_{0.6}K_{0.4}Fe_2As_2$ stands apart because the effect on T_c was not observed in it altogether [123].

On a separate note, there are studies on the electron irradiation of $BaFe_2(As_{1-x}P_x)_2$ [105] and $SrFe_2(As_{1-x}P_x)_2$ [119], where apparently 'accidental' nodes in the nodal $s_\pm$ state were removed with increasing disorder, as was predicted earlier theoretically in Ref. [104]. However, this effect was not observed with the proton irradiation of $BaFe_2(As_{1-x}P_x)_2$ [118].

Summarizing, there is a suppression of superconductivity in most cases. At the same time, the T_c decrease rate is much lower than expected from the Abrikosov–Gor'kov expression.

7. Dynamical properties of dirty superconductors

One of the important features of the discussed $s_\pm \to s_{++}$ and $s_{++} \to s_\pm$ transitions is gapless superconductivity, which has a direct relation to experiments on iron-based materials. In particular, since one of the gaps changes sign it necessarily goes through zero, corresponding to the gapless state. Therefore, the transition should manifest itself in various dynamical properties of the superconducting state. Those properties are: first, the density of states (17) that can be probed in tunneling experiments and ARPES; second, the temperature dependence of the London penetration depth λ_L (19), and, third, the frequency dependence of the optical conductivity $\sigma(\omega)$ (20). A more subtle effect impurity scattering has on a dynamical spin susceptibility and, thus, on $1/T_1T$ — the spin–lattice relaxation rate $1/T_1$, measured by NMR and normalized to the temperature T. We discuss these points in detail in the following Sections 7.1–7.4. Our choice of coupling constants will be the same as in Section 5.2.

7.1 Density of states and penetration depth

First, we discuss the transition from the $s_\pm$ to the s_{++} state induced by nonmagnetic impurities. A total density of states $N(\omega)$ calculated using expression (17) for systems with $\langle\lambda\rangle > 0$ is plotted in Fig. 15a. Upon increasing the impurity scattering rate, the smaller gap closes, resulting in a finite residual density of states at the zero frequency, $N(\omega = 0)$, and then reopens. Such behavior is reflected in the temperature

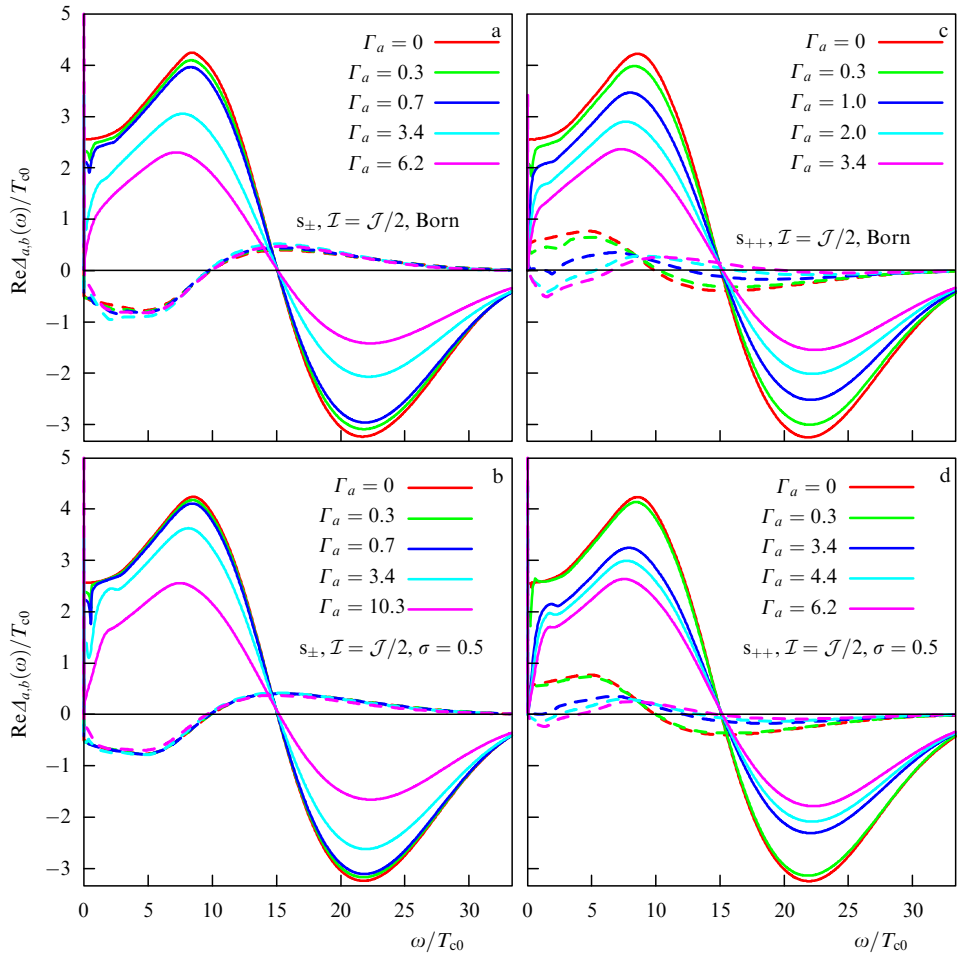

Figure 14. (Color online.) Frequency dependences of the gap function $\mathrm{Re}\,\Delta_\alpha(\omega)$ for the $s_\pm$ (a, b) and the s_{++} (c,d) superconductors with $\mathcal{I} = \mathcal{J}/2$ and for various values of Γ_a. Γ_a is given in units of T_{c0}. Gap in the band $\alpha = a\,(\alpha = b)$ is shown by the straight (dashed) curve. Born limit, $\sigma = 0$, is shown in panels a and c, while the intermediate impurity scattering limit with $\sigma = 0.5$ is shown in panels b and d.

dependence of the London penetration depth (19), shown in Fig. 15b. Here, we present results correspondingly normalized to the plasma frequency $\omega_{p\alpha}$. Evidently, $1/\lambda_L^2$ in a clean limit has an activation temperature dependence determined by the smaller gap, then transforms into the T_c behavior in the gapless state, and finally shows a new activation regime in the s_{++} state. In other words, at $\Gamma_a = 0$ we have a typical two-gap dependence [168]. For larger values of the scattering rate, when the two gaps are almost equal, the temperature dependence of the penetration depth becomes like that in a single-band superconductor.

The density of states $N(\omega)$ and the inverse square of the penetration depth $1/\lambda_L^2$ in the case of magnetic impurities with $\mathcal{I} = \mathcal{J}/2$ and $\sigma = 0.5$ are shown in Fig. 16 for the $s_\pm$ and s_{++} superconductors. In the former case, we see the expected behavior with gradually decreasing gaps. Gapless superconductivity with the residual $N(\omega = 0)$ occurs for $\Gamma_a > 10T_{c0}$ when $\mathrm{Re}\,\Delta_\alpha(\omega = 0)$ vanishes, which is seen in Fig. 14b. As for the s_{++} state, the smaller gap vanishes upon increasing the impurity scattering rate Γ_a, leading to a finite residual density of states $N(\omega = 0)$. Then, the gap reopens and $\Delta_{bn} \neq 0$ until T_c reaches zero at $\Gamma_a \sim 20T_{c0}$. Still, the superconductivity stays gapless with the finite $N(0)$, because $\mathrm{Re}\,\Delta_\alpha(\omega = 0) \to 0$, as seen in Fig. 14d. Penetration depth in the clean limit shows the activation behavior determined by the smaller gap. In the case of the s_{++} state, the penetration depth becomes proportional to T^2 in the gapless regime, causing its significant reduction near $\Gamma_a \sim 4T_{c0}$ (Fig. 16d), and then the penetration depth shows an activation temperature dependence in the $s_\pm$ state after the transition.

7.2 ARPES

The presence of the gapless state should definitely manifest itself in ARPES spectra. The total measured photoemission current intensity $I(\mathbf{k}, \omega)$ in the sudden approximation is given by

$$I(\mathbf{k}, \omega) = \sum_\alpha \left|M_\alpha(\mathbf{k}, \omega)\right|^2 f(\omega)\, A_\alpha(\mathbf{k}, \omega)\,, \tag{75}$$

where $M(\mathbf{k}, \omega)$ is the matrix element of one-electron dipole interaction, depending on the initial and final states of the photoelectron, photon energy, and its polarization, $f(\omega)$ is the Fermi function, and $A_\alpha(\mathbf{k}, \omega)$ is the spectral function. The last can be expressed through the analytical continuation of Green's function (6) to the real frequencies as

$$\begin{aligned} A_\alpha(\mathbf{k}, \omega) &= -\frac{1}{2\pi}\,\mathrm{Tr}\big(\mathrm{Im}\,\hat{G}^{\alpha\alpha}(\mathbf{k}, \omega)\,\hat{\tau}_0\big) \\ &= -\frac{1}{\pi}\,\mathrm{Im}\,\frac{\tilde{\omega}_\alpha(\omega)}{\tilde{\omega}_\alpha^2(\omega) - \xi_{\mathbf{k}\alpha}^2 - \tilde{\phi}_\alpha^2(\omega)}\,. \end{aligned} \tag{76}$$

Notice that here we have to deal with a 'bare' dispersion $\xi_{\mathbf{k}\alpha}$, because the self-energy in our approximation does not depend

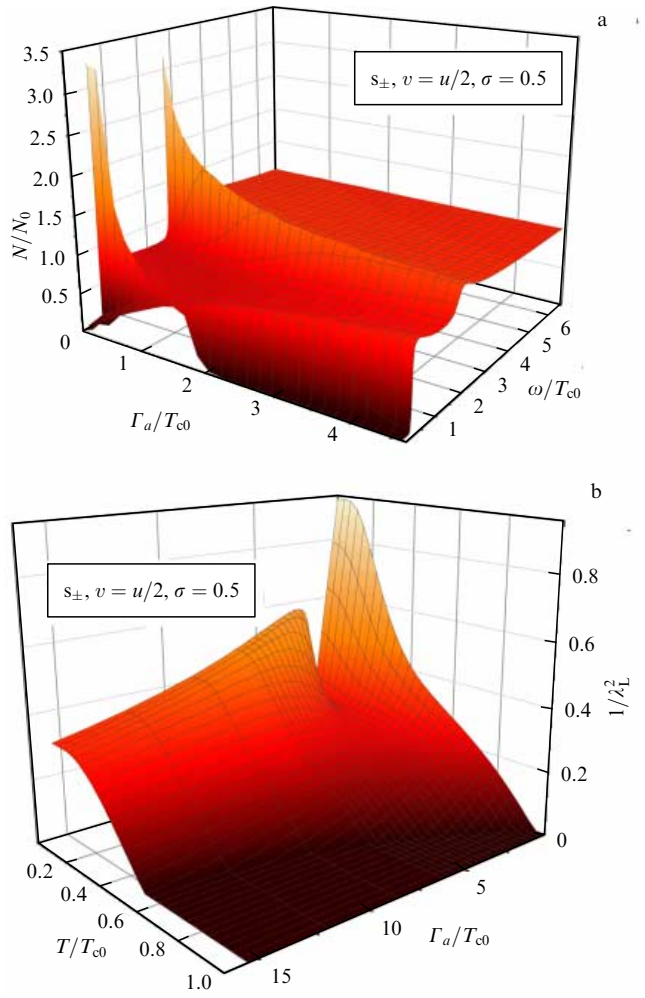

Figure 15. (a) Density of states $N(\omega)$ normalized to the density of states N_0 in the normal state as a function of frequency ω and nonmagnetic impurity scattering rate Γ_a in $s_\pm$ superconductors with $\langle\lambda\rangle > 0$, $\sigma = 0.5$, $\eta = 0.5$, and $N = N_a + N_b$. (b) $1/\lambda_L^2$ normalized to the total plasma frequency as a function of Γ_a and temperature T.

on momentum and makes corresponding contributions neither to the dispersion nor to the chemical potential shift.

The contribution from the electron–boson interaction to the self-energy $\Sigma_{0\alpha}(\mathbf{k},\omega)$ vanishes in the weak coupling approximation [169]. Therefore, we have $\Sigma_{0\alpha}(\omega) \to 0$ and $\Sigma_{2\alpha}(\omega) \to \Delta_\alpha(\omega)$ in the model with the isotropic self-energy. Then, the spectral function takes the following form [169]:

$$A_\alpha(\mathbf{k},\omega) = \frac{1}{\pi}\,\mathrm{Im}\,\frac{\omega}{D_\alpha}\left(1 + \mathrm{i}\sum_\beta \frac{\Gamma_{\alpha\beta}}{\sqrt{\omega^2 - \Delta_\beta^2(\omega)}}\right), \qquad (77)$$

where

$$D_\alpha = \xi_{\mathbf{k}\alpha}^2 + \left(\Delta_\alpha^2(\omega) - \omega^2\right)\left(1 + \mathrm{i}\sum_\beta \frac{\Gamma_{\alpha\beta}}{\sqrt{\omega^2 - \Delta_\beta^2(\omega)}}\right)^2. \qquad (78)$$

To be more specific, let Δ_b be the smaller gap. Two cases of superconductivity should be distinguished — one with the full total gap, and the other gapless. In the first case, $A_\alpha(\mathbf{k},\omega)$ vanishes for energies below Δ_α. On the other hand, the spectral function of the same band in the gapless regime with $\Delta_b \to 0$ will behave in the same fashion as it would in the normal state:

$$A_b(\mathbf{k},\omega) = \frac{1}{\pi}\,\mathrm{Im}\,\frac{\omega(1 + \mathrm{i}\sum_\beta \Gamma_{b\beta}/|\omega|)}{\xi_{\mathbf{k}b}^2 - \omega^2(1 + \mathrm{i}\sum_\beta \Gamma_{b\beta}/|\omega|)^2}. \qquad (79)$$

The fermionic spectral function $A_b(\mathbf{k},\omega)$ for the band b calculated via expression (76) is plotted in Fig. 17. For the sake of argument, we show the calculations for $|\Delta_b| < |\Delta_a|$ and the scattering on nonmagnetic impurities with $\eta = 0.5$ and $\sigma = 0.5$, although these results are retained for the case of magnetic impurities. In the clean limit (Fig. 17a), the behavior of $A_b(\mathbf{k},\omega)$ at small ω and $\xi_{\mathbf{k}b}$ is determined by the presence of the superconducting gap in the spectrum of excitations. On the other hand, at the $s_\pm$-to-s_{++} disorder-induced transition, $A_b(\mathbf{k},\omega)$ shows an absence of the gap (Fig. 17b). With a further increase in the scattering rate Γ_a, when the transition already happened, the gap in the spectrum of the b-band reappears. Therefore, ARPES measurements in the superconducting state at different impurity concentrations would help to detect the disorder-induced transition.

7.3 Optical conductivity

Considering nonmagnetic impurities as an example, here we demonstrate how the optical conductivity changes its behavior with increasing impurity scattering rate and, in particular, near the transition between the $s_\pm$ and s_{++} states. Figure 18 shows the optical conductivity $\mathrm{Re}\,\sigma(\omega) = \sum_\alpha \mathrm{Re}\,\sigma_\alpha(\omega)$ calculated as the solution of equations (20) and (23) at different rates of disorder with $\eta = 0.5$ and $\sigma = 0.5$. Due to the presence of the superconducting gap, in the clean limit we have $\mathrm{Re}\,\sigma_\alpha(\omega) = 0$ at small frequencies $\omega < 2\Delta_\alpha$. With an increase in the impurity scattering rate in the $s_\pm$ state, as opposed to the s_{++} superconductor, the range of the zero value of $\mathrm{Re}\,\sigma_b(\omega)$ for the band b diminishes and the peak above $2\Delta_b$ becomes narrower. This is surely due to a decrease in the gap Δ_b upon approaching the $s_\pm \to s_{++}$ transition (Fig. 10b). It is clearly seen in Fig. 18b that the Drude peak appears near the $s_\pm \to s_{++}$ transition at $\Gamma_a \sim 1.2T_{c0}$. This peak is typical for a normal metal because of vanishing the gap in the b-band, i.e., the gapless superconductivity regime in the course of transition. With a further increase in Γ_a, the optical conductivity regains the form of the full gap superconductor, though with a smaller width of the gap compared with its initial value.

The behavior described differs significantly from the behavior of the s_{++} superconductor, shown in Figs 18c and d, where the gaps converge in the limit of the infinite impurity scattering rate.

The temperature dependence of the optical conductivity $\mathrm{Re}\,\sigma(\omega)$ at a fixed frequency for the $s_\pm$ superconductor is plotted in Fig. 19. Evidently, the low-temperature contribution to the optical conductivity of the band b increases with increasing scattering rate Γ_a before the transition to the s_{++} state at $\Gamma_a \sim 1.1T_{c0}$, and then the contribution decreases.

The imaginary part of the optical conductivity, $\mathrm{Im}\,\sigma(\omega)$, is proportional to the real part of the polarization operator $\Pi(\omega)$, as seen from its definition (20). The frequency dependence of $\Pi(\omega)$ for the $s_\pm$ and s_{++} states in the presence of impurity scattering is illustrated in Fig. 20. There is a dip at frequency $\omega = 2\Delta_\alpha(\omega)$ in the case of the s_{++} superconductor. This agrees with the results for single-band superconductors [170]. In the $s_\pm$ state, interesting features are observed for the band b: first, the location of the dip is a nonmonotonic

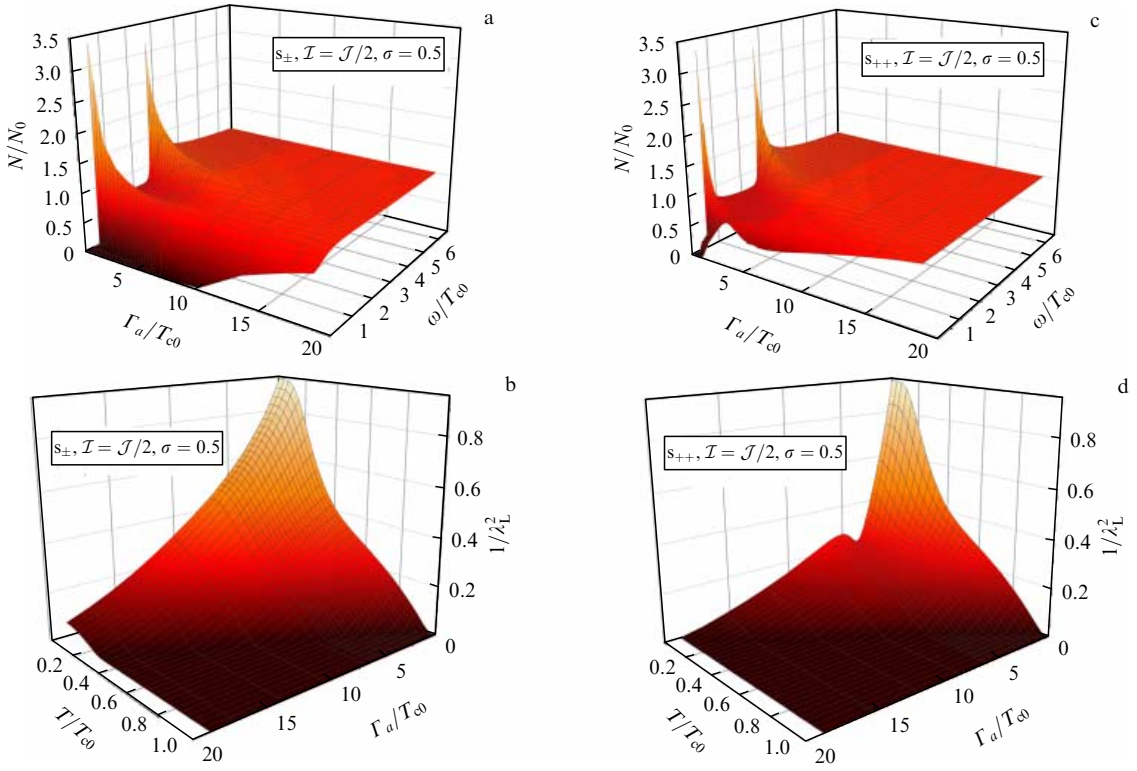

Figure 16. (a, c) Density of states $N(\omega)$ normalized to the density of states N_0 in the normal state as a function of frequency ω and magnetic impurity scattering rate Γ_a. (b, d) Dependence of $1/\lambda_L^2$ normalized to the total plasma frequency on Γ_a and temperature T for the $s_{\pm}$ superconductor (panels a and b) and the s_{++} superconductor (panels c and d) with $\mathcal{I} = \mathcal{J}/2$ and $\sigma = 0.5$. Notice the transition from the s_{++} state to the $s_{\pm}$ state at $\Gamma_a \sim 4T_{c0}$ and a gapless region emerged immediately after it.

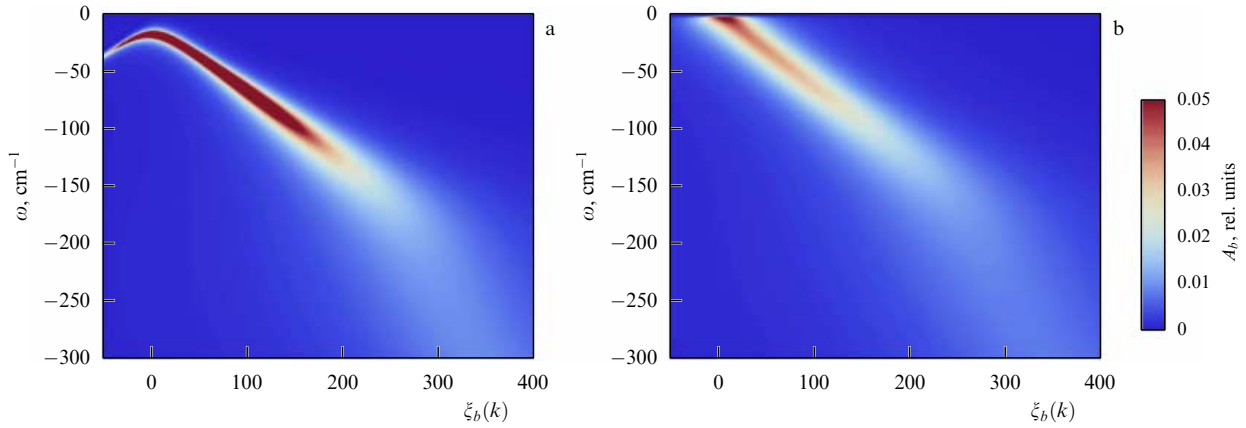

Figure 17. (Color online.) Spectral function $A_b(\mathbf{k}, \omega)$ of the band b with a smaller gap in the clean limit (a), and in the gapless regime (b) with the finite nonmagnetic impurity scattering rate $\Gamma_a = 1.33T_{c0}$ [169].

function of the scattering rate, and, second, the dip disappears in the gapless regime near the $s_{\pm} \to s_{++}$ transition.

A comparison of theoretical and experimental temperature dependences of the optical conductivity and the London penetration depth on the dose of proton irradiation at THz frequencies [117] is drawn in Fig. 21. It is interesting to trace the behavior of the coherence peak in the real part of the optical conductivity $\sigma_1(T, \omega \to 0)$. The peak is analogous to the Hebel–Slichter peak discussed in Section 7.4. With an increase in the irradiation dose, the peak disappears and then reappears (Fig. 21c). Such a behavior is a signature of the gradual closing of the smaller gap and its later reopening. It is exactly the process taking place at the $s_{\pm} \to s_{++}$ transition. The general trend of the penetration depth behavior is the same in the theory and in the experiment, as evident from a comparison of Figs 21b and d. In the experiment, however, it was not possible to 'catch' the region of the $s_{\pm} \to s_{++}$ transition itself. The latter is marked in Fig. 21b by the red arrow.

7.4 NMR spin-lattice relaxation rate

In addition to the Knight shift, which allows one to distinguish between singlet and triplet pairing, NMR can probe the spin-lattice relaxation rate $1/T_1$. Since we are going to discuss Fe-based materials, later we imply NMR in iron nuclei. The effect of the nuclei form factors is not very

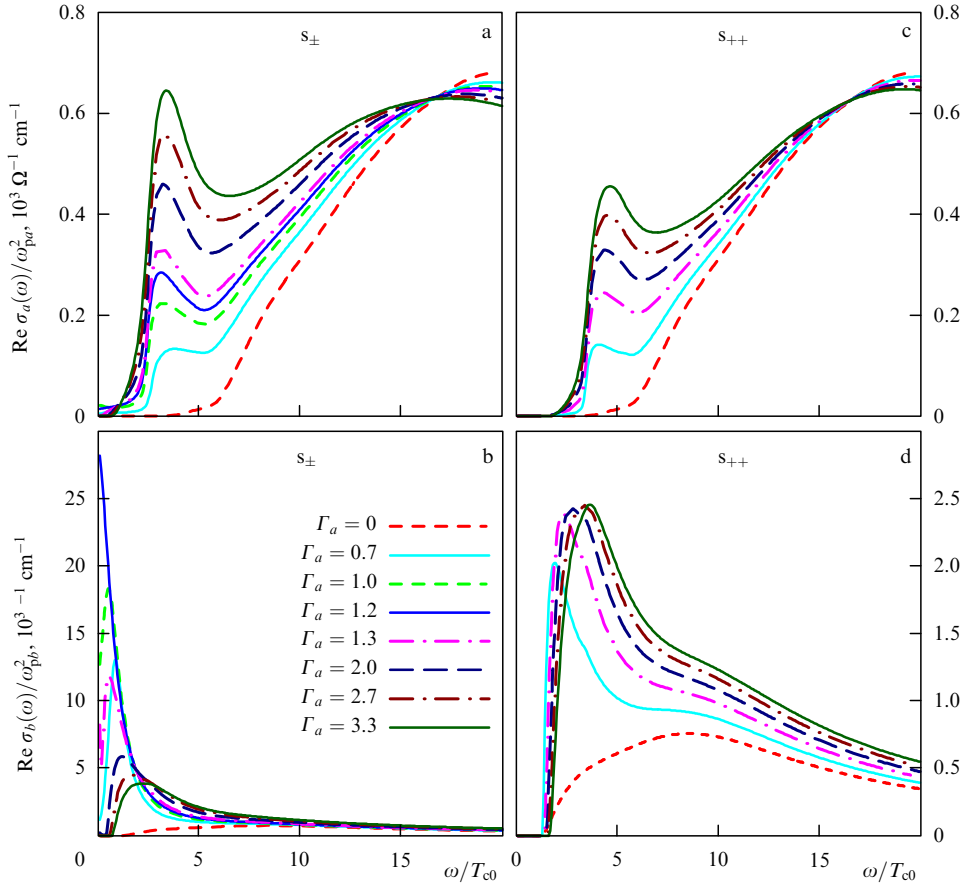

Figure 18. (Color online.) Frequency dependences of the real part of the optical conductivity, $\mathrm{Re}\,\sigma_\alpha(\omega)$, of bands $\alpha = a$ (a, c) and $\alpha = b$ (b, d) for the $s_\pm$ (panels a and b) and s_{++} (panels c and d) superconductors at different nonmagnetic impurity scattering rates Γ_a (in units of T_{c0}). Temperature is $T = 0.03T_{c0}$, $\sigma = 0.5$, and $\eta = 0.5$ [169].

important here compared to cuprates, for example. It is confirmed by a good agreement between $1/T_1T$ data on different nuclei (^{57}Fe, ^{75}As, ^{59}Co, and ^{139}La) in 122 and 1111 systems [92, 95, 171, 172]. It was also experimentally examined [91] that the hyperfine coupling $A_{hf}(\mathbf{q})$ most probably does not depend on the wave vector $\mathbf{q}$.

The spin-lattice relaxation rate is determined by the spin susceptibility integrated over the Brillouin zone, viz.

$$\frac{1}{T_1T} \propto \lim_{\omega\to 0} \sum_{\mathbf{q}} \frac{\mathrm{Im}\,\chi(\mathbf{q},\omega)}{\omega}\,. \tag{80}$$

As in the case with the spin resonance [15, 173–175], $1/T_1$ carries information about the underlying gap symmetry and structure. For example, an isotropic s-wave state is characterized by a Hebel–Slichter peak just below T_c and an exponential low-T temperature dependence. It is well known that d-wave superconductors exhibit a weak or no peak and demonstrate $T_1^{-1} \sim T^3$ behavior for $T \ll T_c$.

In the case of iron-based materials, the situation is somewhat more complicated. Typical data are given in Fig. 22a. Apparently, there is no peak below T_c and the temperature dependence does not follow the same simple power or exponential law. However, simple arguments can enable us to understand the main features revealed in experiments.

In the case of a weakly coupled clean two-band superconductor below T_c, assuming that the main contribution to

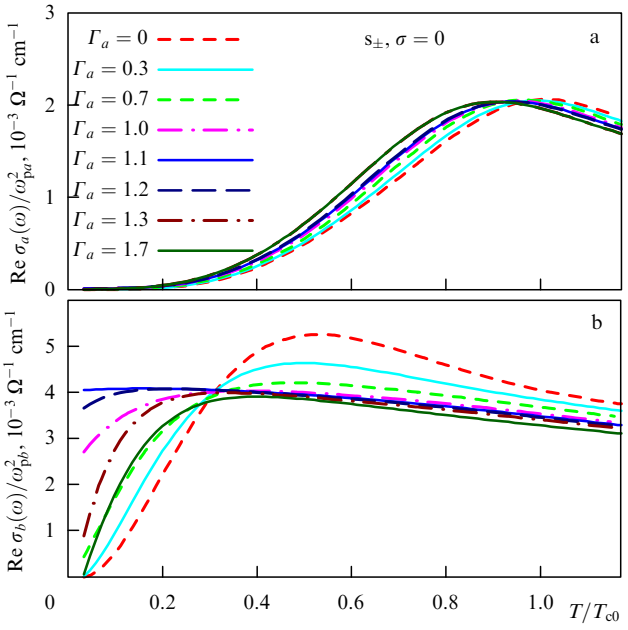

Figure 19. (Color online.) Temperature dependences of the real part of the polarization operator at a fixed frequency, $\mathrm{Re}\,\sigma_\alpha(\omega = 5\ \mathrm{cm}^{-1})$, for the two bands $\alpha = a$ (a) and $\alpha = b$ (b) in the $s_\pm$ state at different nonmagnetic impurity scattering rates Γ_a (in units of T_{c0}). Intraband scattering rate was chosen to be equal to $\Gamma_{intra} = 6.7T_{c0}$ for the sake of presentation [169].

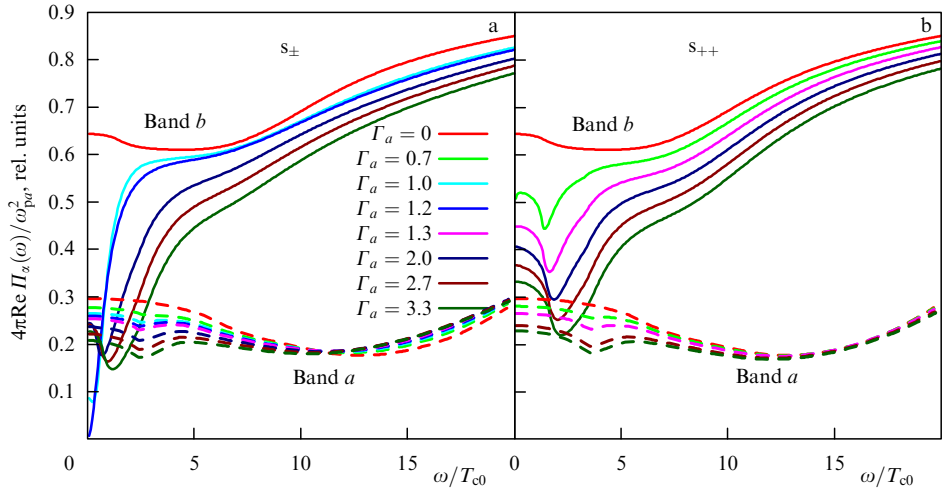

Figure 20. (Color online.) Real part of the polarization operator, $\mathrm{Re}\,\Pi_a(\omega)$, for $s_{\pm}$ (a) and s_{++} (b) superconductors at different nonmagnetic impurity scattering rates Γ_a (in units of T_{c0}). Temperature is $T = 0.03T_{c0}$, $\sigma = 0.5$, and $\eta = 0.5$ [169].

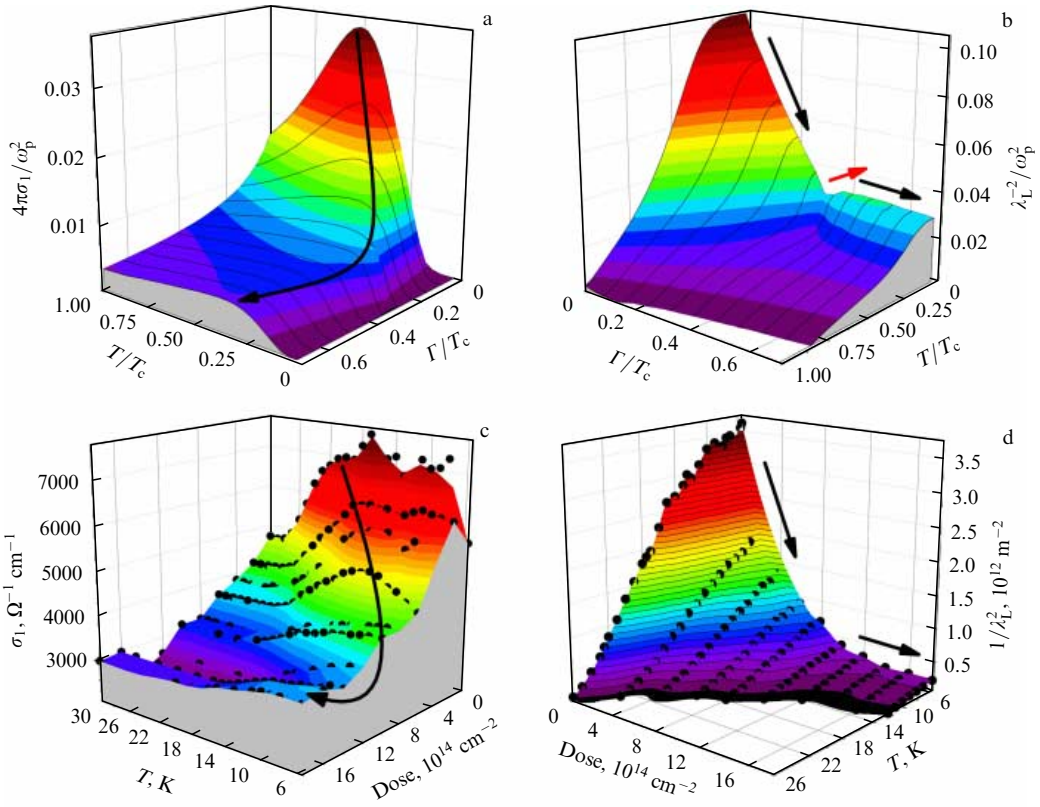

Figure 21. (Color online.) Calculated (a, b) and experimental (c, d) dependences of the real part of the optical conductivity σ_1 (panels a and c) and λ_L^{-2} (panels b and d) on temperature T and level of disorder. The latter is related to the nonmagnetic impurity scattering rate Γ_a in the theoretical calculations, and in the experiment on superconducting $Ba(Fe_{0.9}Co_{0.1})_2As_2$ to the proton irradiation dose (number of protons per 1 cm^2) [117].

$\mathrm{Im}\,\chi(\mathbf{q},\omega)$ comes from interband interactions, we derive the following expression for the inverse NMR spin-lattice relaxation rate:

$$\frac{1}{T_1 T} \propto \sum_{\mathbf{k}\mathbf{k}'} \left[1 + \frac{\Delta_{\mathbf{k}}\Delta_{\mathbf{k}'}}{E_{\mathbf{k}}E_{\mathbf{k}'}}\right] \left(-\frac{\partial f(E_{\mathbf{k}})}{\partial E_{\mathbf{k}}}\right) \delta(E_{\mathbf{k}} - E_{\mathbf{k}'}), \quad (81)$$

where $E_{\mathbf{k}}$ is the quasiparticle energy in the superconducting state, while $\mathbf{k}$ and $\mathbf{k}' = \mathbf{k} + \mathbf{q}$ lie on hole and electron Fermi sheets, respectively. Thus, $\mathbf{q}$ is the vector connecting hole and electron pockets. The above equation follows from the expression for the 'bare' susceptibility $\chi_0(\mathbf{q},\omega)$ at zero temperature and for a vanishing frequency. It is written out in a special way to emphasize the role of coherence factors for the dominating interband processes. The coherence factor in square brackets in formula (81) gives rise to an important distinction between different symmetries of the gap. They play a similar role in the formation of the spin resonance peak in inelastic neutron scattering [173]. In the NMR $1/T_1$ coherence factors, the internal sign is different from that in

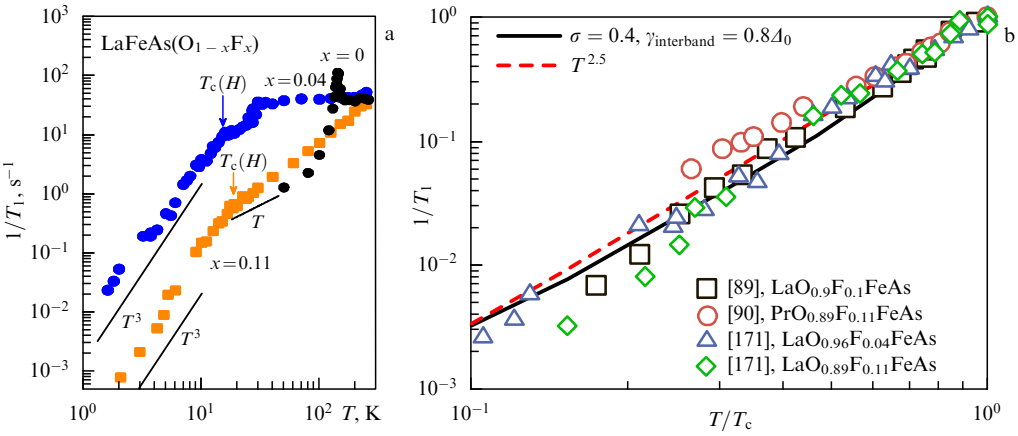

Figure 22. Temperature dependences of $1/T_1$ in iron-based materials. (a) Experimental results for the 1111 system from Ref. [171]. (b) Log-log plot summarizing experimental data from several groups [89, 90, 171], theoretical curve for the $s_{\pm}$ superconductor with intermediate impurity scattering rate ($0 \leqslant \sigma \leqslant 1$) and pairbreaking parameter $\gamma_{\text{interband}} = 0.4\Delta_0$, and $T^{2.5}$ curve for demonstrating a power-law dependence [132].

coherence factors entering the spin susceptibility related to neutron scattering. For the isotropic s_{++}-state with $\Delta_{\mathbf{k}} = \Delta_{\mathbf{k}'} = \Delta$, we obtain

$$\frac{1}{T_1} \propto \int_{\Delta(T)}^{\infty} dE \, \frac{E^2 + \Delta^2}{E^2 - \Delta^2} \operatorname{sech}^2\left(\frac{E}{2T}\right). \tag{82}$$

The denominator gives rise to a peak for temperatures $T \lesssim T_c$ near T_c, which is just the Hebel–Slichter peak. As pointed out earlier [16], it must be suppressed for the $s_{\pm}$-state. Indeed, if $\Delta_{\mathbf{k}} = -\Delta_{\mathbf{k}'} = \Delta$, then we have

$$\frac{1}{T_1} \propto \int_{\Delta(T)}^{\infty} dE \, \frac{E^2 - \Delta^2}{E^2 - \Delta^2} \operatorname{sech}^2\left(\frac{E}{2T}\right) = \int_{\Delta(T)}^{\infty} dE \, \operatorname{sech}^2\left(\frac{E}{2T}\right), \tag{83}$$

which is a monotonically decreasing function with a decrease in temperature for $T < T_c$. The same can be demonstrated for a more general $s_{\pm}$-state with $|\Delta_{\mathbf{k}}| \neq |\Delta_{\mathbf{k}'}|$ [132].

It is well known that pair-breaking impurity scattering dramatically increases the subgap density of states just below T_c, and even a weak magnetic scattering can broaden and eliminate the Hebel–Slichter peak in conventional superconductors. In the case of a sign-changing gap, the similar effect manifests itself due to nonmagnetic interband scattering [145]. Since the Hebel–Slichter peak is not present in iron-based materials, even in the clean case [see equation (83)], the pair-breaking effect is more subtle: it changes an exponential behavior for $T < T_c$ to a more power-law one. If the impurity-induced bound state lies at the Fermi level, the relaxation rate acquires a low-temperature Korringa-like term linear in temperature over a range of temperatures corresponding to the impurity bandwidth [176].

Qualitative arguments suggest that neither pure Born nor pure unitary limits with a simple isotropic $s_{\pm}$-state are well suited for explaining the observed $1/T_1$ behavior: the former leads to an exponential behavior at low temperatures in a relatively clean system, while the latter to Korringa behavior. Various data on 1111 systems appeared to be between these two limits [89, 90, 171] (see Fig. 22b). Results of the $1/T_1$ calculation for the simple $s_{\pm}$ state are also shown there [132]. We observe that the $s_{\pm}$-state result exhibits no coherence peak and, as opposed to the Born and unitary limits, the intermediate case with σ not equal to 0 or 1 is capable of reproducing the experimental behavior of $1/T_1$ [132, 146–148, 177]. This result, taken alone, should not be seen as evidence for an isotropic $s_{\pm}$ state, since a strong gap anisotropy is probably present in some of these systems, and will also lead to a higher density of states for quasiparticles contributing at intermediate temperatures.

Regarding other systems, data obtained on $BaFe_2(As_{1-x}P_x)_2$ shows a term linear in temperature in $1/T_1$ for an optimally doped sample, crossing over to something roughly approximating $\sim T^3$ above $T \gtrsim 0.1T_c$ [95, 178], consistent with reports of line nodes in this material from other probes. In $Ba_{0.68}K_{0.32}Fe_2As_2$, $1/T_1$ shows an exponential decrease below $T \approx 0.45T_c$, consistent with a full $s_{\pm}$ gap [179]. Finally, NMR in the LiFeAs system also shows a full gap, which is consistent with other measurements [94].

8. Conclusions

Summarizing, the disorder in multiband systems may have an unexpected impact on superconductivity. It is especially important in cases of MgB_2, iron pnictides, and iron chalcogenides, as well as for the approximate treatment of d-wave superconductors like cuprates, where parts of the Fermi surface with different signs of the gap to some extent can be considered to be different bands. As an example, here we considered the problem of scattering on nonmagnetic and magnetic impurities in two-band superconductors with s_{++} and $s_{\pm}$ order parameter types.

For nonmagnetic disorder, T_c is more stable against impurity scattering than the trivial generalization of the Abrikosov–Gor'kov theory (33). The exact rate of T_c suppression depends on the relation between intra- and interband coupling constants. Depending on the sign of the averaged coupling constant, $\langle\lambda\rangle$, originating from interelectron interactions, $s_{\pm}$ superconductors can be divided into two types. The first belongs to the case with $\langle\lambda\rangle < 0$ largely discussed in the literature, where the superconductivity is primarily determined by interband scattering. In such systems, T_c is suppressed with increasing disorder and vanishes when the scattering rate reaches the critical value.

The second type of $s_\pm$ state exhibits $\langle\lambda\rangle > 0$ and is characterized by a finite value of T_c with increasing disorder, while the signs of order parameters for different bands become equal. This last notion implies a transition from the $s_\pm$ state to the s_{++} state. The case of $\langle\lambda\rangle > 0$ corresponds to a sizeable intraband attraction. In spite of this attraction, even a weak interband repulsion leads to the opposite phases of order parameters in two different bands, i.e., to the $s_\pm$ state. Notice that the strong intraband attraction in the two-band model considered here may be a consequence of a large intraband pairing amplitude, as well as a result of the downfolding procedure of the realistic multiband model onto the two-band model. The large intraband pairing amplitude could be a result of electron–phonon interaction and/or orbital fluctuations. The downfolding procedure of the multiband model with a small intraband attractive pairing potential and the large band-asymmetric interband repulsion may also lead to the *effective* strong intraband attraction in the two-band model. Such a case was considered in Ref. [134] for the initial four-band model.

Regarding the magnetic disorder, generally, the superconducting state is destroyed with an increase in scattering on magnetic impurities. There are, however, a few special cases with the absence of complete T_c suppression, in which it saturates for a large impurity scattering rate. Such a situation occurs in the unitary limit and in the s_{++} and $s_\pm$ states with the interband-only impurity potential. Remarkably, the s_{++} superconductor is robust in this case against magnetic disorder not by itself, but due to the transition to the $s_\pm$ state insensitive to impurity scattering. This is in line with qualitative arguments on the analogy between magnetic impurities in the $s_\pm$ state and nonmagnetic impurities in the isotropic s_{++} state — that is, the equations have the same form and, since the s_{++} state is robust against nonmagnetic impurities, the $s_\pm$ state is robust against magnetic ones. Notice that the finite intraband component of the scattering potential leads to complete T_c suppression, though with a rate slower than the Abrikosov–Gor'kov theory prediction for single-band superconductors. In this case, even the $s_{++} \to s_\pm$ transition cannot save the superconductivity from collapse.

Summary plots of the T_c dependence on the impurity scattering rate Γ_a for the $s_\pm$ and s_{++} superconductors are displayed in Fig. 23. For both the $s_\pm$ state with the positive averaged coupling constant and the s_{++} state, the nonmagnetic disorder does not completely destroy superconductivity. The reason for this in the case of an $s_\pm$ superconductor is, however, different from that for the s_{++} state: there is a transition to the s_{++} state in the former case. Similarly, the reason for the absence of complete T_c suppression by the interband ($\eta = 0$) magnetic disorder for the s_{++} state is the transition to the $s_\pm$ state, which is robust against scattering on magnetic impurities due to an analog of Anderson's theorem. In the unitary limit, the results for all cases are the same except for the uniform impurity potential ($\eta = 1$) with a fall in T_c. Notice that while the exact form of the impurity potential is not known, it is hard to imagine that its intra- and interband parts would be equal in different cases, e.g., upon adding Zn or proton irradiation. This means that practically the case with $\eta = 1$ is highly improbable.

The general conclusion on the transition between states with different gap structures is the following: if the system has two interactions in the clean limit, dominating (1) and subdominating (2), and interaction (2) may induce a superconducting state that is robust against impurities, then the system will transform into this state as soon as the order due to the interaction (1) is destroyed by a disorder. That is, the $s_\pm$ state occurs due to the interband interaction, while the s_{++} state originates mainly from the intraband one. And if initially there was an $s_\pm$ state without the intraband component, then the interband nonmagnetic impurities would completely destroy this state and suppress T_c to zero. If there is an $s_\pm$ state with an intraband component (even a small one) of the interaction, then the same impurities would suppress the $s_\pm$ state but, due to the residual intraband interaction, the s_{++} state that cannot be destroyed by nonmagnetic impurities would stabilize. This is the $s_\pm \to s_{++}$ transition. For magnetic impurities, the situation is reversed. If initially there was an s_{++} state without the interband component of the superconducting interaction, then the interband magnetic impurities would destroy it.

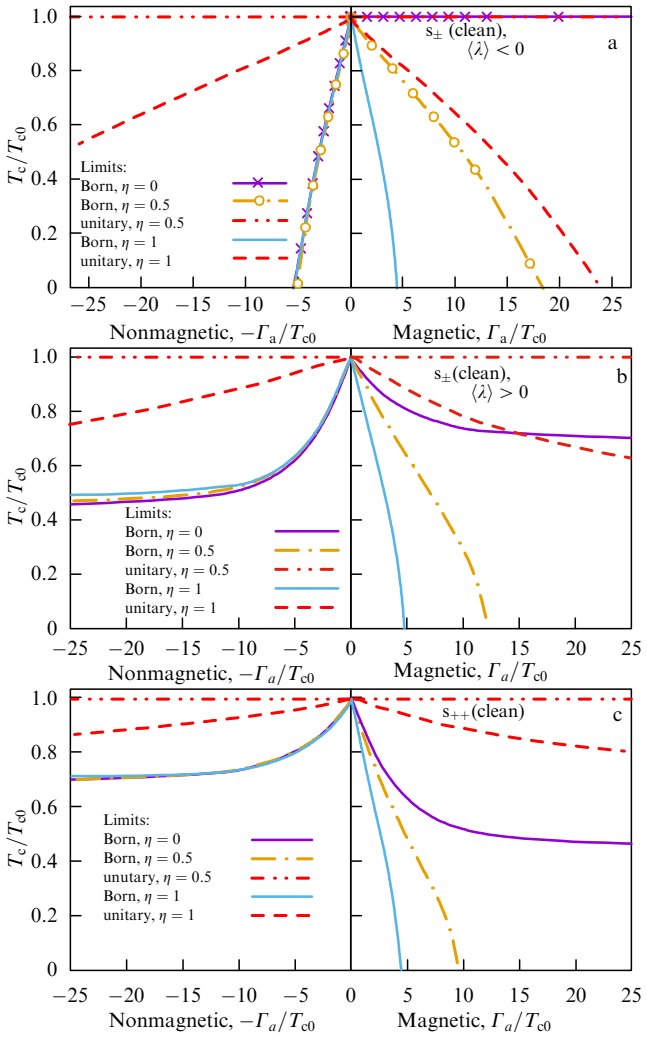

Figure 23. Dependences of T_c on nonmagnetic (left panel) and magnetic (right panel) impurity scattering rates Γ_a. (a) $s_\pm$ superconductor with the negative averaged coupling constant. (b) Superconductor with the positive averaged coupling constant that has the $s_\pm$ gap symmetry in the clean case ($\Gamma_a = 0$): for nonmagnetic impurities, a transition from the $s_\pm$ to the s_{++} state occurs at particular values of Γ_a. (c) Superconductor with the s_{++} gap symmetry in the clean case: for magnetic impurities, a transition to the $s_\pm$ state occurs at particular values of Γ_a. Various curves represent Born ($\sigma = 0$) and unitary ($\sigma = 1$) limits obtained for different relations between intra- and interband impurity potentials: the absence of the intraband potential ($\eta = 0$), the interband potential is twice the intraband one ($\eta = 0.5$), and the uniform impurity potential ($\eta = 1$).

However, the presence of even a small interband interaction would result in emerging the $s_{\pm}$ state after suppressing the s_{++} state by the magnetic disorder. It would be the $s_{++} \to s_{\pm}$ transition.

Since these transitions proceed through the gapless regime, they should manifest themselves in thermodynamical and transport properties. For example, they can be observed in optical and tunneling experiments, as well as in photoemission spectroscopy and tunneling conductivity in iron-based superconductors and other multiband systems. That is, since the smaller gap vanishes near the transition, ARPES should demonstrate the gapless spectra, and the optical conductivity would reveal the 'recovery' of the Drude-like frequency dependence of $\mathrm{Re}\,\sigma(\omega)$.

Acknowledgments

We would like to thank A Bianconi, A A Golubov, B P Gorshunov, I M Eremin, M V Eremin, D V Efremov, B Keimer, I I Mazin, R Prozorov, M V Sadovskii, D J Scalapino, M Tanatar, P J Hirschfeld, and A V Chubukov for many useful discussions. M M K is grateful to Max-Planck Institut für Festkörperforschung, and to B Keimer in particular, for the hospitality during his visit in Stuttgart. We acknowledge partial support by RFBR (grant 16-02-00098) and Government Support of the Leading Scientific Schools of the Russian Federation (NSh-7559.2016.2).

References

1. Bardeen J, Cooper L N, Schrieffer J R *Phys. Rev.* **108** 1175 (1957)
2. Abrikosov A A, Gorkov L P, Dzyaloshinski I E *Methods of Quantum Field Theory in Statistical Physics* (Englewood Cliffs, N.J.: Prentice-Hall, 1963); Translated from Russian: *Metody Kvantovoi Teorii Polya v Stasisticheskoi Fizike* (Moscow: Fizmatgiz, 1962)
3. Volovik G E, Gor'kov L P *JETP Lett.* **39** 674 (1984); *Pis'ma Zh. Eksp. Teor. Fiz.* **39** 550 (1984)
4. Volovik G E, Gor'kov L P *JETP* **61** 843 (1985); *Zh. Eksp. Teor. Fiz.* **88** 1412 (1985)
5. Mineev V P, Samokhin K V *Introduction to Unconventional Superconductivity* (Amsterdam: Gordon and Breach Sci. Publ., 1999); Translated from Russian: *Vvedenie v Teoriyu Neobychnoi Sverkhprovodimosti* (Moscow: Izd. MFTI, 1998)
6. Riseborough P S, Schmiedeshoff G M, Smith J L, in *Superconductivity* Vol. 2 *Novel Superconductors* (Eds K Bennemann, J B Ketterson) (Berlin: Springer-Verlag, 2008) p. 1031
7. Vonsovsky S V, Izyumov Yu A, Kurmaev E Z *Superconductivity of Transition Metals, Their Alloys and Compounds* (Berlin: Springer-Verlag, 1982); Translated from Russian: *Sverkhprovodimost' Perekhodnykh Metallov, ikh Splavov i Soedinenii* (Moscow: Nauka, 1977)
8. Bednorz J G, Müller K A *Z. Phys. B* **64** 189 (1986)
9. Sigrist M, Ueda K *Rev. Mod. Phys.* **63** 239 (1991)
10. Hebard A F et al. *Nature* **350** 600 (1991)
11. Nagamatsu J et al. *Nature* **410** 63 (2001)
12. Kamihara Y et al. *J. Am. Chem. Soc.* **130** 3296 (2008)
13. Drozdov A P, Eremets M I, Troyan I A, arXiv:1412.0460
14. Drozdov A P et al. *Nature* **525** 73 (2015)
15. Hirschfeld P J, Korshunov M M, Mazin I I *Rep. Prog. Phys.* **74** 124508 (2011)
16. Mazin I I et al. *Phys. Rev. Lett.* **101** 057003 (2008)
17. Graser S et al. *New J. Phys.* **11** 025016 (2009)
18. Kuroki K et al. *Phys. Rev. Lett.* **101** 087004 (2008)
19. Maiti S et al. *Phys. Rev. B* **84** 224505 (2011)
20. Korshunov M M *Phys. Usp.* **57** 813 (2014); *Usp. Fiz. Nauk* **184** 882 (2014)
21. Kontani H, Onari S *Phys. Rev. Lett.* **104** 157001 (2010)
22. Boeri L, Dolgov O V, Golubov A A *Phys. Rev. Lett.* **101** 026403 (2008)
23. Kulić M L, Drechsler S-L, Dolgov O V Europhys. Lett. **85** 47008 (2009)
24. Fujioka M et al. *Appl. Phys. Lett.* **105** 102602 (2014)
25. Qing-Yan W et al. *Chinese Phys. Lett.* **29** 037402 (2012)
26. Liu D et al. *Nature Commun.* **3** 931 (2012)
27. Shaolong He et al. *Nature Mater.* **12** 605 (2013)
28. Shiyong Tan et al. *Nature Mater.* **12** 634 (2013)
29. Jian-Feng Ge et al. *Nature Mater.* **14** 285 (2015)
30. Golubov A A et al. *JETP Lett.* **94** 333 (2011); *Pis'ma Zh. Eksp. Teor. Fiz.* **94** 357 (2011)
31. Kordyuk A A *Low Temp. Phys.* **41** 319 (2015); *Fiz. Nizk. Temp.* **41** 417 (2015)
32. Kuchinskii E Z, Sadovskii M V *JETP Lett.* **88** 192 (2008); *Pis'ma Zh. Eksp. Teor. Fiz.* **88** 224 (2008)
33. Sawatzky G A et al. *Europhys. Lett.* **86** 17006 (2009)
34. Nakamura K, Arita R, Ikeda H *Phys. Rev. B* **83** 144512 (2011)
35. Brouet V et al. *Phys. Rev. B* **80** 165115 (2009)
36. Kuroki K et al. *Phys. Rev. B* **79** 224511 (2009)
37. Mizuguchi Y et al. *Supercond. Sci. Technol.* **23** 054013 (2010)
38. Kuchinskii E Z, Nekrasov I A, Sadovskii M V *JETP Lett.* **91** 518 (2010); *Pis'ma Zh. Eksp. Teor. Fiz.* **91** 567 (2010)
39. Hirschfeld P J C. R. Physique **17** 197 (2016)
40. Anderson P W *J. Phys. Chem. Solids* **11** 26 (1959)
41. Abrikosov A A, Gor'kov L P *Sov. Phys. JETP* **12** 1243 (1961); *Zh. Eksp. Teor. Fiz.* **39** 1781 (1960)
42. Tarascon J M et al. *Phys. Rev. B* **42** 218 (1990)
43. Jayaram B, Chen H, Callaway J *Phys. Rev. B* **52** 3742 (1995)
44. Brinkmann M, Bach H, Westerholt K *Phys. Rev. B* **54** 6680 (1996)
45. Markert J T, Dalichaouch Y, Marle M B, in *Physical Properties of High Temperature Superconductors I* (Ed. D N Ginsberg) (Singapore: World Scientific, 1989) Ch. 6, p. 265
46. Xiao G et al. *Phys. Rev. B* **42** 8752(R) (1990)
47. Ting S T et al. *Phys. Rev. B* **46** 11772 (1992)
48. Ovchinnikov S G *Phys. Solid State* **37** 2007 (1995); *Fiz. Tverd. Tela* **37** 3645 (1995)
49. Gaididei Yu B, Loktev V M *Phys. Status Solidi B* **147** 307 (1988)
50. Kluge T et al. *Phys. Rev. B* **52** R727 (1995)
51. Davydov S A et al. *JETP Lett.* **47** 234 (1988); *Pis'ma Zh. Eksp. Teor. Fiz.* **47** 193 (1988)
52. Aleksashin B A et al. *Sov. Phys. JETP* **68** 382 (1989); *Zh. Eksp. Teor. Fiz.* **95** 678 (1989)
53. Anan'ev A V *JETP Lett.* **67** 182 (1998); *Pis'ma Zh. Eksp. Teor. Fiz.* **67** 172 (1998)
54. Ovchinnikov S G *Phys. Usp.* **40** 993 (1997); *Usp. Fiz. Nauk* **167** 1043 (1997)
55. Kulić M L *Phys. Rep.* **338** 1 (2000)
56. Hussey N E *Adv. Phys.* **51** 1685 (2002)
57. Hirschfeld P J, Atkinson W A *J. Low Temp. Phys.* **126** 881 (2002)
58. Balatsky A V, Vekhter I, Zhu J -X *Rev. Mod. Phys.* **78** 373 (2006)
59. Alloul H et al. *Rev. Mod. Phys.* **81** 45 (2009)
60. Pogorelov Yu G, Santos M C, Loktev V M *Low Temp. Phys.* **37** 633 (2011); *Fiz. Nizk. Temp.* **37** 803 (2011)
61. Radtke R J et al. *Phys. Rev. B* **48** 653(R) (1993)
62. Preosti G, Kim H, Muzikar P *Phys. Rev. B* **50** 1259 (1994)
63. Fehrenbacher R, Norman M R *Phys. Rev. B* **50** 3495(R) (1994)
64. Balatsky A V, Salkola M I, Rosengren A *Phys. Rev. B* **51** 15547 (1995)
65. Harań G, Nagi A D S *Phys. Rev. B* **54** 15463 (1996)
66. Franz M et al. *Phys. Rev. B* **56** 7882 (1997)
67. Kulić M L, Oudovenko V *Solid State Commun.* **104** 375 (1997)
68. Kulić M L, Dolgov O V *Phys. Rev. B* **60** 13062 (1999)
69. Chen Q, Schrieffer J R *Phys. Rev. B* **66** 014512 (2002)
70. Fujita K et al. *Phys. Rev. Lett.* **95** 097006 (2005)
71. Hirschfeld P J et al. *Phys. Rev. B* **40** 6695 (1989)
72. Hirschfeld P J, Goldenfeld N *Phys. Rev. B* **48** 4219(R) (1993)
73. Hirschfeld P J, Putikka W O, Scalapino D J *Phys. Rev. B* **50** 10250 (1994)
74. Quinlan S M, Hirschfeld P J, Scalapino D J *Phys. Rev. B* **53** 8575 (1996)
75. Hirschfeld P J, Quinlan S M, Scalapino D J *Phys. Rev. B* **55** 12742 (1997)
76. Duffy D, Hirschfeld P J, Scalapino D J *Phys. Rev. B* **64** 224522 (2001)

77. Atkinson W A, Hirschfeld P J *Phys. Rev. Lett.* **88** 187003 (2002)
78. Tsai S-W, Hirschfeld P J *Phys. Rev. Lett.* **89** 147004 (2002)
79. Zhu L, Atkinson W A, Hirschfeld P J *Phys. Rev. B* **67** 094508 (2003)
80. Preosti G, Muzikar P *Phys. Rev. B* **54** 3489 (1996)
81. Shimizu K et al. *Nature* **412** 316 (2001)
82. Bose S K et al. *Phys. Rev. B* **67** 214518 (2003)
83. Lebègue S *Phys. Rev. B* **75** 035110 (2007)
84. Singh D J, Du M-H *Phys. Rev. Lett.* **100** 237003 (2008)
85. Cao C, Hirschfeld P J, Cheng H-P *Phys. Rev. B* **77** 220506(R) (2008)
86. Kordyuk A A *Low Temp. Phys.* **38** 888 (2012); *Fiz. Nizk. Temp.* **38** 1119 (2012)
87. Brouet V et al. *Phys. Rev. B* **86** 075123 (2012)
88. Ning F et al. *J. Phys. Soc. Jpn.* **78** 013711 (2009)
89. Grafe H-J et al. *Phys. Rev. Lett.* **101** 047003 (2008)
90. Matano K et al. *Europhys. Lett.* **83** 57001 (2008)
91. Matano K et al. *Europhys. Lett.* **87** 27012 (2009)
92. Yashima M et al. *J. Phys. Soc. Jpn.* **78** 103702 (2009)
93. Jeglič P et al. *Phys. Rev. B* **81** 140511(R) (2010)
94. Li Z et al. *J. Phys. Soc. Jpn.* **79** 083702 (2010)
95. Nakai Y et al. *Phys. Rev. B* **81** 020503(R) (2010)
96. Zhang X et al. *Phys. Rev. Lett.* **102** 147002 (2009)
97. Hicks C W et al. *J. Phys. Soc. Jpn.* **78** 013708 (2009)
98. Geshkenbein V B, Larkin A I *JETP Lett.* **43** 395 (1986); *Pis'ma Zh. Eksp. Teor. Fiz.* **43** 306 (1986)
99. Maier T A et al. *Phys. Rev. B* **83** 100515(R) (2011)
100. Wang F et al. *Europhys. Lett.* **93** 57003 (2011)
101. Das T, Balatsky A V *Phys. Rev. B* **84** 014521 (2011)
102. Maiti S et al. *Phys. Rev. Lett.* **107** 147002 (2011)
103. Mazin I I *Phys. Rev. B* **84** 024529 (2011)
104. Mishra V et al. *Phys. Rev. B* **79** 094512 (2009)
105. Mizukami Y et al. *Nature Commun.* **5** 5657 (2014)
106. Karkin A E et al. *Phys. Rev. B* **80** 174512 (2009)
107. Cheng P et al. *Phys. Rev. B* **81** 174529 (2010)
108. Li Y et al. *New J. Phys.* **12** 083008 (2012)
109. Nakajima Y et al. *Phys. Rev. B* **82** 220504(R) (2010)
110. Tropeano M et al. *Phys. Rev. B* **81** 184504 (2010)
111. Kim H et al. *Phys. Rev. B* **89** 174519 (2014)
112. Prozorov R et al. *Phys. Rev. X* **4** 041032 (2014)
113. Tarantini C et al. *Phys. Rev. Lett.* **104** 087002 (2010)
114. Tan D et al. *Phys. Rev. B* **84** 014502 (2011)
115. Grinenko V et al. *Phys. Rev. B* **84** 134516 (2011)
116. Li J et al. *Phys. Rev. B* **85** 214509 (2012)
117. Schilling M B et al. *Phys. Rev. B* **93** 174515 (2016)
118. Smylie M P et al. *Phys. Rev. B* **93** 115119 (2016)
119. Strehlow C P et al. *Phys. Rev. B* **90** 020508(R) (2014)
120. Cho K et al. *Phys. Rev. B* **90** 104514 (2014)
121. Kim H et al. *Phys. Rev. B* **82** 060518(R) (2010)
122. Murphy J et al. *Phys. Rev. B* **88** 054514 (2013)
123. Salovich N W et al. *Phys. Rev. B* **87** 180502(R) (2013)
124. Gerashenko A et al., arXiv:0911.2127
125. Zhao J et al. *Nature Mater.* **7** 953 (2008)
126. Efremov D V et al. *Phys. Rev. B* **84** 180512(R) (2011)
127. Korshunov M M, Efremov D V, Golubov A A, Dolgov O V *Phys. Rev. B* **90** 134517 (2014)
128. Castellani C, Natoli C R, Ranninger J *Phys. Rev. B* **18** 4945 (1978)
129. Oleś A M *Phys. Rev. B* **28** 327 (1983)
130. Berk N F, Schrieffer J R *Phys. Rev. Lett.* **17** 433 (1966)
131. Allen P B, Mitrovic B, in *Solid State Physics*: *Advances in Research and Applications* Vol. 37 (Eds H Erenreich, F Zeitz, D Turnbull) (New York: Academic Press, 1982) pp. 1 – 92
132. Parker D et al. *Phys. Rev. B* **78** 134524 (2008)
133. Popovich P et al. *Phys. Rev. Lett.* **105** 027003 (2010)
134. Charnukha A et al. *Phys. Rev. B* **84** 174511 (2011)
135. Ohashi Y *Physica C* **412 – 414** 41 (2004); *Proc. of the 16th Intern. Symp. on Superconductivity, ISS 2003. Advances in Superconductivity XVI, Tsukuba, Japan, 27 – 29 October 2003*
136. Bickers N E et al. *Phys. Rev. B* **42** 67 (1990)
137. Nam S B *Phys. Rev.* **156** 470 (1967)
138. Nam S B *Phys. Rev.* **156** 487 (1967)
139. Lee W, Rainer D, Zimmermann W *Physica C* **159** 535 (1989)
140. Dolgov O V, Golubov A A, Shulga S V *Phys. Lett. A* **147** 317 (1990)
141. Marsiglio F *Phys. Rev. B* **44** 5373(R) (1991)
142. Akis R, Carbotte J P *Solid State Commun.* **79** 577 (1991)
143. Sadovskii M V *Phys. Rep.* **282** 225 (1997)
144. Sadovskii M V *Superconductivity and Localization* (Singapore: World Scientific, 2000)
145. Golubov A A, Mazin I I *Phys. Rev. B* **55** 15146 (1997)
146. Chubukov A V, Efremov D V, Eremin I *Phys. Rev. B* **78** 134512 (2008)
147. Senga Y, Kontani H *J. Phys. Soc. Jpn.* **77** 113710 (2008)
148. Bang Y, Choi H-Y, Won H *Phys. Rev. B* **79** 054529 (2009)
149. Golubov A A, Mazin I I *Physica C* **243** 153 (1995)
150. Kemper A F et al. *Phys. Rev. B* **80** 104511 (2009)
151. Korshunov M M, Togushova Yu N, Dolgov O V *J. Supercond. Novel Magnet.* **29** 1089 (2016)
152. Schopohl N, Scharnberg K *Solid State Commun.* **22** 371 (1977)
153. Ummarino G A *J. Supercond. Novel Magnet.* **20** 639 (2007)
154. Yao Z-J et al. *Phys. Rev. B* **86** 184515 (2012)
155. Chen H et al. *Phys. Rev. B* **88** 184509 (2013)
156. Ambegaokar V, Griffin A *Phys. Rev.* **137** A1151 (1965)
157. Li J, Wang Y *Europhys. Lett.* **88** 17009 (2009)
158. Stanev V G, Koshelev A E *Phys. Rev. B* **86** 174515 (2012)
159. Peng Cheng et al. *Europhys. Lett.* **104** 37007 (2013)
160. Li J et al. *Phys. Rev. B* **84** 020513(R) (2011)
161. Suzuki S, Miyasaka S, Tajima S *Physica C* **470** S330 (2010); *Proc. of the 9th Intern. Conf. on Materials and Mechanisms of Superconductivity*
162. Bezusyy V l et al. *Acta Phys. Polon. A* **121** 816 (2012)
163. Guo Y F et al. *Phys. Rev. B* **82** 054506 (2010)
164. Lee S C et al. *J. Phys. Soc. Jpn.* **79** 023702 (2010)
165. Satomi E e al. *J. Phys. Soc. Jpn.* **79** 094702 (2010)
166. Wang A F et al. *Phys. Rev. B* **89** 064510 (2014)
167. Maiti S, Korshunov M M, Chubukov A V *Phys. Rev. B* **85** 014511 (2012)
168. Golubov A A et al. *Phys. Rev. B* **66** 054524 (2002)
169. Efremov D V, Golubov A A, Dolgov O V *New J. Phys.* **15** 013002 (2013)
170. Marsiglio F et al. *Phys. Rev. B* **53** 9433 (1996)
171. Nakai Y et al. *J. Phys. Soc. Jpn.* **77** 073701 (2008)
172. Ning F et al. *J. Phys. Soc. Jpn.* **77** 103705 (2008)
173. Korshunov M M, Eremin I *Phys. Rev. B* **78** 140509(R) (2008)
174. Maier T A, Scalapino D J *Phys. Rev. B* **78** 020514(R) (2008)
175. Inosov D S *C. R. Physique* **17** 60 (2016)
176. Hirschfeld P J, Wölfle P, Einzel D *Phys. Rev. B* **37** 83 (1988)
177. Senga Y, Kontani H *New J. Phys.* **11** 035005 (2009)
178. Nakai Y et al. *Phys. Rev. Lett.* **105** 107003 (2010)
179. Li Z et al. *Phys. Rev. B* **83** 140506(R) (2011)